Annual Report on Major Results and Progress of Naka Fusion Research Establishment of JAERI from April 1 to September 30, 2005 and Fusion Research and Development Directorate of JAEA from October 1, 2005 to March 31, 2006

Fusion Research and Development Directorate

Japan Atomic Energy Agency
Naka-shi, Ibaraki-ken

(Received July 31, 2006)

This annual report provides an overview of major results and progress on research and development (R&D) activities at Naka Fusion Research Establishment of Japan Atomic Energy Research Institute (JAERI) during the period from April 1 to September 30, 2005 and at Fusion Research and Development Directorate of Japan Atomic Energy Agency (JAEA) from October 1, 2005 to March 31, 2006, including those performed in collaboration with other research establishments of JAERI, research institutes, and universities.

In JT-60, ferritic steel tiles (FSTs) were installed inside the vacuum vessel of JT-60U to reduce the toroidal field ripple. After the installation of FSTs, a high normalized beta plasma at β_N~2.3 was sustained for 28.6s with ELMy H-mode confinement as required for an ITER hybrid operation scenario. National Centralized Tokamak was placed as the ITER satellite tokamak in collaboration with the EU fusion community, and the facility design was modified strongly in support of ITER.

In theoretical and analytical researches, studies on H-mode confinement, ITB in reversed shear plasmas, aspect ratio effects on external MHD modes and magnetic island evolution in a rotating plasma were progressed. Progress was also made in the NEXT project in which the behaviors of collisionless MHD modes and the dynamics of zonal flows were simulated.

In fusion reactor technologies, R&Ds for ITER and fusion DEMO plants have been carried out. For ITER, a steady state operation of the 170GHz gyrotoron up to 1000 s with 0.2MW was demonstrated. Also current density of the neutral beam injector has been extended to 134A/m^2 at 0.75MeV. In the ITER Test Blanket Module (TBM), designs of Water and Helium Cooled Solid Breeder TBMs and R&Ds of tritium breeder/multiplier materials were progressed. Tritium processing technology for breeding blankets was also progressed. For the DEMO reactors, high temperature superconductor such as Bi2212 has been examined. In plasma facing components, critical heat flux of a screw tube has been examined. Neutronics integral experiments with a blanket mockup were also progressed. For ITER TBMs and DEMO blankets, irradiation effects on F82H characteristics were progressed using HFIR, JMTR and so on. In the IFMIF program, transitional activities were also progressed. Vacuum technology and its application to industries have been examined.

In the ITER Program, under the framework of the ITER Transitional Arrangements, the Design and R&D Tasks have been carried out by the Participant Teams along the work plan approved on September 2005. In FY 2005, JAERI/JAEA has performed sixty-six Design Tasks and has completed thirty-four Tasks that make the implementation of preparing the procurement documents for facilities and equipments that are scheduled to be ordered at an early stage of ITER construction. The work plan for the “Broader Approach” Program has been continuously discussed through the bilateral negotiation meetings between Japan and the EU, and JAERI/JAEA provided the technical support for the meetings.

Finally, in fusion reactor design studies, a reactor concept of SlimCS was proposed to demonstrate an electric power generation of 1GW level, self-sufficiency of tritium fuel and year-long continuous operation.

Keywords; JAERI, JAEA, Fusion Research, Fusion Technology, JT-60, ITER, Broader Approach, IFMIF, Fusion Power, DEMO Plant, Fusion Reactor

---

Editors: Yoshida, H., Oasa, K., Hayashi, T., Nakamura, H., Ogawa, H.

Contents

I. JT-60 PROGRAM

1. Experimental Results and Analyses

1.1 Insertion of the Ferritic Steel Tile and Extended Plasma Regimes

Modification of the control systems for the operation, heating and diagnostics has brought a new regime in the advanced tokamak plasma research with longer time scales than the current relaxation time (τ_R) on JT-60U. However, fur ther pursuit of long sustainment of high performance plasmas has been prevented by the loss of fast ions due to the toroidal field ripple, since the loss decreases the net heating power, increases heat load to the wall and lower hybrid (LH) wave launcher located at a horizontal port, and limits controllability of the toroidal rotation (V_T) profile due to formation of an inward electric field. In order to reduce the toroidal field ripple, ferritic steel tiles (FSTs), which cover ~10% of the vacuum vessel surface, have been installed inside the JT-60U vacuum vessel on the low field side [1.1-1]. After the installation of FSTs, high normalized beta (β_N) of 2.3 is successfully maintained for 28.6 s with good confinement close to ITER hybrid operation scenario [1.1-2].

1.1.1 Ferritic Tile Insertion

Specifications of the FST is described in the section 2.1.2. Installation of the FSTs was optimized based on a typical large bore discharge (I_p=1.1MA, B_t=1.86T) in which the fast ion loss is larger using fully three Dimensional magnetic field orbit-following Monte-Carlo code (F3D OFMC) [1.1-1]. The final design is shown in Fig. I.1.1-1. With this design, the evaluation results show that total absorbed NB power can be increased by about 13%, and the increase in the absorbed power of the perpendicular beams can be 15%. Moreover, the heat load to the LH launcher can be reduced by a factor of ~3.

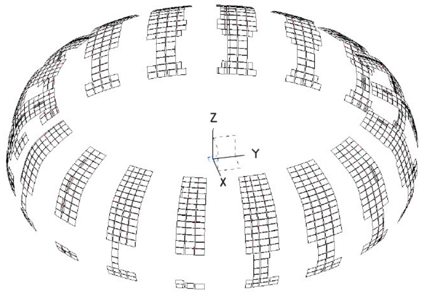

Fig. I.1.1-1 Bird's eye view of ferritic insertion. Thickness of the FST is 23mm

After the installation, the heat load to the outer wall was evaluated by the infrared camera, and found to be consistent with the calculation.

1.1.2 Sustainment of High β_N with High Confinement

The reduction of toroidal field ripple increases absorbed heating power at the same injection power. The increase in absorbed power can reduce the required NB units to sustain a given β_N and then increase flexibility of combination of tangential NB units to vary torque input. The reduction of fast ion losses can also reduce formation of an inward electric field, which may induce a counter toroidal rotation. All these factors can be expected to contribute in extending the sustainable

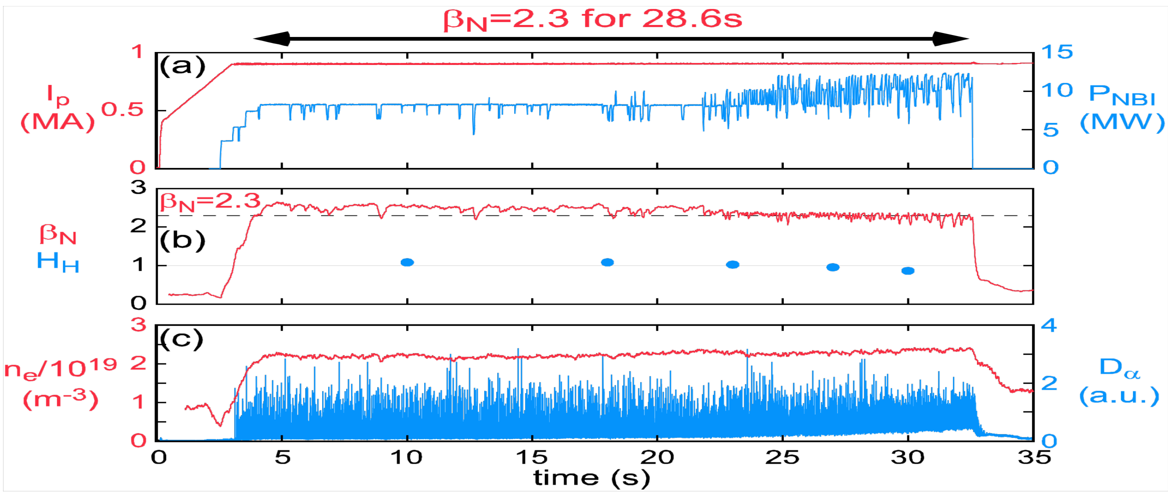

Fig. I.1.1-2 Waveforms of a typical high β_N long-pulse plasma (E45436), (a) plasma current and heating power, (b) normalized beta, β_N, and confinement factor, H_{98}, and (c) line-averaged density and divertor D_α intensity.

duration of high β_N plasma. Therefore, optimization had been carried out, and high β_N of 2.3 was successfully sustained for 28.6s. The typical waveforms of the discharge (I_p=0.9MA, B_T=1.58T, q_{95}~3.3) are shown in Fig. I.1.1-2. Increase in the absorbed power and plasma confinement has enabled to sustain high β_N with smaller injection power. As the result, enough power to keep β_N is maintained until the end of the pulse. Smaller injection power also prevented increase in the temperature of the divertor tiles, which causes increase in the particle recycling. The increase in the particle recycling would degrade plasma confinement. In this discharge, the particle recycling is increasing (Fig. I-1.1-2 (c)), but limited low. It should be noted that in this discharge, a high bulk energy confinement ($H_{98(y,2)}$) of about 1.1 is maintained up to t~22s with β_N ≥2.4 as shown in Fig. I-1.1-2. Also in this discharge high value of the product $\beta_N H_{98(y,2)}$, which is a measure of the fusion performance, is maintained above 2.2 for 23.1s (>~12τ_R). It is noted that this value of $\beta_N H_{98(y,2)}$ can satisfy the ITER Hybrid scenario.

References

1.1-1 Shinohara, K., and the JT-60 Team, "Review of Recent Steady-State Advanced Tokamak Research, and Its Further Pursuit by Reduction of TF Ripple on JT-60U," to be published in *J. Korean Phys. Soc.*.

1.1-2 Oyama, N., *et al.*, "Enhanced ELMy H-mode Performance with Reduced Toroidal Field Ripple in JT-60U," *Proc. 33rd EPS Conf. on Plasma Phys.*.

1.2 Heat, particle and rotation transport

1.2.1 Temporal Variation of Density Fluctuation and Transport in Reversed Shear Plasmas [1.2-1]

In reversed shear (RS) plasmas, an internal transport barrier (ITB) is formed due to suppression of anomalous turbulent transport. Many types of fluctuation with various spatial scales exist in plasmas. The anomalous turbulent heat transport for ion and electron channels and also the anomalous turbulent particle transport could be dominated by different types of fluctuation with different spatial scale such as ion temperature gradient (ITG) mode, trapped electron mode (TEM) and electron temperature gradient (ETG) mode. In a JT-60U RS plasma, further reduction of the transport was induced by a pellet injection after the ITB formation. The temporal variation of the density fluctuation and its relation to the electron and ion heat transport and the particle transport were investigated for the further reduction of the transport.

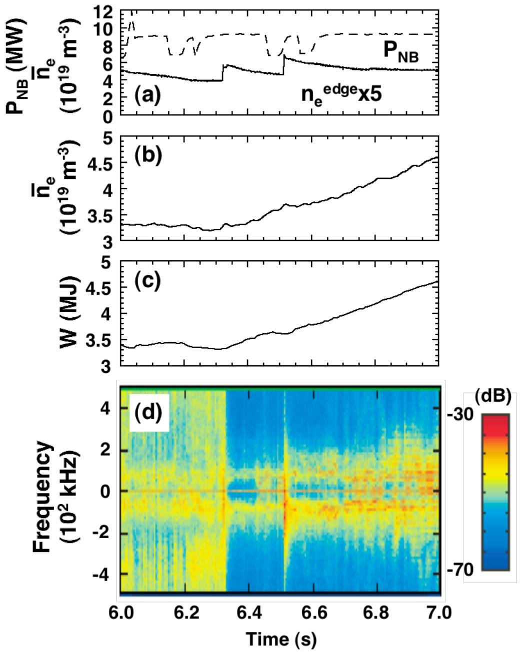

Fig. I.1.2-1 Wave-forms in a RS plasma with pellet injections. (a) The solid line shows edge line-averaged electron density. The dashed line shows NB heating power. (b) Center line-averaged electron density, (c) stored energy and (d) spectrogram of the O-mode reflectometer signal.

Figure I.1.2-1 shows wave-forms in a RS plasma with further reduction of the transport after the pellet injection. Pellets were injected into the RS plasma from the high-field-side at the top after the ITB formation. The plasma current (I_p) was 2.2MA, the toroidal magnetic field (B_T) was 4.3T, and the safety factor at 95% flux surface (q_{95}) was 3.8. The first pellet was injected at t=6.32s, as shown by the edge density jump, during the I_p flat-top phase with constant heating power of neutral beam (NB). After the first pellet injection, the central density and the stored energy started to increase. A high frequency component (|f|>200kHz) of the O-mode reflectometer signal was drastically reduced, as well as a low frequency component (50kHz>|f|>20 kHz), ~5ms after the pellet injection. In this case, the cut-off layer was located in the ITB region (r/a=0.45-0.5). The central density and the stored energy seemed to start to increase simultaneously with the reduction of the high and low frequency components. The reduction of the high and low frequency components of the O-mode reflectometer signal indicated change of density fluctuation level. The density fluctuation level was estimated to be 1-2% before and 0.4-0.5% after the first

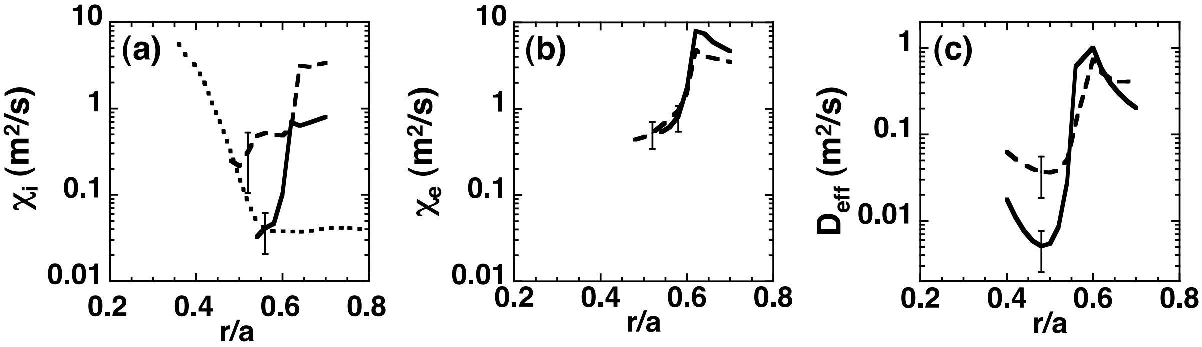

Fig. I.1.2-2 (a) Ion thermal diffusivity, (b) electron thermal diffusivity and (c) effective particle diffusivity. The dashed lines show the data before the first pellet injection at t=6.3s and the solid lines show the data after the pellet injection at t=7.0s. The dotted line in (a) shows the neoclassical ion thermal diffusivity.

pellet injection, respectively, [1.2-2] based on the analytical solution of time-dependent 2D full-wave equation [1.2-3]. The wave number of the measured density fluctuation was estimated to be of the order of 1cm^{-1}, which was consistent with the spatial scale of ITG and/or TEM. After another pellet injection at t=6.51s, the spectrum of the O-mode reflectometer signal was unchanged, and the central density and the stored energy continued to increase. The energy confinement time (τ_E) and the confinement enhanced factor over ITER-89P L-mode scaling (H_{89PL}) increased from τ_E=0.5s and H_{89PL}=1.6 at t=6.3s to τ_E=1.0s and H_{89PL}=2.6 at t=7s.

The density substantially increased inside the ITB foot, while the edge density slightly increased. The ion and electron temperature profiles did not changed significantly. The profiles of the ion and electron thermal diffusivities (χ_i and χ_e) and the effective particle diffusivity (D_{eff}) estimated by the particle and power balance analysis without consideration of the pinch term (considering only the diffusion term) are shown in Fig. I.1.2-2. The values of χ_i and D_{eff} decreased by one order of magnitude after the pellet injection. However, no reduction of χ_e was observed. The equi-partition heat transfer from ions to electrons increased due to the substantial increase in the central density, but no change of difference between ion and electron temperature was observed. The ion temperature gradient in the ITB region was maintained with the decreased ion heat flux after the pellet injections due to χ_i reduced to a neoclassical level. The increase in the electron stored energy (density increase with a constant electron temperature) was attributed to the increase in the equi-partition heat transfer from ions. The particle and power balance analysis indicated that the particle and ion heat transport are coupled with the measured density fluctuation with spatial scale of the order of 1cm^{-1}, while the electron heat transport was decoupled.

1.2.2 Degradation of Internal Transport Barrier by ELM Crashes [1.2-4]

In order to sustain burning plasmas in ITER and the steady-state tokamak power plants, we need to achieve high values of the energy confinement improvement factor (HH_{y2}), normalized beta (β_N), bootstrap and non-inductively driven current fractions, plasma density, fuel purity and radiation power simultaneously. It is widely recognized that the high H-mode pedestal pressure and the ITB formation are important for achieving the above highly integrated plasma performance. However, high pedestal pressure may induce large ELMs. The compatibility of large ELMs with the ITB is important issue to develop the highly integrated plasma. In JT-60U, the compatibility of type I ELMs and the ITB has been good enough to sustain a HH_{y2} factor value of 1–2 in long pulse discharges of the high β_p H-mode (weak positive magnetic shear) and the RS H-mode [1.2-5]. Up to I_p=1.5MA, the sustainable maximum plasma stored energy and β_N have been limited by the appearance of neoclassical tearing modes (NTM) for the positive shear cases (q_{95}=3.2–9 at I_p=1 MA, q_{95}=4–5 at I_p=1.5MA) [1.2-5]. However, at higher I_p=1.8MA (q_{95}=4.1), we found some cases where the plasma stored energy was degraded by type I ELMs.

Figure I.1.2-3 shows the time evolution of the high β_p ELMy H-mode discharge E39713 (I_p=1.8MA, B_T=4.05T, q_{95}=4.1), where a full non-inductive current drive was achieved [1.2-6]. The total plasma stored energy (W_{dia}) reached 7.6MJ, which was the highest value achieved so far at I_p=1.8MA in JT-60U. In the flat

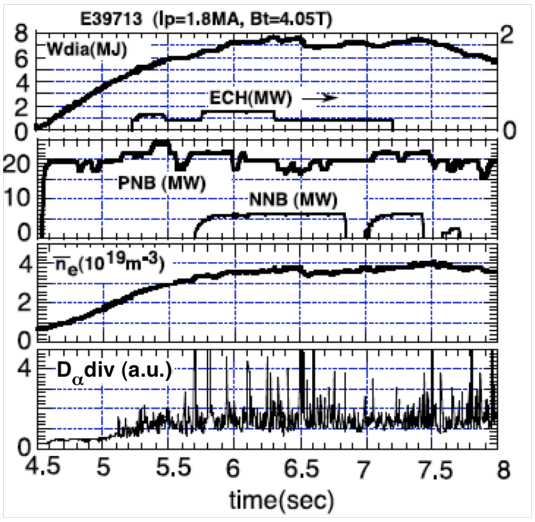

Fig. I.1.2-3 Time evolutions of total stored energy, heating powers for EC wave injection and for positive and negative ion based NBs, line averaged electron density and Dα emission intensity from the divertor area in the high β_p ELMy H-mode discharge at I_p=1.8MA.

top phase of W_{dia}, the ITB-foot location was around 65% of the minor radius and the location of the top of the pedestal was around 90% of the minor radius. The central safety factor (measured by MSE) was 1.4 and thus there was no sawtooth activity. In Fig. I.1.2-3, a drop of W_{dia} was seen at t~6.5s to coincide with a drop in the line averaged density and an increase in the Dα emission from the divertor area. In this phase, no signature of an NTM was observed.

In order to evaluate the penetration of an ELM crash, we performed ECE measurement using the heterodyne radiometer system with a radial resolution of 2cm. The minor radius of this discharge was 79cm. Figure I.1.2-4 shows the measured profiles of the electron temperature (T_e) and the relative change in T_e at the ELM crashes (=$\Delta T_e/T_e$) at t=5.35s and t=6.49s in the discharge shown in Fig. I.1.2-3. In order to evaluate the ELM crash itself (the eigenfunction of the instability), $\Delta T_e/T_e$ was calculated within 600μs. We defined the ELM penetration radius by the deepest radial location with $\Delta T_e/T_e$> 1%. At t=5.35s, the ELM crash depth was away from the ITB-foot, while at t=6.49s, it reached the ITB-foot.

In the early phase (t<5.8s) the ITB-foot radius expanded and the ELM penetration radius deepened gradually. This deepening of the ELM penetration seemed to coincide with an increase in pedestal stored energy (while the pedestal electron collisionality was almost constant). Then the ELM penetration radius and the ITB-foot met each other at t~5.8s. After that, the 'balanced phase' lasted for ~0.7s. Interestingly, the ITB-foot seemed to behave as a barrier against ELM crash penetration, and after around ten ELM attacks the ITB-foot shrank. Then the ELM penetration followed the shrinking ITB-foot. This behavior was shown in greater detail in T_e at various radial locations. Before t=6.492s, a sudden drop in T_e was seen up to r/a=0.615 (~ITB-foot), while no change in T_e at each ELM occurs inside the ITB. At t=6.492s, the ITB was broken at the original ITB-foot radius. Then degradation of T_e penetrated gradually into the inner region and, at the same time, T_e in the outer region increased and the ELM period shortend due to a release of the stored energy. As the result of this degradation of the ITB from t=6.492s to t=6.56s, the stored energy decreased by about 10% (0.8MJ). ELM control for small amplitude such as type

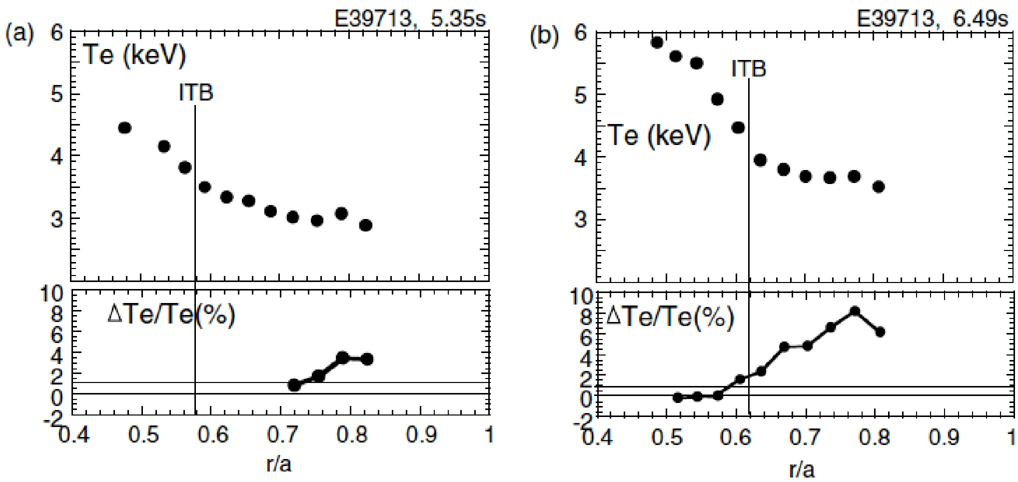

Fig. I.1.2-4 Profiles of electron temperature (T_e) and relative change of T_e within 600 μs at an ELM crash (=$\Delta T_e/T_e$) appeared at (a) t=5.35s and (b) t=6.59s in the high β_p ELMy H-mode discharge shown in Fig. I.1.2-3.

II ELM is important not only to reduce transient heat load to the divertor plates but also to achieve highly integrated plasma performance.

1.2.3 Response of Toroidal Rotation Velocity to Electron Cyclotron Wave Injection [1.2-7]

In tokamak plasmas, toroidal rotation velocity and its shear (or radial electric field (E_r) shear) play an important role in stability and transport. In present tokamak devices, the toroidal rotation velocity profile can be easily controlled by toroidal momentum input from NBs. In contrast, the control of toroidal rotation velocity profile by NBs will be difficult in a burning plasma. Therefore, the development of other actuators to control the toroidal rotation velocity profile is important for the control of a burning plasma. Recently, the change in toroidal rotation velocity profile induced by ICRF heating has been reported [1.2-8]. In JT-60U, the spontaneous toroidal rotation velocity under the no/low direct toroidal momentum input was investigated using electron cyclotron (EC) wave injection.

In order to investigate the response of the toroidal rotation velocity to on-axis EC wave injection, EC power of 2.7MW was injected into L-mode plasma (I_p=1MA, B_T=1.9T for the second harmonic EC central injection, q_{95}=3.4 and n_e~$1.0\times10^{19}m^{-3}$ at the centre). In this plasma, low power NBs were applied, which consisted of counter-NB (0.9MW) for the motional Stark effect (MSE) diagnostic and perpendicular-NB (2.3MW) for the CXRS diagnostic. Since the fundamental O-mode (or the second harmonic X-mode) with an oblique toroidal injection angle was launched from the low-field-side for the current drive in JT-60U, EC injection was not for the electron heating only but also for the current drive. Figure I.1.2-5 shows the profiles of the toroidal rotation velocity and electron temperature just before and during the EC wave injection. As EC wave was injected, the central electron temperature increased from 2 to 6keV. The ion temperature just outside the EC wave deposition (r/a~0.25) and the electron density at r/a~0.13 were kept almost constant during EC wave injection. The toroidal rotation velocity at r/a~0.25 was changed from ~100 to ~60km/s in the counter-direction during the EC wave injection as shown in Fig. I.1.2-5. The region of change in toroidal rotation velocity was up to r/a~0.6 from the centre, which was wider than the EC wave power deposition profile. Although the change in toroidal rotation velocity at the core region coincided with the increase in electron temperature, the timescale of change in the toroidal rotation velocity was slower than that in the electron temperature. It should be mentioned that the change in toroidal rotation velocity at r/a~0.37 was delayed from that at r/a~0.25. This indicated that the change in the toroidal rotation velocity propagated from the centre to the peripheral.

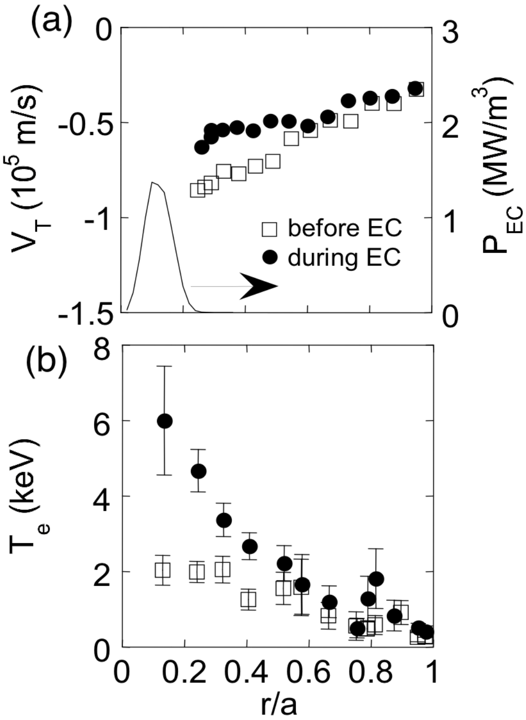

Fig. I.1.2-5 Profiles of (a) toroidal rotation velocity and (b) electron temperature just before (squares) and during (circles) EC wave injection. The solid line in (a) shows profile of the EC wave power deposition.

In order to investigate the propagating response of the toroidal rotation velocity to EC wave injection (2MW), the short pulse (0.1s) off-axis EC wave injection into the L-mode plasma heated by diagnostics NBs (counter-NB: 0.76MW, perpendicular-NB: 2MW) was performed, as shown in Fig. I.1.2-6. Here, I_p, B_T and q_{95} were 0.8MA, 2.1T and 5.1 for the second harmonic EC injection, the line averaged electron density was ~$0.8\times10^{19}m^{-3}$. Figure I.1.2-6 shows response of the toroidal rotation velocity in the core region to the short pulse of the off-axis EC wave injection. The peak of the absorbed EC wave power deposition was located at r/a~0.7, and there was no EC wave power source in the region of r/a<0.5. The perturbation of the toroidal rotation velocity towards co-direction (or reduced counter-rotation) was observed

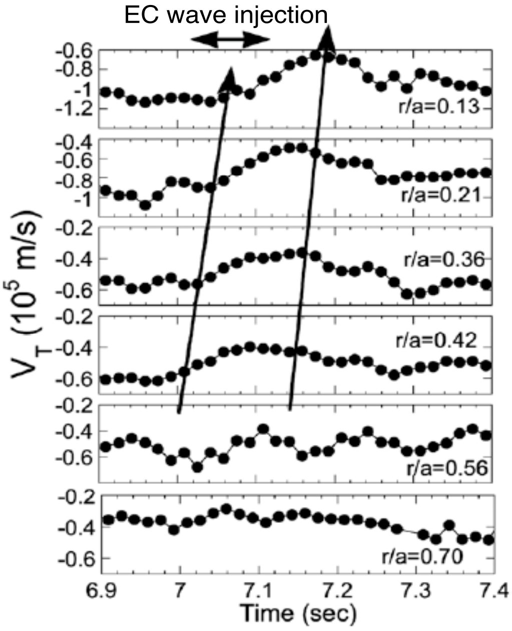

Fig. I.1.2-6 Propagating perturbations in toroidal rotation velocity at several radii, induced by the short pulse off-axis EC wave injection (t=7.02-7.12s).

clearly in the region of r/a<0.5 and it propagated from the half of the minor radius to the centre, as shown in Fig. I.1.2-6. On the other hand, the propagation of the perturbation of the toroidal rotation velocity in the opposite direction was not obvious in this discharge. The propagation of the heat pulse was also observed in the electron temperature. The propagation speed for the perturbation of the toroidal rotation velocity was much slower than that of electron temperature. This suggests that the toroidal rotation velocity was not simply determined by the local electron pressure gradient. The perturbation amplitude of the toroidal rotation velocity increased when the perturbation propagated, suggesting existence of an inward pinch in momentum transport. The turbulence driven theory predicted that the density and/or temperature gradient, as well as the velocity gradient, generate the momentum flux [1.2-9]. The investigation of the response of the toroidal rotation velocity to the EC wave injection is necessary with various plasma parameters to clarify the mechanisms determining the momentum transport.

References

1.2-1 Takenaga, H., *et al., Plasma Phys. Control. Fusion,* **48**, A401 (2006).
1.2-2 Oyama, N., *et al., Plasma Phys. Control. Fusion,* **46**, A355 (2004).
1.2-3 Bruskin, L.G., *et al., Plasma Phys. Control. Fusion,* **44**, 2305 (2002).
1.2-4 Kamada, Y., *et al., Plasma Phys. Control. Fusion,* **48**, A419 (2006).
1.2-5 Kamada, Y., *et al., Nucl. Fusion,* **41**, 1311 (2001).
1.2-6 Isayama, A., *et al., Nucl. Fusion,* **43**, 1272 (2003).
1.2-7 Sakamoto, Y., *et al., Plasma Phys. Control. Fusion,* **48**, A63 (2006).
1.2-8 Noterdaeme, J.-M., *et al., Nucl. Fusion,* **43**, 274 (2003).
1.2-9 Itoh , S.-I., *Phys. Fluids,* **B4**, 796 (1992).

1.3 MHD Instabilities and Control

1.3.1 Stabilization of the Neoclassical Tearing Mode

In a fusion reactor such as ITER, stationary sustainment of a high-beta and high confinement plasma is essential. From the viewpoint of MHD stability, suppression of neoclassical tearing modes (NTMs) is the most critical issue in optimizing the discharge scenario of the high-performance plasmas. In JT-60U, in addition to the experimental demonstration of NTM suppression, progress has been made in simulation of NTM evolution by extending the transport code TOPICS [1.3-1, 1.3-2].

(1) Simulation of Evolution of Magnetic Island

Evolution of magnetic island associated with an NTM is described by the modified Rutherford equation. The equation is composed of the effects of the equilibrium current profile, the bootstrap current, the toroidal geometry (Glasser-Greene-Johnson effect), the ion polarization current, and the EC-driven current. Since each term contains a coefficient which cannot be determined with high accuracy by theory alone, in JT-60U, the coefficients have been determined by comparing between TOPICS simulation and NTM experiments.

Temporal evolution of magnetic island width of an m/n=3/2 NTM evaluated with the TOPICS code is shown in Fig. I.1.3-1 (a). Here, m and n are the poloidal and toroidal mode numbers, respectively. In this simulation, equilibrium and pressure profile in an NTM experiment are used, and EC wave power P_{EC} of 2.6MW, which corresponds to 4-unit injection in JT-60U, is injected from t=7.6s. Other typical parameters are as follows: plasma current I_p=1.5MA, toroidal field B_t= 3.6T, safety factor at 95% flux surface q_{95}=3.9, island width before EC wave injection W(7.5s)=0.125, full-width at half-maximum (FWHM) of ECCD profile δ_{EC}=0.12, mode rational surface ρ_s=0.4 in the volume-averaged normalized minor radius ρ. If EC wave is deposited at the island center, the 3/2 NTM is completely stabilized in 1.3s at t=8.8s (case A in Fig. I.1.3-1(a)). If the deposition location is misaligned by 0.01 in ρ, time for stabilization is prolonged (case B in Fig. I.1.3-1(a)). Figure I.1.3-1 (b) shows the island width at t=10s, W(10s), for different deposition locations. As shown in this figure, stabilization effect by ECCD is significantly decreased with increasing the distance between ρ_s and ECCD location ρ_{EC}. Complete stabilization can be achieved within the misalignment of $|\rho_{EC} - \rho_s|/W(7.5s) \lesssim 0.5$, that is, about a half of the island width. This suggests that precise adjustment of ECCD location is essential, as recognized in experiments in JT-60U. It is notable that island width increases when the deposition location is misaligned by about W. The simulation also shows that it is mainly attributed to a destabilization effect of the ECCD term due to the misaligned injection.

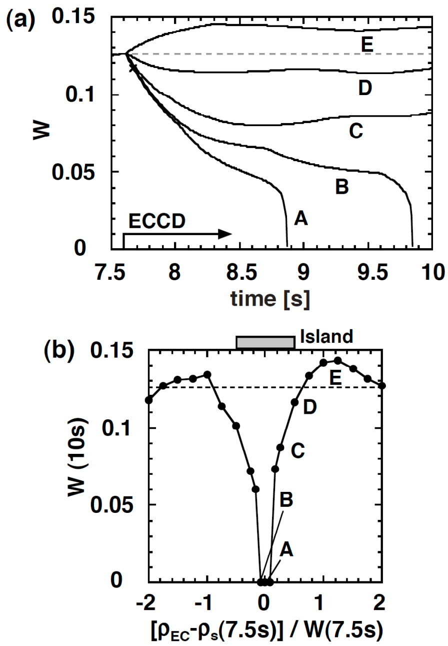

Fig. I.1.3-1 (a) Temporal evolution of magnetic island width for different ECCD locations and (b) island width at t = 10s. ECCD location is fixed at ρ=0.40 (A), 0.39 (B), 0.43 (C), 0.46 (D) and 0.55 (E).

(2) Effect of ECCD Profile on Stabilization

In NTM stabilization, ECCD profile is important as well as injection power. The effect has been numerically evaluated by TOPICS simulation. Figure I.1.3-2 (a) shows the dependence of magnetic island width during ECCD on P_{EC} for different ECCD width. Here, W^* and δ_{EC}^* are the island width and FWHM of ECCD profile normalized by the island width before ECCD, respectively. It can be seen that the stabilization effect strongly depends on the width of ECCD profile. Since the maximum value of the ECCD profile decreases with increasing δ_{EC}^* at fixed EC power, both δ_{EC}^* and P_{EC} must be considered in evaluating the stabilization effect. In Fig. I.1.3-2 (b), W^* is plotted as a function of δ_{EC}^* and P_{EC}. In general, magnetic island associated with an NTM is spontaneously decays due to the polarization current effect when its width is decreased to a certain value. In JT-60U, complete stabilization can be achieved for $W^* \lesssim 0.3$. The TOPICS code simulation shows that the threshold for complete stabilization increases with $P_{EC}^{0.6}$, which indicates that EC wave power required for complete stabilization can be significantly reduced by narrowing the ECCD width. In NTM experiments in JT-60U, EC-driven current density J_{EC} is comparable to the bootstrap current density J_{BS} at the mode rational surface. Since the ECCD profile is close to the Gaussian distribution function, the maximum current density linearly increases with decreasing the FWHM under a fixed injection power. This suggests that complete stabilization can be achieved even with J_{EC}/J_{BS}<1 if narrow ECCD profile is obtained.

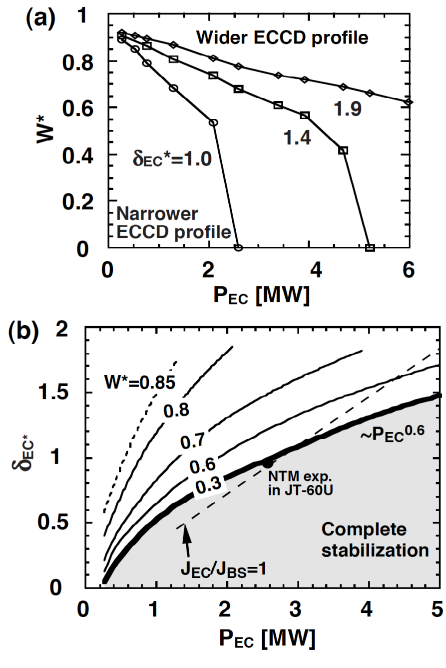

Fig. I.1.3-2 (a) Dependence of magnetic island width on EC wave power, and (b) contour plot of island width during ECCD as a function of ECCD width and EC wave power.

1.3.2 Stability of Resistive Wall Mode

Steady-state high-β plasma is required for future fusion reactors. In ideal MHD stability, achievable β is mostly limited by pressure-driven instabilities such as the kink-ballooning modes. Although these instabilities can be stabilized by placing a perfectly conducting wall (ideal wall), the actual wall has a finite resistivity and then generates an other branch as a resistive wall mode (RWM). Therefore, the stabilization of the RWM is required for a high performance plasma. To stabilize the RWM, mainly two methods are proposed; active feedback control and plasma rotation effect. As for the RWM experiment, an advantage of JT-60U is various tangential NBs; therefore, the plasma rotation can be controlled. We have performed the RWM experiments focused on the stabilization effects due to the wall and the plasma rotation.

(1) Current-Driven RWM Experiment

1) Wall Stabilization Effect

To investigate the basic features of the RWM, we have performed current-driven RWM experiments. When q_{eff} was below 3, a instability grew with about 10 ms without oscillation and a plasma collapse was observed. Note that this mode has m/n = 3/1 mode structure. Since the wall skin time of JT-60U is about 10ms, this mode can be identified as the RWM. To confirm the wall stabilization effect on RWM, plasma is systematically shifted away from the outer wall. FigureI.1.3-3 shows experimental growth rates γ versus the normalized wall radius. In Fig. I.1.3-3, solid line shows the dispersion relation without plasma rotation and dissipation in cylindrical geometry. When the plasma is moved away from the wall, the growth rates of RWM become larger, as is consistent with the dispersion relation.

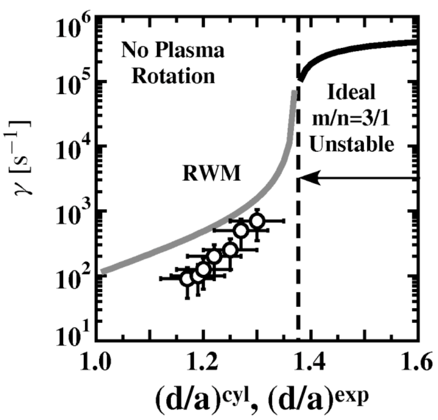

Fig. I.1.3-3 Experimental growth rates versus normalized wall radii. Solid lines show a dispersion relation without plasma rotation and dissipation.

2) Plasma Rotation Effect

To investigate the stabilization effect of the plasma rotation, we performed experiments with different plasma rotation which was controlled by tangential NBs. Figure I.1.3-4 (a) shows two profiles of the toroidal plasma rotation V_{tor} at δL = 10cm, where δL denotes the clearance between the plasma surface and the first wall at low field side. The experimental growth rates at δL = 10, 20, 30 and 40cm with different plasma rotation are shown in Fig. I.1.3-4 (b). Note that the experimental data at zero rotation are in ohmic discharges. For the δL = 10 and 20cm case, the growth rates with a slow plasma rotation become twice smaller than that with a fast plasma rotation. However, for δL = 30cm case, the growth rates become larger. In the case δL $\leq$ 30, the instabilities were occurred with $q_{\mathrm{eff}} \leq 3$, while in the δL = 40cm case, the instabilities were observed with $q_{\mathrm{eff}} \leq 4$. Although the resistive wall can stabilize m/n = 4/1 mode with wall positions δL $\leq$ 30, the wall can no longer stabilize this mode in the δL = 40cm case. These data shows that the plasma rotation tends to stabilize RWM. However, in this experiment, NBs, which were injected to control plasma rotation, increased a plasma pressure. Therefore, not only a current but also pressure must be considered as driving force of instabilities. Further analysis taking into account both driving force is required.

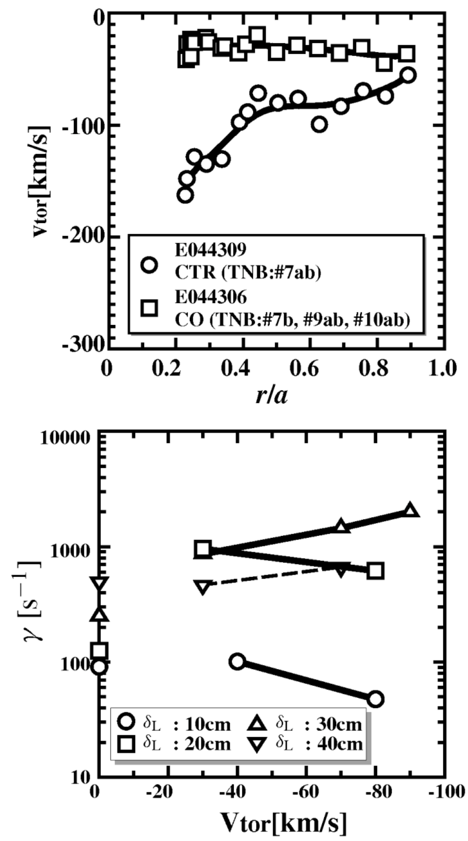

Fig. I.1.3-4 (a) Profiles of toroidal plasma rotation for current-driven RWM experiment. (b) Growth rates versus toroidal plasma rotation at the edge (r/a = 0.9).

(2) Pressure-Driven RWM Experiment

To induce RWM near the wall, a lot of NBs were injected to a negative shear plasma ($l_i \sim 0.7$), which has a lower critical β_N. At β_N reached 2.4, plasma disrupted with an instability (Fig. I.1.3-5). According to ideal MHD stability calculation, $\beta_{no-\ wall\ N}$ is about 2.2. The decomposed magnetic fluctuations show that $n = 1$ was dominant and the growth rate is 10ms which is similar to the wall penetration time. Consequently, we have identified that this mode is the $n = 1$ pressure-driven RWM.

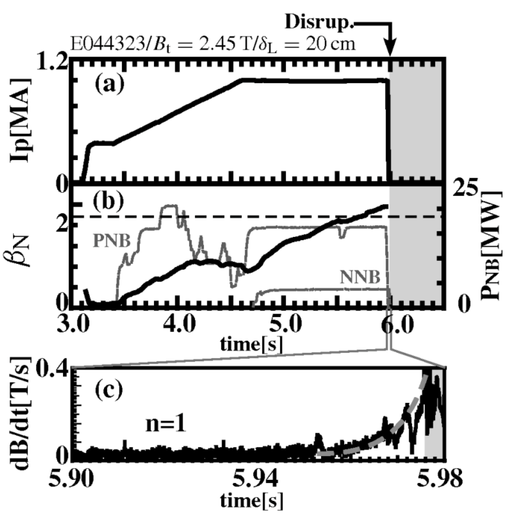

Fig. I.1.3-5 Waveforms of the pressure-driven RWM experiment. (a) Plasma current, (b) β_N and NB heating powers. (c) Normal magnetic fields fluctuation decomposed as n = 1.

1.3.3 Confinement Degradation of Energetic Ions due to Alfvén Eigenmodes

MHD instabilities driven by energetic ions, such as TAE, has been widely studied, because these instabilities can enhance the transport of α-particles from core region of the plasma, and then degrade the performance of burning plasmas. Recently, AEs, whose frequency rapidly sweeps and then saturate as the minimum value of the safety factor, q_{min}, decreases, which are mainly observed in reversed-shear plasmas, have been extensively studied. These frequency behavior can be explained by reversed-shear induced AEs (RSAEs) [1.3-3] or Alfvén Cascades (ACs) [1.3-4] and its transition to TAEs. In the previous studies in JT-60U, it has been reported that the transition phase was most unstable. However, the effect of these AEs on confinement of energetic ions has not been understood yet. In this work, the effect due to these AEs has been investigated. Figure I.1.3-6 shows time trace of (a) q_{min} and (b) frequency spectrum of n = 1 instabilities measured by Mirnov coils in the NNB injected weak reversed shear plasma (E43978, B_T = 1.7T, I_P = 1.0MA, P_{NNB} = 4.0MW, E_{NNB} = 370keV). Frequency of these instabilities swept up rapidly and saturated as q_{min} decreased from 4.6 to 5.5s. After that, these instabilities were almost stabilized. Thick broken lines in Fig. I.1.3-6 (b) denote estimated frequency of n = 1 AEs with RSAE model described in Ref. 1.3-3. As shown in Fig. I.1.3-6 (b), observed frequency behavior can be explained by RSAEs and its transition to TAEs. Solid line in Fig. I.1.3-6 (c) shows time trace of total neutron emission rate (Sn). Increase of Sn was suppressed with RSAEs and TAEs. After these AEs were stabilized at t ~ 5.5s, the increasing rate of Sn was enhanced rapidly. This suggests confinement degradation of energetic ions due to these AEs. Then, in order to evaluate how confinement of energetic ions was degraded, Sn was calculated with OFMC code, taking into account the changes in the bulk plasma. The calculation was performed assuming that the confinement was classical and beam-thermal neutron was dominant. Actually, beam-thermal neutron emission rate accounted for ~ 90% of total neutron emission rate according to the

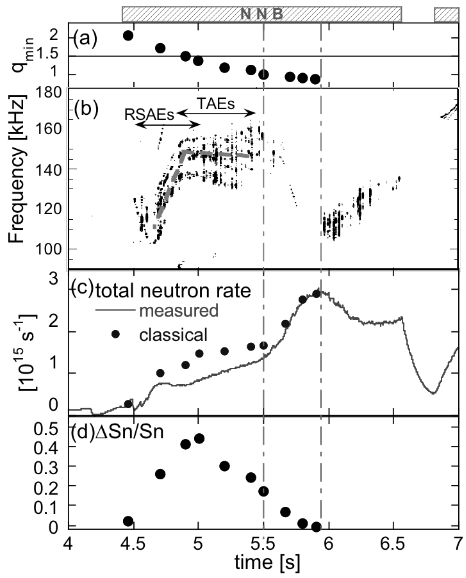

Fig. I.1.3-6 Time trace of (a) q_{min}, (b) frequency spectrum of magnetic fluctuation. Thick broken lines denote estimated frequency from the RSAE model. Frequency behavior can be explained by RSAEs and its transition to TAEs. Time trace of (c) measured total neuron emission rate (solid line) and calculated one by classical theory (classical) (circle) (d) reduction rate of Sn.

calculation with a transport code TOPICS. Shown in circles of Fig. I.1.3-6 (c) is calculated Sn by classical theory. It is found that measured Sn is smaller than calculated one in the presence of these AEs. Whereas, after AEs were stabilized, measured one became close to calculated one, then was consistent with that at t ~ 5.9s. This evaluation indicates confinement degradation of energetic ions due to AEs was confirmed. Fig. I.1.3-6 (d) shows time trace of reduction rate of Sn, which was estimated from the ratio of measured Sn to calculated one. One can see that the rate is largest in the transition phase from RSAEs to TAEs. The previous studies that the transition phase from RSAEs to TAEs was most unstable [1.3-3] support this result. Here, the maximum reduction rate is estimated as $(\Delta Sn/Sn)_{max}$ ~ 45% at t ~5.0s. Confinement degradation of energetic ions in the presence of RSAEs and TAEs is quantitatively evaluated for the first time [1.3-5].

References

1.3-1 Isayama, A., *et al.*, *Plasma Sci. Technol.*, **8**, 36 (2006).
1.3-2 Nagasaki, K., *et al.*, *Nucl. Fusion,* **45**, 160 (2005).
1.3-3 Akechi, M., *et al., Phys. of Plasmas.,* **12,** 82509 (2005).
1.3-4 Berk, H.L., *et al., Phys. Rev. Lett.*, **87**, 185002 (2001).
1.3-5 Ishikawa, M., *et al.*, "Observation of Confinement Degradation of Energetic Ions due to Alfvén Eigenmodes in Weak Shear Plasmas on JT-60U," submitted to *Nucl. Fusion.*.

1.4 H-mode and Pedestal Research

1.4.1 Roles of Plasma Rotation and Toroidal Field Ripple on H-mode Confinement in JT-60U [1.4-1]

The edge pedestal structure characterized by the formation of the H-mode edge transport barrier (ETB) is known to determine the boundary condition of the heat transport in the plasma core. It has prevalently been believed that the **E** x **B** flow shear in the peripheral region plays an important role in suppressing the level of turbulence and in reducing correlation length of the turbulence that helps the formation of the ETB structure. In ITER, the toroidal field ripple is estimated as 0.5-1%. However, the influence of the toroidal field ripple on the pedestal structure and plasma confinement quality is not known. It is presumed that the toroidal field ripple induces the toroidal rotation towards the counter direction. It is likely that in the peripheral region the ripple loss of fast ions produces an inward electric field, which drives the counter-directed toroidal rotation. In this study, conducting the power scans for a variation of the toroidal momentum sources, the characteristics of the H-mode confinement have been investigated. Although it is hard to modify the arrangement of the toroidal field coils from the viewpoint of the technological constraint, the effect of the toroidal field ripple can be examined by changing the plasma configuration.

The experiments were carried out at three cases of geometrical configurations. With increasing the plasma volume V_p from 'small' (V_p~52m^3), 'medium' (V_p~65m^3)

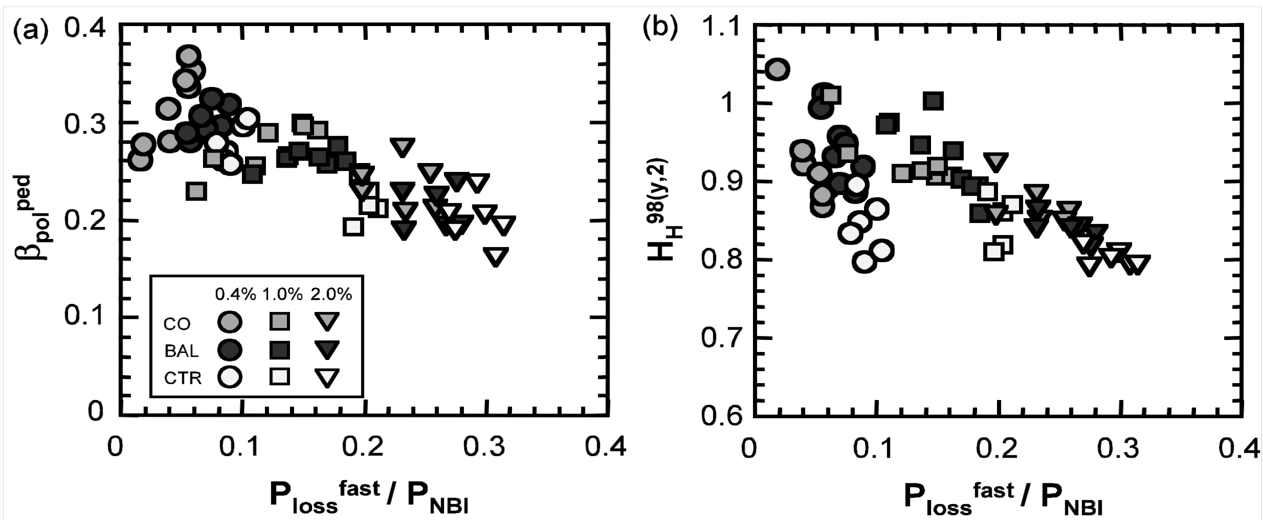

Fig. I.1.4-1 (a) Dependence of the β_{pol}^{ped} on P_L^{fast} / P_{in}. (b) Dependence of the H_H-factor based on the IPB98(y,2) scaling on P_L^{fast} / P_{in}.

and 'large' size (V_p~75m^3) in turn, the toroidal field ripple increases from 0.4, 1.0 and 2.0%, respectively. Figure I.1.4-1(a) shows the dependence of the β_{pol}^{ped} on the ratio of the loss power of the fast ions to the NB injection power or P_L^{fast}/P_{in}. It is found that the β_{pol}^{ped} tends to increase when the fast ions' loss power fraction decreases. The observed increase of β_{pol}^{ped} at fixed toroidal field ripple and momentum source comes from the increased absorbed power. When β_{pol} in the plasma core is raised by high power heating, it has been known that the MHD stability boundary at the plasma edge is improved. Figure I.1.4-1(b) shows the dependence of the H_H-factor on P_L^{fast}/P_{in}. It is shown that operating at smaller loss power fraction of fast ions does not always produce high energy confinement while the achievable confinement performance tends to decrease with increasing P_L^{fast}/P_{in}. The H-mode plasmas with the toroidal momentum source heading for the co-direction are sensitive to the ripple loss of fast ions.

The H-mode plasmas with small ripple loss at the momentum source for co-direction clearly show the highest performance. However, the energy confinement with the toroidal momentum source heading for the ctr-direction does not vary when the ripple loss of fast ions is changed.

One can find that the toroidal plasma rotation for co-direction displays its potential on the improvement of the energy confinement through the enhanced pedestal pressure. The temperature profiles in the H-mode plasmas are in many cases characterized by the minimum critical scale length of the temperature gradient L_T. Thus, it will be investigated whether the high confinement with the momentum source in the co-direction is due to the change of the critical L_T or the increase of the pedestal temperature.

1.4.2 Characterization of Type-I ELMs in Tangential Co-, Balanced-, and Counter- Plus Perpendicular NBI Heated Plasmas on JT-60U [1.4-2]

Effects of plasma rotation on the Type-I ELM characteristics have been systematically studied in the JT-60U tokamak, scanning combinations of NBI (tangential co-, balanced-, and counter-NBI plus perpendicular NBI) in the three different plasma volume to change the toroidal field ripple at the plasma edge, corresponding ripple amplitude for small, medium and large volume plasma were δ_r~0.4, 1.0 and 2.0%, respectively. We performed the following experiment under the condition of the plasma current, I_P=1-1.2MA and toroidal magnetic field, B_T=2.6T at the n_e/n_{GW}~0.4-0.5 with q_{95}~4.1.

Figure I.1.4-2 shows the ELM characteristics in the small volume plasma case. As can be seen in Fig.I.1.4-2(a), ELM frequency, f_{ELM}, increased with the heating power crossing the separatrix, P_{SEP}, as $df_{ELM}/dP_{SEP} \geq 0$. This power dependence in the f_{ELM} was

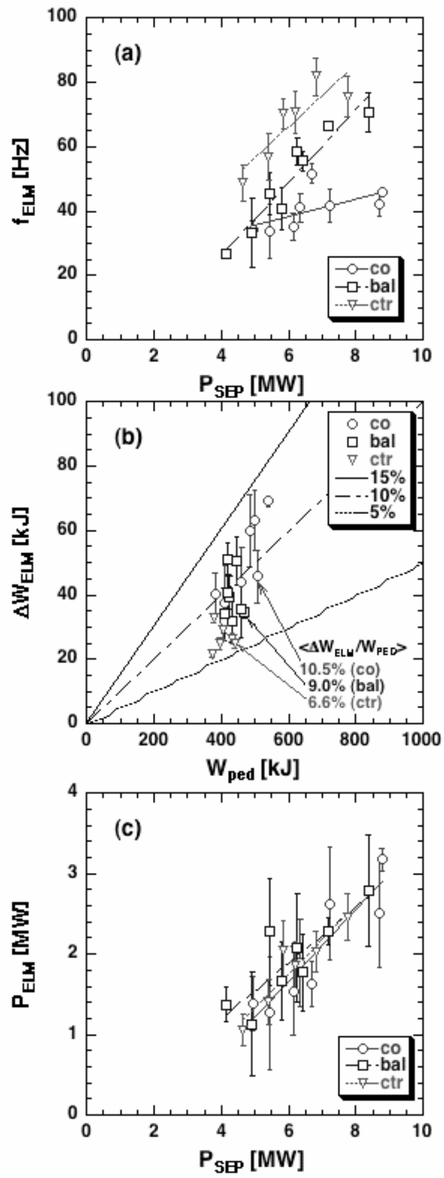

Fig. I.1.4-2 Plots of (a) ELM frequency versus heating power crossing the separatrix, (b) ELM energy loss versus pedestal stored energy, and (c) power loss due to ELM, P_{ELM} (= $\Delta W_{ELM} \times f_{ELM}$), normalized by P_{SEP}. These data are taken in the small volume configuration. Circles, squares and inverse-triangles indicate the tangential co-, balanced-, and counter-, plus perpendicular-NBI heated plasmas, respectively.

confirmed in all plasma configurations and so that observed ELM in these scan could be classified into type-I ELM.

The ELM energy loss normalized by pedestal stored energy, $\Delta W_{ELM}/W_{ped}$, appears to be smaller when the external momentum input is in the counter direction, especially in small volume configuration case as shown in Fig.I.1.4-2(b). Although each data point has somewhat large statistic error, the averaged value, $<\Delta W_{ELM}/W_{ped}>$, in the co-NBI discharge is significantly higher than that in the counter-NBI. In this analysis, it is noted that each ΔW_{ELM} is the averaged value during ELM cycles over an interval of $\Delta T\sim$ 100ms, and the corresponding error bar is its statistical error of this averaging process.

The most interesting point is the dependences of the power loss due to ELM, P_{ELM} (= $\Delta W_{ELM} \times f_{ELM}$), normalized by P_{SEP}, which is constant among co-, balanced, and counter-NBI, suggesting that the power loss due to inter-ELM transport, $P_{inter\text{-}ELM}$, is almost unchanged among co-, balanced, and ctr-NBI plasmas (i.e. $P_{inter\text{-}ELM}/P_{SEP}\sim 1-P_{ELM}/P_{SEP}$). As a result, we have demonstrated that ELM energy loss can be controlled by means of counter-NBI in a clear Type-I ELM regime, while keeping confinement quality fixed. On the other hand, when the plasma configuration changed from small to middle and large, the P_{ELM}/P_{SEP} decreases with increasing the plasma volume, suggesting an increase in the inter-ELM transport.

1.4.3 Pedestal Conditions for Small ELM Regimes in Tokamaks [1.4-3]

Several small/no ELM regimes such as EDA, grassy ELM, HRS, QH-mode, type II and V ELMs with good confinement properties have been obtained in Alcator C-Mod, ASDEX-Upgrade (AUG), DIII-D, JET, JFT-2M, JT-60U and NSTX. All these regimes show considerable reduction of instantaneous ELM heat load onto divertor target plates in contrast to conventional type I ELM, and ELM energy losses are evaluated as less than 5% of the pedestal stored energy. In order to compare the pedestal conditions in these many regimes, they have been categorized into four main groups (grassy ELM regime, type II ELM regime, QH-mode regime and enhanced recycling with high ν_e^* regime) in terms of ELM energy loss and pedestal electron collisionality ν_e^*, which plays a significant role in pedestal stability through modification of the edge bootstrap current. Moreover, ITER will have a low collisionality pedestal.

Achieved pedestal pressure in the type II ELM regime is comparable to the usual type I ELM regime in spite of the existence of edge fluctuations. Moreover, higher pedestal pressure can be obtained in JET. Because of a requirement of high density, the edge collisionality remained at moderate values ($\nu_e^* > 0.8$). It should be noted that a narrow operational window in density ($0.85 < \bar{n}_e^{ped}/n_{GW} < 0.95$) is observed in AUG.

On the other hand, the grassy ELM regime was found in JT-60U as another small ELM regime at lower ν_e^* in high β_p plasmas with simultaneously high q_{95} and high δ. In recent experiments on JET and AUG, grassy-like ELMs were also observed following the grassy ELM prescription with high β_p plasmas ($\beta_p > 1.7$) at high q_{95} ($q_{95}\sim 7$) and high triangularity ($\delta > 0.4$).

Figure I.1.4-3 shows the comparison of the non-dimensional operational regime in β_p-δ space between high n_e type II ELM and grassy ELM regimes.

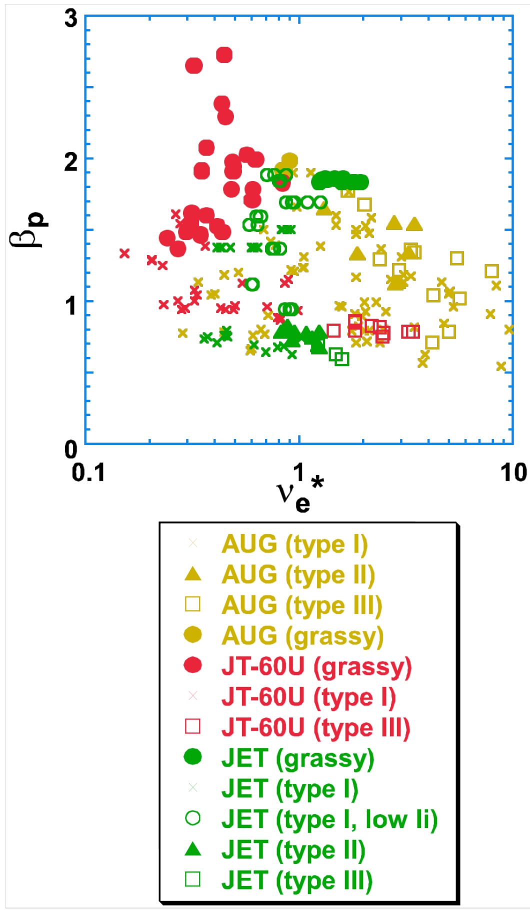

Fig. I.1.4-3 Operational space in ν_e^* versus β_p for small/no ELM regimes and type I/III ELM regime.

It suggests that there is not a large requirement of poloidal beta β_p for type II ELM in contrast to the grassy ELM regime. On the other hand, a quasi-double null (QDN) configuration is required in AUG, where the typical operational value is $\delta > 0.4$.

As can be seen in Fig. I.1.4-3, grassy ELMs can be obtained at low collisionality of ~ 0.3 in JT-60U. Nevertheless, achieved ν_e^* in grassy ELM plasmas was comparable to type II ELM plasmas in JET. It is noted that no significant edge fluctuations related to enhanced losses were observed in any devices with grassy ELMs.

The required condition to enter the small/no ELM regimes in terms of the plasma shape is also important to investigate further, because ITER cannot operate using a double null configuration and Δ_{sep} (the distance between the separatrix and the flux surface through the upper X-point at the outer midplane) should be kept larger than 4cm. So far, a QDN configuration is required both for type II ELMs and for grassy ELMs in AUG. In JET, type II ELM does not require QDN configuration, while grassy ELM has been observed in QDN configuration so far. Grassy ELMs in JT-60U have often been observed for lower single null (LSN) operation without a second separatrix and type V ELM in NSTX also requires LSN configuration. On the other hand, higher δ is an important condition for small ELM regimes. Since it is difficult to separate between effects of δ and Δ_{sep} in some devices due to the hardware limitations, we should consider these issues in further experiments.

References

1.4-1 Urano, H., *et al.*, *Plasma Phys. Control. Fusion,* **48**, A193 (2006).

1.4-2 Kamiya, K., *et al.*, *Plasma Phys. Control. Fusion,* **48**, A131 (2006).

1.4-3 Oyama, N., *et al.*, *Plasma Phys. Control. Fusion,* **48**, A171 (2006).

1.5 Divertor/SOL Plasmas and Plasma-Wall Interaction

1.5.1 Fluctuations in High- and Low-Field-Side SOL

Study of the ELM radial propagation to the first wall was presented in the 32nd EPS [1.5-1] with improving sampling rate of 500kHz for the Mach probes (at outer midplane and X-point) and magnetic pick-up coils. In 2005, measurement of the plasma fluctuations both at HFS and LFS SOLs has been, for the first time, performed in JT-60U since electrodes of the HFS reciprocating Mach probe was repaired. Statistical analysis such as a probability distribution function (p.d.f.) described intermittent (non-diffusion) transport in SOL plasma fluctuations as shown in Fig.I.1.5-1 [1.5-2]. Fluctuation level of the ion saturation current ($\delta j_s/\langle j_s \rangle$) at HFS was 1/3-1/10 smaller than that at LFS. It was found that the positive bursty events appeared most frequently at LFS midplane distance from separatrix (Δr) ~ 5cm, and flat far SOL was formed in outer flux surfaces (Δr > 5cm). Positive bursty events were seen in wide SOL radii (Δr < 7cm) only at LFS midplane, where the "flow reversal" of the SOL plasma was observed. Influences of the radial transport of the convective blobby plasma on the SOL formation and the flow reversal were investigated.

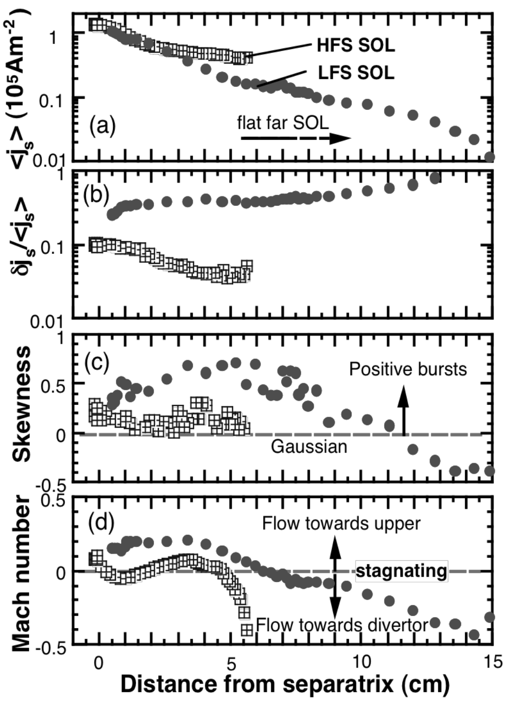

Fig. I.1.5-1 (a) j_s profiles measured with LFS midplane (circles) and HFS (squares) Mach probes in L-mode. (b) fluctuation level of j_s, (c) Skewness, (d) Mach number. HFS baffle is located at the flux surface of 6cm LFS midplane distance.

1.5.2 Modeling of Divertor Pumping Using SOLDOR/ NEUT2D Code

To characterize the divertor pumping for particle and heat control in the SOL/divertor, simulations using the SOLDOR/ NEUT2D code developed originally [1.5-3] were performed to the JT-60U long pulse discharge [1.5-4]. The simulation reproduces the neutral pressure and pumping flux in the exhaust chamber at the experiment by treating the desorbed flux from the wall similar as the gas puff flux (Fig. I.1.5-2). Heat loads on the divertor targets satisfy the heat balance consistently. Parametric survey shows the pumping efficiency (ratio of pumping flux to generated flux around the divertor targets) [1.5-5] increasing with the pumping speed. It is found that the pumping speed higher than the present capability (26m^3/s) is necessary for the active particle control under the wall saturation condition. On the other hand, shortening the strike-point distance (distance from extension point of the private dome wing on the divertor target to the strike point) from 10cm to 2cm, the pumping efficiency is enlarged by a factor of 1.5 with increase of the viewing angle from strike point to pumping slot and the incident flux into exhaust chamber.

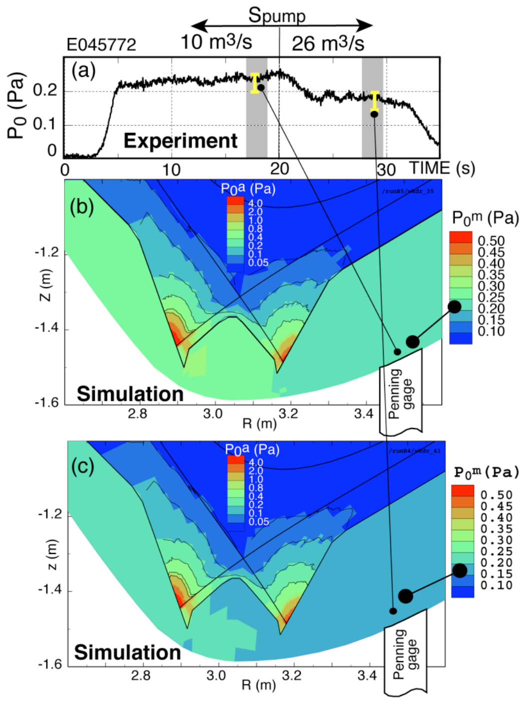

Fig. I.1.5-2 (a); Time evolutions of neutral pressure in front of penning gage, when the pumping speed S_{pump} is increased from 10m^3/s to 26m^3/s at t = 20s in JT-60U long pulse discharge under the wall saturation condition. (b) and (c); Simulated contour plots of neutral pressure (molecular pressure in the exhaust chamber and atom pressure in the divertor region) for (b) S_{pump}=10m^3/s and (c) S_{pump}=26m^3/s.

A virtual tilt of the divertor targets to 15º vertically enhances the pumping efficiency by a factor of 1.2 with a low target heat load.

1.5.3 Two-Dimensional Structure of Volume Recombination of Hydrogen and Impurity Ions

In order to investigate two-dimensional structure of divertor plasmas, a spectrometer with 92 viewing chords (vertically 60ch and horizontally 32ch) has been prepared, and a computer tomography technique using a maximum entropy method has been developed. Figure I.1.5-3 shows reconstructed emission profiles of D I (n=2–5) and C IV (n=6-7) during an X-point MARFE. The emission peaks of D I (n=2-5) are found above the outer and the inner strike point. In contrast, the emission peak of C IV (n=6-7) is found in the main plasma just above the X-point. Because these two lines are emitted predominantly, resulting from volume recombination of D^+ and C^{4+}, respectively, these emission profiles are interpreted as the two-dimensional structures of volume recombination.

Because the ratio of D I (n=2-6) to D I (n=2-5) gives electron temperature of recombining plasma, the two-dimensional structure of electron temperature can

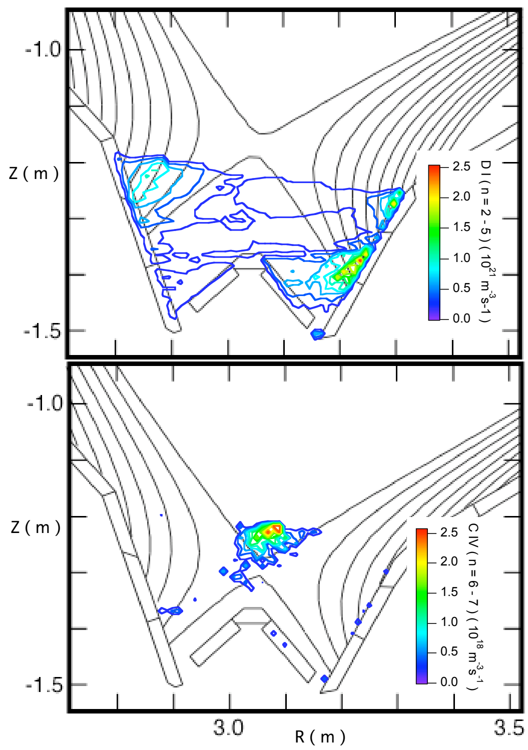

Fig. I.1.5-3 Emissivity of (a) D I (n = 2-5) and (b) C IV (n = 6–7) during an X-point MARFE, reconstructed by a computer tomography technique (tentative version for demonstration).

be obtained from the ratio of the reconstructed emission profiles of these lines. This method is in progress.

1.5.4 Emission Rates of CH/CD and C_2 Spectral Bands for Loss-Events of CD_4 and C_2H_6

To evaluate hydrocarbon sputtering flux from emission intensities of CH/CD and C_2 spectral bands, the numbers of CH/CD and C_2 photons until one hydrocarbon molecule is ionized in plasma, are required. The reciprocals of these numbers, hereafter called loss-events / photon, have been measured.

To measure the CD_4-loss-evnets / CD photon, CD_4 was injected at a known rate into the outer divertor plasma. The CD emission was measured along two similar viewing chords: one views the plasma in front of the gas-puff nozzle and the other does not. The difference of the CD emission measured with the two viewing chords is originated from the injected CD_4. Hence, the CD_4-loss-events/CD photon was determined as the ratio of injected CD_4 flux to the difference of the CD emission. Similar measurements for C_2H_6 to determine the C_2H_6-loss-events/CH photon and the C_2H_6-loss-events/C_2 photon were done [1.5.6].

Figure I.1.5-4 shows the measured loss-events/photon. The loss-events/photon is positive dependence on the electron temperature, which is similar to those measured in PISCES [1.5.7]. It was found that that dependence of C_2H_6-loss-events/C_2 photon is stronger than that of C_2H_6-loss-events/CH photon. In addition, at 20eV, the absolute values agree within a factor of 2. The data obtained in the present work will be used to measure the CH_4/CD_4 and C_2H_x/C_2D_x sputtering yields.

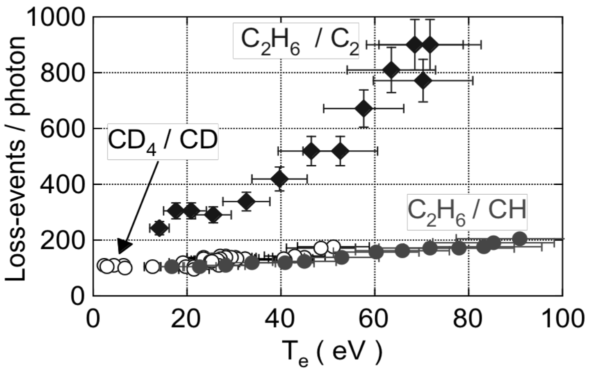

Fig. I.1.5-4 Loss-events as a function of electron temperature. Open circles indicate the ratio of CD_4-loss-events to a CD-spectral-band photon, closed circles and diamonds the ratios of C_2H_6-loss-events to a CD- and to a C_2-spectral-band photon, respectively.

1.5.5 Carbon Deposition and Hydrogen Isotope Retention in the JT-60U Plasma Facing Wall

Erosion/deposition analyses for the plasma facing wall showed that deposition was dominant at the inner divertor (A) and the outer dome wing (C), whereas erosion dominant at the outer divertor (D) and the inner dome wing (B) (Fig. I.1.5-5). The upper area of the first wall was mainly eroded, while the bottom area of the inboard wall was deposition dominated [1.5-8]. In deposition analyses for the plasma shadowed area, thick deposition (~several 10μm) was observed on the bottom side of the outer dome wing tile, and no deposition was found on the bottom edge of the inner divertor tile. These results indicated that local transport of eroded carbon to inboard direction plays an important role on the carbon redeposition process.

Distribution of deuterium and hydrogen retained in graphite tiles placed in the divertor region of JT-60U with the both side pumping geometry was investigated by thermal desorption spectroscopy. The retention of hydrogen isotopes is nearly proportional to the thickness of carbon redeposited layers, though their concentration changes with the location of the tiles. The least concentration of ~ 0.02 in (H+D)/C is found in the redeposited layers on the inner divertor tile. This value agrees well with H/C of ~0.030 observed for the redeposited layers on the divertor tiles exposed to HH discharges in the JT-60 open divertor, and H+D/C of ~0.032 in the inner divertor tiles exposed to the DD discharges in the JT-60U with the inner side pumping system. Rather high hydrogen concentration is found in the redeposited layers on plasma-shadowed area.

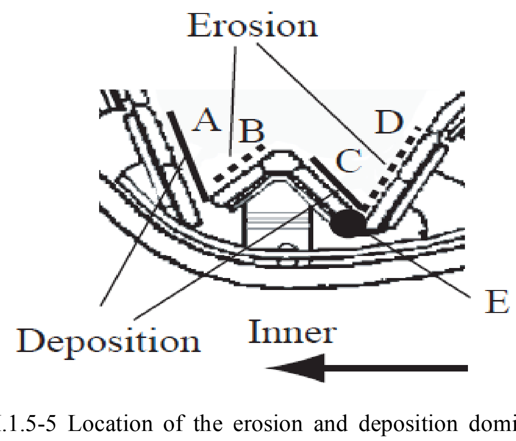

Fig. I.1.5-5 Location of the erosion and deposition dominated area in the JT-60U W-shaped divertor. The results showed the eroded carbon was transported to the inboard direction. The highest hydrogen isotope retention was found at the bottom side of the outer dome wing tile (E).

In particular, the redeposited layers on the bottom side of the outer wing tile (see Fig. I.1.5-5,E) shadowed from plasma and facing to the pumping slot shows the highest concentration of 0.13 in (H+D)/C [1.5-9]. In JT-60U, however, the deposition at the shadowed area is very small, which is a candidate to explane the smallest total retention in the divertor area compared with other large tokamaks.

1.5.6 ^{13}C Tracing and Deposition

To clarify the transport and deposition places of carbon impurities, the $^{13}CH_4$ gas puffing experiment was carried out in JT-60U [1.5-10]. Figure I.1.5-6 shows the location of the gas puffing port and a plasma configuration for the experiment. The total of ~2 x 10^{23} $^{13}CH_4$ molecules was puffed into 13 L-mode plasma discharges. Deposition layers of thicker than 200μm were observed on the outer divertor tile adjacent to the gas puffing port. The poloidal distribution of the ^{13}C deposition adjacent to the $^{13}CH_4$ gas puffing port agrees well with that of the positioning frequency on the outer divertor tiles. Therefore it is considered that a large amount of carbon impurity generated at the outer divertor re-deposited near eroded place and was transported by repetition of erosion and redeposition.

Although the first wall located in the inner side was thought to be exposed to SOL plasma during the discharges, deposited ^{13}C on the first wall was the lowest among the analyzed tiles. This suggests that carbon impurities transport from the inner to the outer divertor region through SOL takes a long term. The ^{13}C surface density peaked at the lower side of the inner striking point on the inner divertor tile as shown in Fig. I.1.5-7. It is suggested that a large part of ^{13}C puffed from the outer divertor is transported through the drift flux toward the inner divertor. This result indicates the existence of another transport path of carbon impurities generated in the outer divertor region in addition to the SOL flow.

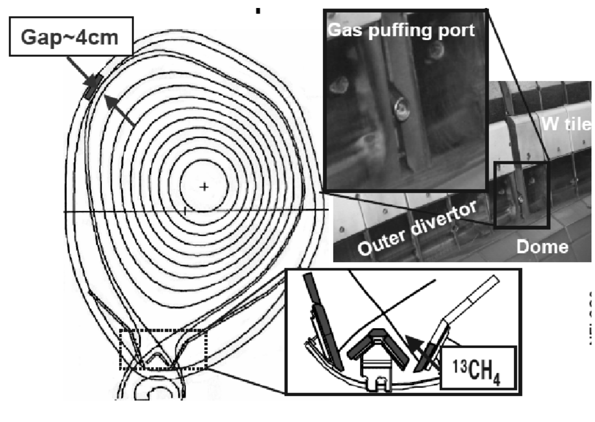

Fig. I.1.5-6 Location of the gas puffing port and a plasma configuration for the experiment. Thirteen L-mode discharges were performed at almost same plasma configuration. Totally, 2.0 x 10^{23} ^{13}C were puffed during the discharges.

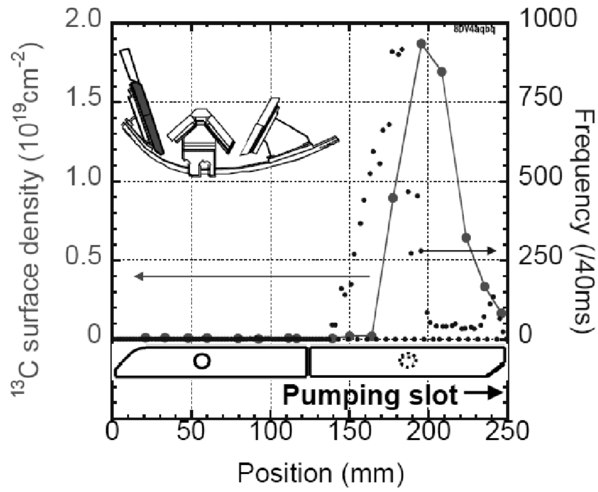

Fig. I.1.5-7 ^{13}C surface density of the inner divertor tile and frequency distribution of inner divertor leg. The peak position of the ^{13}C surface density was found at the lower side (i.e. near pumping slot) of the strike point.

References

1.5-1 Asakura, N., *et al.*, Proc. *32nd EPS Plasma Phys. Conf.,* P5.006 (2005).

1.5-2 Miyoshi, H., *et al., Proc. 32nd EPS Plasma Phys. Conf.,* P1.045 (2005).

1.5-3 Kawashima, H., *et al.*, *Plasma and Fusion Res.*, **1**, 031 (2006).

1.5-4 Kawashima, H., *et al., Proc. 17th PSI conf., Hefei* P1-78 (2006).

1.5-5 Kawashima, H., *et al., Fusion Eng. Design,* **81**, 1613 (2006).

1.5-6 Nakano, T., *et al.*, Proc. *32nd EPS Plasma Physics Conf.,* P-5.007 (2005).

1.5-7 Pospieszczyk, Y.R., *et al.*, *UCLA-PPG-1251* (1989).

1.5-8 Oya, Y., *et al.,* "Hydrogen Isotope Behavior in the First Wall of JT-60U after DD Discharge," Proc. *12th ICFRM* (2005) to be published in *J. Nucl. Mater.*.

1.5-9 Hirohata, Y., *et al.,* "Distribution of Hydrogen Isotopes Retained in the Divertor Tiles Used in JT-60U," *Proc. 12th ICFRM* (2005) to be published in *J. Nucl. Mater.*.

1.5-10 Ishimoto, Y., *et al.,* "Transport of Carbon Impurity Using 13CH4 Gas Puffing in JT-60U," *Proc. 12th ICFRM* (2005) to be published in *J. Nucl. Mater.*.

2. Operation and Machine Improvements

Two cycles of the JT-60 operation were implemented in FY 2005, which included 945 shots of plasma pulse discharge, 104 shots of commissioning pulse sequence, 30 hours of Taylor-type discharge cleaning and 323 hours of glow discharge cleaning.

In order to reduce a large ripple of toroidal field, which had been considered to limit operational performance of large-volume plasmas in JT-60U, ferritic steel tiles were newly installed as a part of the first wall in place of carbon tiles during the maintenance period in 2005. To compensate the magnetic influence of the ferritic tile insertion on plasma equilibrium, a new real-time program was developed to correct the magnetic sensor signals including poloidal magnetic field and flux from the ferritic steel magnetized by the toroidal magnetic field. The plasma magnetic surface calculated in consideration of the ferritic tiles agrees to the separatrix line reproduced by CXRS measurement results near the upper port within a few centimeters in the largest magnetization case at Bt=2T. After careful confirmation of position and shape reconstruction accuracy, JT-60 experiments were successfully performed on schedule.

2.1 Tokamak Machine

2.1.1 Improvement of Pellet Injector for Long Pulse Operation

In order to extend the JT-60 operation to high density regime and to investigate the impact of particle fuelling on confinement and pedestal parameters, the pellet injector has been under modification to have long injection duration (~60 s) and high repetitive injection frequency (≤20 Hz). The pellet extruder was changed from the piston type to the screw type (Fig. I.2.1-1). This screw type pellet extruder can produce a 2.1 mm x 2.1 mm ice rod with an extrusion speed of 46 mm/s for 60 s or with a extrusion speed of 38 mm/s for 360 s. The new screw type pellet extruder was assembled into the present centrifugal pellet injector used for JT-60U. The production of a transparent ice rod has been confirmed in some operation conditions. The liquefier and nozzle temperatures are being optimized.

2.1.2 Installation of Supersonic Molecular Beam Injector

Supersonic molecular beam injectors (SMBI) were installed both at the high-field-side and low-field-side of the JT-60U Vacuum Vessel in collaboration with CEA Cadarache. The injector head is the same as that installed in Tore Supra (Fig. I.2.1-2). The SMBI can be operated with a frequency of 8-10 Hz and 2 ms duration per pulse. Theoretical gas flow was evaluated to be 510 Pam^3/s with a Mach number of 4.1 (speed of 2.2 km/s) at operation temperature of 150^{o}C and fueling pressure of 0.5 MPa. The particle fueling to a plasma with the SMBI is expected to be deeper than gas puffing, but shallower than pellet injection. The gas injection test into the JT-60U vacuum vessel was carried out using helium gas at operation temperature of 150^{o}C and fueling pressure of 0.2 MPa. The amount of injected gas from the low-field-side injector was estimated to be 0.14 Pam^3 per pulse.

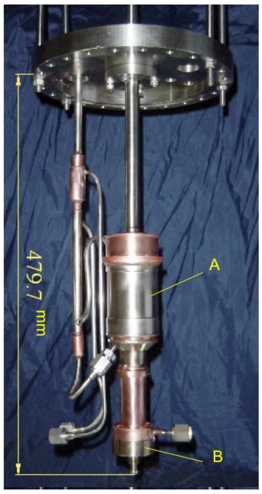

Fig. I.2.1-1 The screw type pellet extruder installed into the centrifugal pellet injector of JT-60 (A: Liquefier, B: Nozzle).

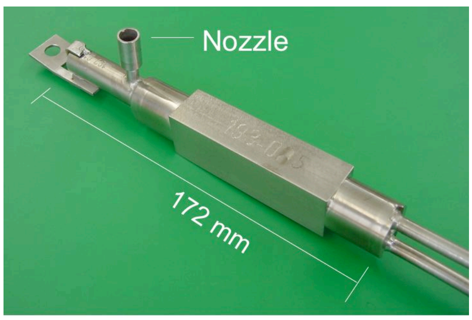

Fig. I.2.1-2 An injector head of the Supersonic molecular beam injector (SMBI) installed both on the inboard and outboard side in the vacuum vessel.

2.1.3 Installation of Ferritic Steel Tiles as the Outboard First Wall [2.1-1]

In order to reduce the toroidal magnetic field (TF) ripple, 8Cr-2W-0.2V ferritic steel tiles were installed at the out board wall inside the vacuum vessel (Fig. I.2.1-3). 8Cr-2W-0.2V ferritic steel was selected among candidate ones such as F82H developed as a low activation ferritic steel, because the saturated magnetization of 8Cr-2W-0.2V ferritic steel was high enough for the experiments planned with the toroidal magnetic field, and the low activation was not critical at the present level of neutron production in JT-60. By August 2005, 1122 carbon tiles near the inside of the TF coils were replaced to ferritic steel tiles with reinforcement of stud nuts. The dimensions of the most tiles are 130 mm(length) x 185 mm(width) x 23 mm(thickness), which is 2 mm thinner than the carbon tiles. The surfaces position of the ferritic tiles were arranged at more than 1.5mm below those of the carbon tiles. Slits were made in each tile to reduce the electromagnetic force due to eddy current.

Fifty-five plates of 8Cr-2W-0.2V ferritic steel were manufactured from the 2.6 ton ingots made by 20 ton vacuum induction melting in January 2006. Magnetic properties of the ferritic steel plates fabricated in large scale melting were investigated. It was shown that the average saturated magnetization was 1.838 Tesla, and the confidence interval of 95% was between 1.833 and 1.843 Tesla at ambient temperature. The variation among the plates fabricated was confirmed to be sufficiently small. The saturated magnetization was 1.66 Tesla at 573 K, the maximum baking temperature of the relaxation of the activation-element. Although it was lower than the expected value, it was confirmed by a numerical calculation that the saturated magnetization of 1.7 Tesla was still sufficient for the JT-60 experiment.

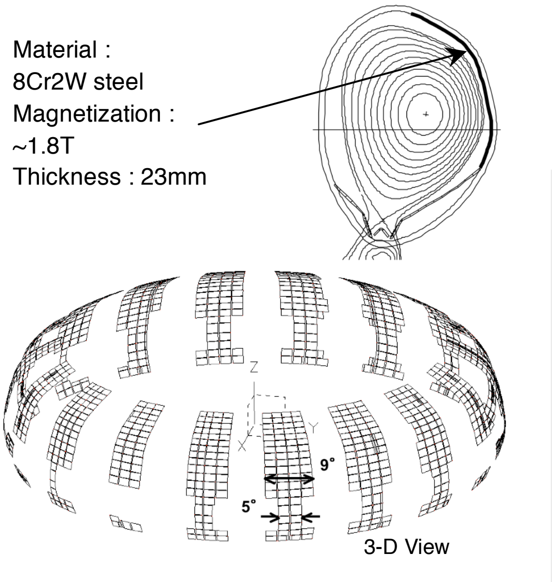

Fig. I.2.1-3 Ferritic steel tiles installed at the out board wall inside the JT-60U vacuum vessel.

2.1.4 Study of the Plasma-Surface Interaction

The cooperative research program between JAEA and universities using the JT-60 first wall tile was initiated in 2001. Under the program, various studies on the plasma facing materials have progressed. Major research activities conducted in FY 2005 except for the results mentioned in Section I.1.5 [1.5-8, 1.5-9, 1.5-10] are as follows:

(1) Measurement of Tritium Distribution at the Tile Gap [2.1-2]

Tritium retention on the side surfaces which locate at gaps between the W-shaped divertor tiles was analyzed by the imaging plate technique and a combustion method. The samples measured were exposed in the plasma discharges from June 1997 to March 2003. Total amount of tritium generated was ~ 5.7 x 10^{19} (~102 GBq) during this period.

Tritium retention was essentially correlated with the carbon deposition profile at the gap. On the both toroidal sides (i.e. toroidal gaps), the tritium concentration exponentially decreased with the distance from the front end to the bottom end with the e-folding length of around 3 mm.

Tritium retention profiles on the poloidal sides (i.e. poloidal gaps) varied with their location. Relatively high tritium retention was found at (i) the gaps between the inner target tiles and (ii) the bottom side of the outer divertor tile facing to the outer pumping slot. According to SEM observation, those side surfaces were covered by the redeposited layers with the maximum thickness of ~80 μm (i) and ~90 μm (ii), indicating that tritium was incorporated in the redeposited layers.

The amount of the tritium retention in the divertor tile gaps determined by the combustion method was approximately 67 MBq (assuming full toroidal symmetry in the tritium retention profiles), which corresponds to ~ 0.07 % of the total generated tritium.

(2) Exhaust Gas Analysis during Experimental Operation [2.1-3, 2.1-4]

The exhaust gas from JT-60U during the experimental operation has been investigated to understand behavior of hydrogen as fuel and to obtain basic data of impurity. Exhaust gas was measured with Mass Spectrometer, Micro Gas Chromatography and Ion Chamber. Because we didn't individually measure hydrogen isotopes (H, D, T) in the experiment, all three hydrogen isotopes are described as H. On the other hand, some impurity species could be individually measured during plasma discharges. The ratio of CH_4, CO_2, C_2H_2+C_2H_4 and C_2H_6 were 44%, 42%, 12% and 2%, respectively. These ratios of impurity species were independent on the wall temperature, even though the amounts of exhausted H and impurities increased with the wall temperature due to high recycling. Concentration of carbon compounds varied in each shot and the maximum amount of exhausted carbon was several mg in a shot. There was a tendency between the exhaust gas and the plasma parameter, indicating that the amounts of exhausted H and impurities increased with the maximum electron density of the plasma.

References

2.1-1 Kudo, Y., *et al.*, "Fabrication of 8Cr-2W Ferritic Steel Tile for Reduction in Toroidal Magnetic Field Ripple on JT-60U," *Proc. 5th Asia Plasma & Fusion Association (2005)*, to be published in *J. Korean Physical Society*.

2.1-2 Sugiyama, K., "Tritium Distribution Measurement of the Tile Gap of JT-60U," *Proc. 12th ICFRM* (2005), to be published in *J. Nucl. Mater.*.

2.1-3 Isobe, K., *et al.*, *Fusion Eng. Des.*, **81**, 827 (2006).

2.1-4 Kobayashi, Y., *et al.*, *Proc. 21th SOFE,* (CD-ROM) (2005).

2.2 Control System

2.2.1 Innovative Integrator Resistant to Plasma Instabilities

In the development of a precise integrator for magnetic measurements aiming at long pulse operation, saturation of an amplifier caused by exposure of excessive voltage input from the sensor is the only remaining issue [2.2-1, 2.2-2].

Figure I.2.2-1 (a) shows a good, accurate integration result for the output of a magnetic probe in a discharge with a disruption; no baseline change was observed before and after plasma discharge. Unexpectedly, soon after a few disruption shots, clear baseline gap was again observed, as shown in Fig. I.2.2-1 (b). This was caused by the damage of the FET-Zener diode elements in the signal input circuit.

To find out a proper method to provide the required durability under the repeated disruptive instabilities, we made and tested three trial signal input circuits; board #I with high voltage (±2kV) resistant diode, board #II with power Mos FET (+1kV/-0.6kV) and board #III with a precise attenuator insertion with an FB compensator. The linearity errors of the board #I and #II exceeded the specification of the employed operational amplifier (±0.001%) for three ranges 10V, 100V, and 1000V. The cause was considered to be a large leakage current of the signal input protection elements. The linearity error of the board #III was smaller than 0.001%. Therefore, the board #III has been applied to the input circuit. Furthermore, to correctly integrate fast varying input signals during disruptions, the time resolution has been improved by increasing the integration cycle from 1.0kHz to 10kHz. Figure I.2.2-2 shows an example of good result. The integration error caused by over-range input had been successfully corrected. This development has been carried out as ITA (ITER Transitional Arrangements) task for ITER.

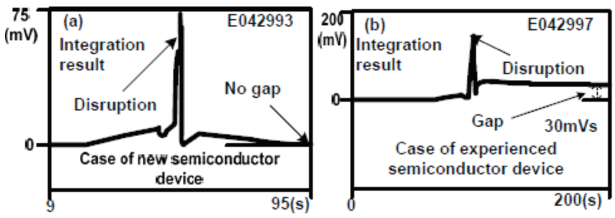

Fig. I.2.2-1 A gap of integral results occurred after several exposures to high voltage at a disruption.

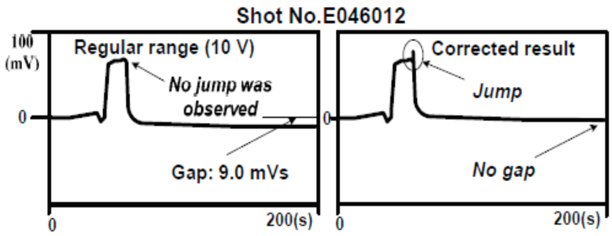

Fig. I.2.2-2 Corrected integration result.

2.2.2 Plasma Movie Database System

A plasma movie is generally expected as one of the most efficient methods to know how plasma discharge has been conducted in the experiment. On this motivation, a real-time plasma shape visualization system has been developed and operated over ten years. The current plasma movie is composed of (1) video camera picture of cross-sectional view of a plasma, (2) computer graphic (CG) picture, and (3) magnetic probe signal as a sound channel.

In order to use this movie efficiently, a new system having the following functions has been developed; (a) to store a plasma movie in the movie database system automatically after a discharge sequence, and (b) to make a plasma movie be available (downloadable) for experiment data analyses at the Web-site, as shown in Fig.I.2.2-3.

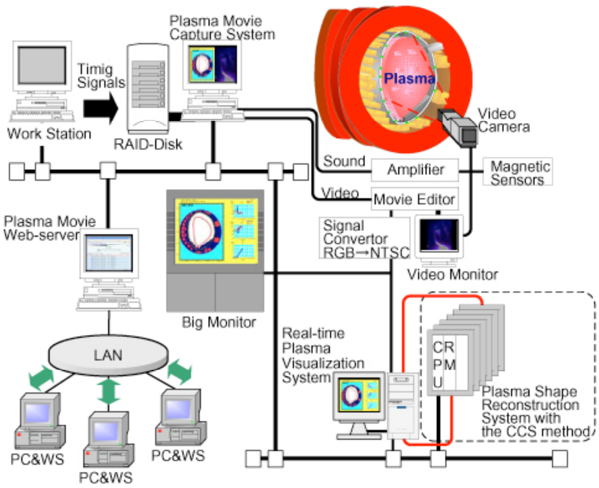

Fig.I.2.2-3 Configuration of the Plasma Movie Database System.

The plasma movie capture system stores the movie file in a format of MPEG2 first. Secondly, it transfers a movie file in a MPEG4 format to the plasma movie web-server. In response to the user's request, the plasma movie web-server transfers a stored movie data. The movie data amount for the MPEG2 format is about 50Mbyte/shot (65s discharge), and that for the MPEG4 format is about 7 Mbyte/shot. It has been confirmed that the transfer of plasma movie takes a few seconds through a local area network. After one plasma discharge sequence is finished, the plasma movie file for the 15s to 65s pulse discharge comes to be available for the web-users in about 6 to 16 minutes.

References

2.2-1 Kurihara, K., *et al., Proc. 17th Symp. on Fusion Eng.*, 799 (1997).

2.2-2 Kawamata, Y., *et al., Proc. 19th Symp. on Fusion Eng.*, 172 (2002).

2.3 Power Supply System

Annual inspections and regular maintenances for the power supply systems have been conducted to maintain availability of high power operations as shown in Table I.2.3-1. These activities contributed to achieve safe operation of the power supplies.

Table I.2.3-1 Inspections and overhaul of the power supply systems.

Item	Term
Overhaul of the Oil-cooled Transformer	April
Detail Inspection of the Motor Generator and the Poloidal Field Coil Power Supply	August~ October
Regular Inspection of the Grounding and Lightning systems	September
Regular Inspection of the Toroidal Field Coil Power Supply	September ~October
Regular Inspection of the Power Supply for Additional Heating Facilities	September ~October
Regular Inspection of the Power Distribution Systems	October

2.3.1 Overhaul of the Oil-Cooled Transformer

The regular gas chromatograph analysis of insulating oil in the oil-cooled transformers for TFC power supply detected abnormal quantities of flammable gas, C_2H_4, C_2H_2, etc., in January, 2005. This transformer for the thyristor drive device of the motor generator has a zero-voltage tap changer. The specifications and outer appearance are shown in Table I.2.3-2 and Fig.I.2.3-1. The pattern of the gas contents showed flammable gas was produced by overheats of the oil. A spring-forced metal contact could produce "creep" on a contact surface. This would result in a temperature rise at the contact surface, and generate carbide layers for a certain period. This scenario seems to be supported by observation of the tap contact as shown in Fig.I.2.3-2. To avoid this phenomenon, the changeable tap contact was replaced by the fixed one.

Table I.2.3-2 Specifications of the oil-cooled transformer.

Capacitor (kVA)	28,000
Primary voltage (V)	10,500~11,500
Secondary voltage (V)	17,000
Oil quantity (L)	10,700
Weight (kg)	40,200

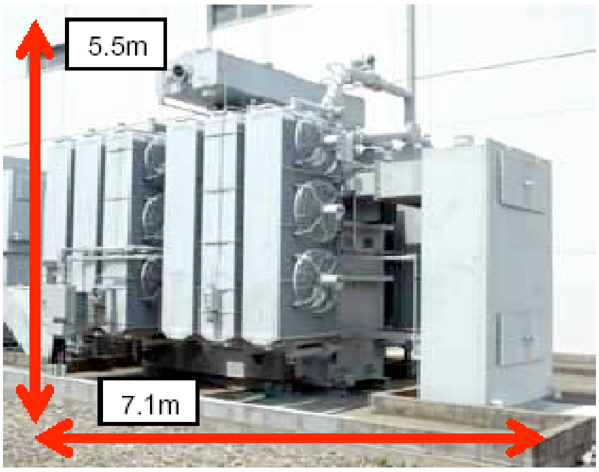

Fig.I.2.3-1 The oil-cooled transformer for the thyristor drive device of the TF-PS motor generator.

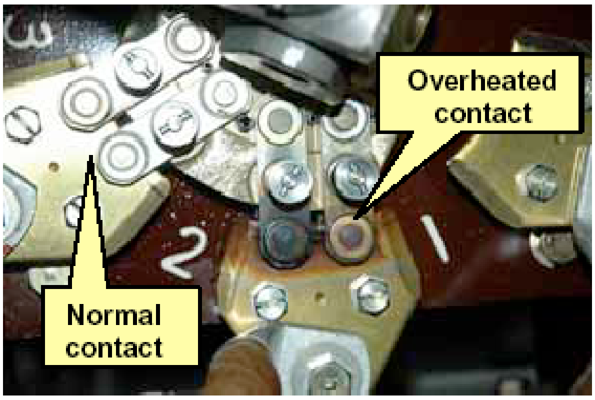

Fig.I.2.3-2 The overheated tap contact.

2.3.2 New AC Power System for Satellite Tokamak

The satellite tokamak, the modification of JT-60 to a super-conducting tokamak, is planned to have a 41MW-100s heating operation through the Japan-Europe negotiation in 2005. The planned powers for the heating facilities are summarized in Table I.2.3-3. AC power of 130MW-100s (13GJ) is necessary for the operation with all the heating facilities, but cannot be supplied by the present motor generator for additional heating facilities (H-MG: 400MVA, 2.65GJ). The reuse of the present power supply is a basic policy of the satellite tokamak project to save the cost. Therefore, we have studied possible AC power systems that are reconstructed with the present JT-60 power supply system.

(1) Configuration of a New AC Power System

The new AC power system would be constituted of the 275kV commercial line (Tr-1) and the motor generator for the current TFC-PS (T-MG). The configuration of the new AC system is shown in Fig. I.2.3-3. The AC powers of 88MW for P-NBI and ECRF and 40MW for NNBI are supplied from the Tr-1 line and from T-MG, respectively.

Table I.2.3-3 Nominal power for Additional Heating Facilities.

Unit	Heating Power (MW)	Active Power (MW)	Reactive Power (MVar)
P-NBI	24.0	60.3	80.1
N-NBI	10.0	40.5	54.0
ECRF	7.0	28.0	21.0

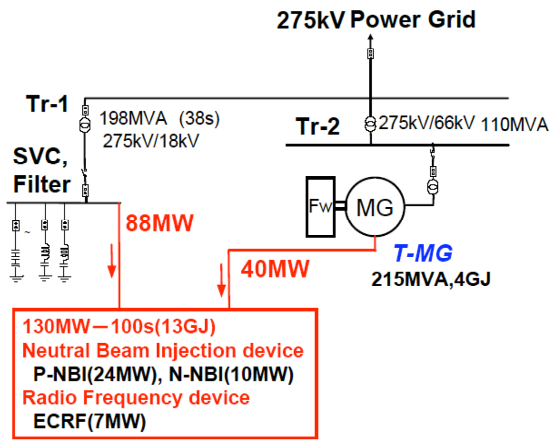

Fig. I.2.3-3 A possible configuration of the new AC power system for additional heating facilities.

(2) Design Study of a New Reactive Power Compensator

Power consumption of 88 MW through Tr-1 would induce voltage variation and higher harmonic currents at 275 kV power grid exceeding the values restricted by the contract with the commercial power company, TEPCO. To reduce such influence on the commercial line, a reactive power compensator consisting of a harmonic filter set and a power-factor improvement capacitor set to be installed in the circuit were designed. In the design, the existing harmonic filters and power-factor improvement capacitors were assumed to be reused as a part of the reactive power compensator.

We made the model of additional heating facilities for the simulation codes PSCAD/EMTDC. First, the response of the circuit without the reactive power compensator was simulated. The results are shown in Table I.2.3-4, and the harmonic current is shown in Fig. I.2.3-4. The equivalent disturbing current calculated with the harmonic current is 4.94A. This value does not satisfy the contract condition with TEPCO, allowable equivalent disturbing current of 1.9A.

Table I.2.3-4 Simulation result from the case without a reactive power compensator.

Active Power (MW)	84.4
Reactive Power (MVar)	105.0
Power Factor	0.63
275kV line Voltage regulation (%)	0.8
18kV line Voltage regulation (%)	10.0

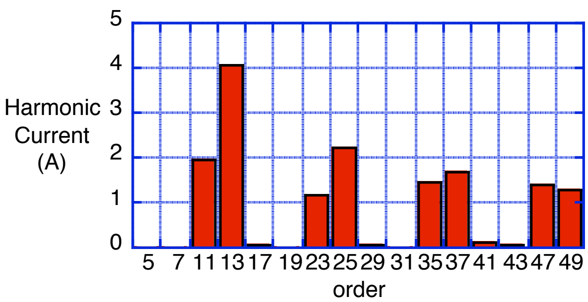

Fig. I.2.3-4 Harmonic current of 275kV power grid without reactive power compensator.

Table I.2.3-5 Simulation result from the case with a reactive power compensator.

Active Power (MW)	87.4
Reactive Power (MVar)	59.2
Power Factor	0.82
275kV line Voltage regulation (%)	0.4
18kV line Voltage regulation (%)	5.5

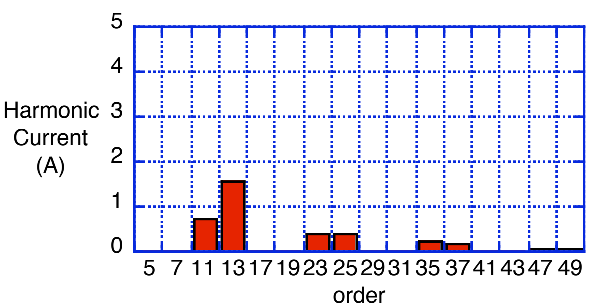

Fig. I.2.3-5 Harmonic current of 275kV power grid with reactive power compensator.

To explore the resolution, the simulation for the case with the reactive power compensator was conducted, and the results are shown in Table I.2.3-5. The harmonic current is shown in Fig. I.2.3-5. In the simulation, it was assumed that 11, 13 order harmonic filters were substituted by the new ones, while 18 and higher order harmonic filters and the power-factor improvement capacitors of 40MVar were reused. The equivalent disturbing current improved to 1.54A, and satisfied the contract condition. It was, therefore, concluded that a new AC power system for the satellite tokamak additional heating facilities was feasible.

2.4 Neutral Beam Injection System

The main objectives of the NBI system is to extend its pulse duration up to 30s so as to study long pulse plasmas whose duration is much longer than the current diffusion time. Four tangential positive ion-based NBI (P-NBI) units have been routinely operated up to 30s with 2MW/unit at 85keV. Also, seven perpendicular P-NBI units have been operated in series for the total pulse duration of 30s. As for the negative ion-based NBI (N-NBI) system, the long pulse operation of 10 s with two ion sources has been achieved. The high performance of NBI system at the injection power of ~10 MW for 30s has been contributed to achieve high β_n~2.3 for 28s. Moreover, the critical issues for long pulse operation are specified, such as stable source plasma control, high voltage holding and reduction of heat load of the accelerator and beamline components. Design of the upgrade of the NBI system has been started, where the total injection power of 34 MW for 100 s is planned for the satellite tokamak.

2.4.1 Renewal of Control System for Cryogenic Facility

The NBI system needs deuterium gas fueling of 3-5Pam^3/s for source plasma production and neutralization. A large cryopumping system with pumping speed of 20000m^3/s is used to quickly exhaust the residual gas so as to avoid re-ionization of the neutral beam. The cryopumping system is cooled down by a liquid He cryogenic facility with a cooling capacity of 2.4kW. The control system of the cryogenic facility was constructed with Distributed Control System (DCS) computer about 20 years ago. Recently, the frequency of troubles in the control system has increased due to its ageing. Therefore, the control system has been renewed using functional and inexpensive commercial Programmable Logic Controllers (PLC). Figure I.2.4-1 shows the block diagram of the new control system. The new control system is composed of four PC computers and PLCs, each of which is connected with Ethernet. The PLCs are connected with double control loops to keep a high reliability. The control program in the original DCS, consisting of about 400 feedback control loop with ~400 digital and ~800 analog data, was transferred to the program in the PLC. A distributed processing method was used to control the cryopumps independently. About 200 control views were created to obtain a high man-machine interface. The new control system was completed in September 2005 and has shown its high reliability without troubles to date. This is a new approach of the commercial PLC to the dynamic control system in the large plant [2.4-1].

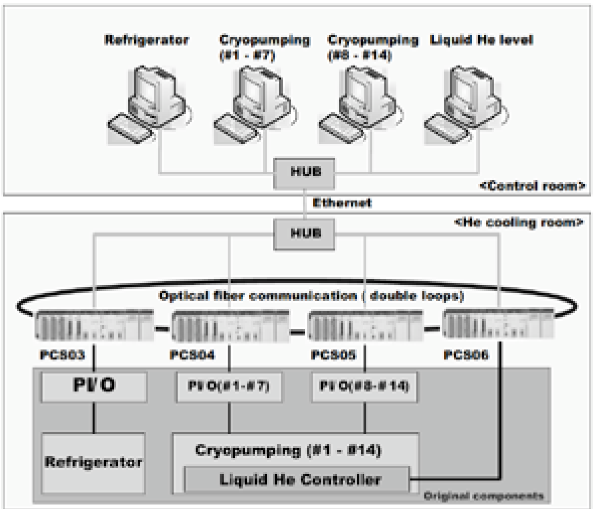

Fig. I.2.4-1 Block diagram of the new control system for a cryogenic facility.

2.4.2 Progress in N-NBI System

The long pulse more than 10 sec was carried out with one ion source only in 2004. In 2005, the optimization of 10 sec operation with two ion sources has been intended. Figure I.2.4-2 shows the progress of the injection power with two ion sources. A long pulse injection at ~3.3MW for 10sec, where the acceleration beam energy and current are 340keV, ~33A, has been achieved.

Some critical issues for long pulse operation have been specified through the optimization study [2.4-2]. The first issue is to keep the negative ion production constant for long pulse operation. Once the arc discharge starts, the discharge current flows into the filament, changing its temperature distribution. Feedback control of the arc current is effective in keeping the source plasma parameters. It is also confirmed that the cesium effect depends on the temperature of the plasma grid in the large ion source. This result indicates that active temperature control of the plasma grid is essential for long pulse operation.

The second issue is to improve the high voltage holding capability of the accelerator. It was found that outgass increased in the range of 10^{-4}Pa during voltage holding even when there was no-breakdown in the ion source (base pressure: 1-2x10^{-4}Pa). When the outgassing was well suppressed after sufficient conditioning, breakdowns were well suppressed. The main component of the outgass was m/e=28. There was no component of m/e=14. Therefore, the outgass was supposed to be hydro-carbon species. This result indicates that the improvement of FRP (fiberglass-reinforced plastic) insulator, which is composed of hydro-carbons, may be a key to achieve high voltage holding in the accelerator.

The third issue is to reduce the heat load of the acceleration grids and beam line components. The investigation of the negative ion beam deflection, which was measured by the infrared camera on the target plate set 3.5m away from the grid, indicates that the spread of beamlet-bundle is in proportion to the current density. Field-shaping plates attached on the extraction grid were effective in modifying the local electric field and reducing the heat load of the acceleration grid [2.4-3]. It was also found that some

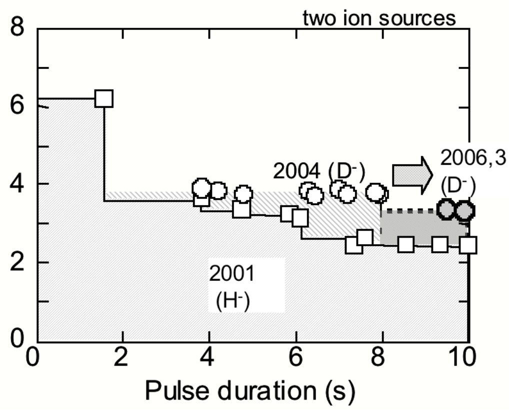

Fig. I.2.4-2 Progress of the injection power and pulse duration with two ion sources.

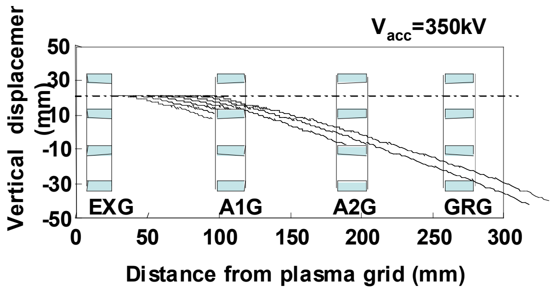

Fig. I.2.4-3 Electron beam trajectory in the three stage accelerator. Some electron produced at the first stage is deflected by the PG magnetic field and is accelerated,. passing through the next accelerator grids (A2G, GRG).

part of the stripped electrons produced at the first stage accelerator were accelerated and passed through the down pitch of the multi-apertures in the next acceleration grid and then collided the beam line as shown in Fig.I.2.4-3. It is important to investigate in detail the negative ion-beam and electron-beam trajectory not only inside of the ion source, but also downstream from the ion source for further long pulse operation [2.4-4].

2.4.3 Design Study of NBI System for the Satellite Tokamak

Modification of JT-60U to the satellite tokamak has been planned to contribute to ITER and DEMO. The NBI system is required to inject 34MW for 100s. The upgraded NBI system consists of P-NBI units and one N-NBI unit. The injection power of each P-NBI unit is 2MW at 85keV, and that of one N-NBI unit will be 10MW at 500keV. There are three types of P-NBI units (perpendicular: 8 units, co-tangential: 2 units, counter-tangential: 2 units) to control deposition profile and plasma rotation. The beam line of the co-tangential N-NBI unit will be shifted downward from the equatorial plane by ~0.6m to drive off-axis plasma current that is necessary for producing reversed shear with a high bootstrap current fraction. Figure I.2.4-4 shows the side view of the NBI system for the satellite tokamak.

The critical issue of the modified NBI system is to extend the pulse duration up to 100s. In long pulse operation of P-NBI unit at 2MW for 30s, the temperature rise of the cooling water in the ion source has been found to get almost saturated at less than 10°C at ~15 s after the start of injection, indicating that the present ion source of P-NBI may operate for 100 s without modification. Under the KBSI-JAERI collaborative program, a long pulse operation of P-NBI ion source has been demonstrated up to 200s at KSTAR NBI test facility though the beam current is ~20A at 60kV due to the power supply capability. In the preliminary study, the present high voltage DC power supply for P-NBI unit can drive the ion source for 100s by modifying some resistances and employing active cooling of the inner conductor in the high voltage feeder duct. The available beam voltage of the present N-NBI is less than 400keV. Thus, the main issue of N-NBI unit is to improve the voltage holding of the ion source up to 500kV. A modification of the accelerator such as the insulator structure is under consideration. The present acceleration power supply of 500kV, 64A with an inverter switching system will also be modified to extend its pulse duration from 10s to 100s by adding more converter-inverter components. The last item is shielding of the leakage magnetic field of the satellite tokamak. The leakage field will be about five times larger from the JT-60U, so attachment of high permeability metal on the ion tank is required, in addition to strengthening the canceling coils. The detailed design study is under development [2.4-5].

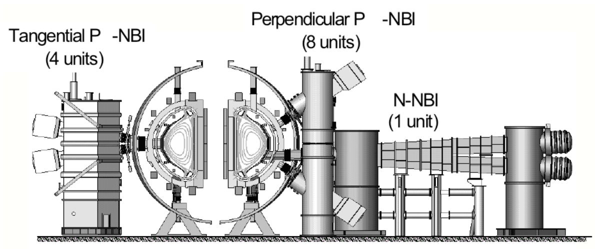

Fig. I.2.4-4 Side view of NBI systems for satellite tokamak.

Reference

2.4-1 Okano, F., *et al.*, *Keiso*, **49**, 22 (2006) (in Japanese).

2.4-2 Ebisawa, N., *et al.*, "Recent Activities of Negative Ion Based NBI System on JT-60U," *Proc. 21st Symp. on Fusion Eng.,* (CD-ROM) (2005).

2.4-3 Ikeda, Y., *et al.*, "Present Status of Negative Ion Based NBI System for Long Pulse Operation on JT-60U," *Proc. 4th IAEA TM on Negative Ion Based Neutral Beam Injectors,* (CD-ROM) (2005).

2.4-4 Umeda, N., *et al.*, *Rev. Sci. Instrum.*, **77**, 03A529 (2006).

2.4-5 Ikeda, Y., *et al.*, "Progress of Neutral Beam Injection System on JT-60U for Long Pulse Operation," *Proc. 5th General Scientific Assembly of Asia Plasma & Fusion Association,* (CD-ROM) (2005).

2.5 Radio-Frequency Heating System

2.5.1 Long-Pulse Operation of the ECH System

Trail of Pulse extension of the ECH system is being carried out to enhance the plasma performance in the recent experiment campaign in JT-60U focusing on long sustainment of high performance plasmas. Improvements of the gyrotron and development of advanced operation techniques are keys to extend the ECH pulse. A difficulty in the pulse extension was to keep the oscillation condition against decreasing collector current because of cathode cooling due to continuous electron emission. The techniques of controlling heater current and anode voltage during the pulse developed by FY2004 [2.5-1] were refined and pulse duration of 17 s at 0.4 MW (at gyrotron) has been achieved.

The mechanism of this control is regarded as follows; the increase in heater current is a direct method to compensate the cathode temperature drop, and the change in anode voltage changes the oscillation condition by modifying the electron pitch angle. As an advanced feature of the real time heater current and anode voltage control, automatic recovery from the oscillation termination was also achieved. The termination was detected from the voltage signal from the directional coupler and the diode detector, then the anode voltage was increased by 2.2 kV and the oscillation successfully recovered as shown in Fig. I.2.5-1.

It is important to estimate the power of injected millimeter waves for the ECH system. However, power measurement by a dummy load, used as a basic and common power measurement method, assumes reproducibility and stability of the gyrotron oscillation. A model calculation showed that the disk edge temperature of the diamond vacuum window (diameter: 60 mm, thickness: 1.72 mm) in the waveguide (inner diameter: 31.75 mm) gap was sufficient to estimate the transmission power at 1 MW and 110 GHz with a response time of ~0.2 s, because of the high thermal conductivity of diamond. This suggests that quasi-real-time power measurement can be achieved using a high response thermometer such as a very thin thermocouple or an infrared radiation thermometer. The initial high power test with a thermocouple (ϕ = 0.5 mm) demonstrated successful power measurement for ~1 MW, 4 s pulses with response time of < 1 s as shown in Fig. I.2.5-2.

2.5.2 Operation and R&D of the LH System

The performance of the modified launcher with the developed carbon grills showed sufficient abilities as a high power LH launcher, for instance, moderate current drive efficiency [2.5-2]. For the modified LH launcher,

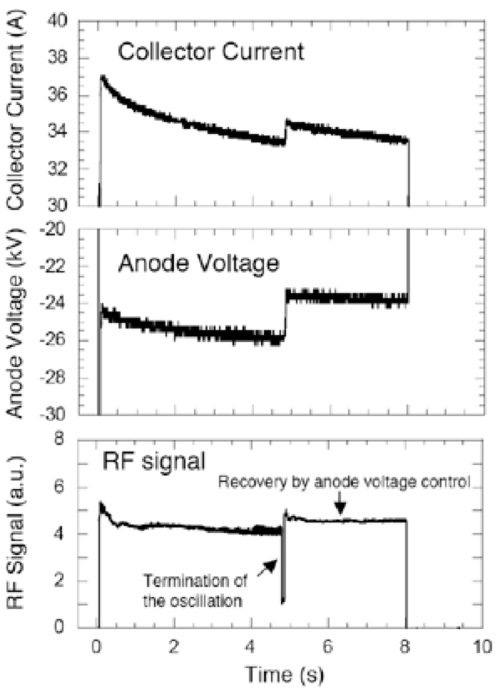

Fig. I.2.5-1 Oscillation recovery by anode voltage control.

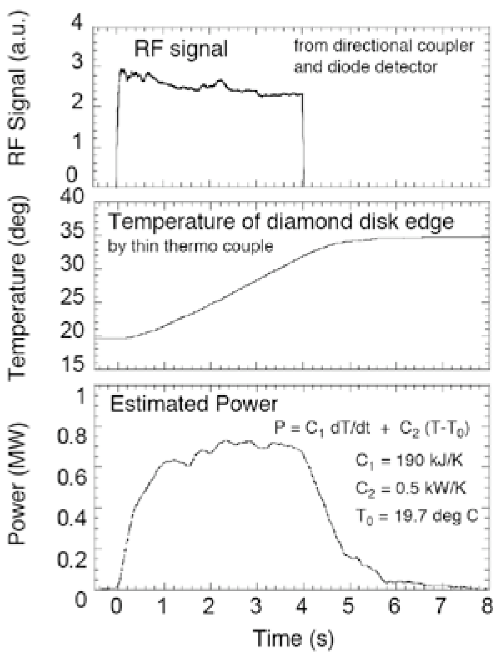

Fig. I.2.5-2 Power measurement by the diamond disk set in the waveguide gap.

the technical key issue was to obtain sufficient electrical contact along the carbon grills, even though for this purpose a thin RF contactor made of copper was inserted between the base frame and the carbon grill mouth. After large energy injection such as ~16 MJ, the carbon grills seemed to be of integrity, however, severe damages were observed around a few base frames by RF breakdown due to insufficient electrical contact and low responses of the arc monitor system to protect them against RF breakdown in the LH launcher. Therefore, at first the arc monitor system was improved such as re-installation of the checking lamps that clearly check whether the protection system works well or not. Next, the eight carbon grills were removed from the base frames welded with the LH launcher, and these base frames were repaired smoothly. Unfortunately, two base frames were so injured that high RF power could not be injected. Conditioning of the LH launcher through the six base frames was performed with plasma by using the power-modulated injection method like as discontinued injection of 50ms-on/10ms-off. The conditioning has progressed up to ~1.5 MW and/or ~9.3 MJ, as shown in Fig. I.2.5-3. Moreover, the real time current profile control by LH injection was successfully demonstrated via real-time adjustment of input power and phase difference with monitoring current profile estimated with MSE measurement.

In order to improve insufficient electrical contact along the carbon grill, a new carbon grill has been developed as shown in Fig. I.2.5-4. The four-divided (4-div.) grill made of graphite is joined with the 4-div. pedestal by a "diffusion bonding method". In this new carbon grill, the position of electrical contact is between the 4-div. pedestal made of stainless steel and the base frame. Enough electrical contact is expected because pressing is stronger than the former type. This new carbon grill shows enough power capability of ~500 kW even in short time. Up to now, high power of 300 kW - 10 s can be transmitted without heavy RF breakdown.

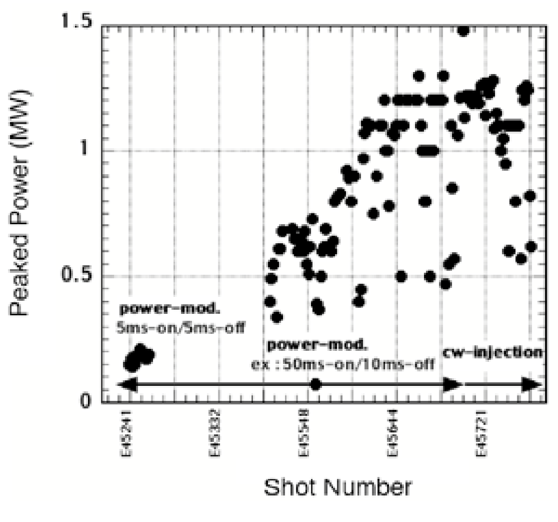

Fig. I.2.5-3 Progress of conditioning using the LH launcher with 6 base frames. A power modulation method is used for efficient conditioning. In the latter phase, power is injected continuously.

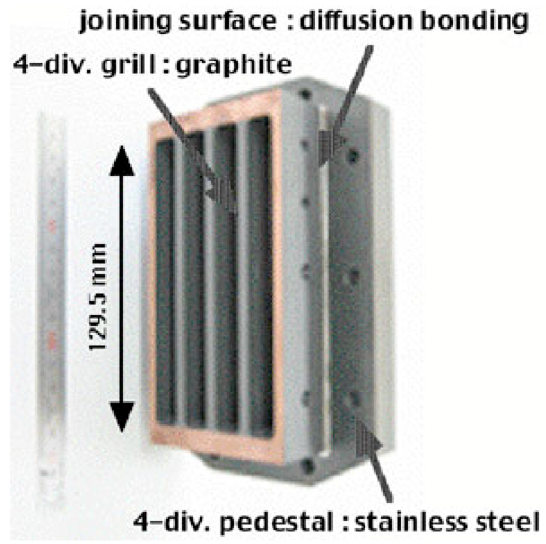

Fig. I.2.5-4 Overview of the new carbon grill.

References

2.5-1 Moriyama, S., *et al.*, *Fusion Eng. Des.*, **74**, 343 (2005).

2.5-2 Seki, M., *et al.*, *Fusion Eng. Des.*, **74**, 273 (2005).

2.6 Diagnostics Systems

2.6.1 High-Repetition CO_2 Laser for Collective Thomson Scattering Diagnostic [2.6-1]

A diagnostic of fusion-generated alpha particles is important for understanding of their contribution to plasma heating and plasma instabilities. However, the effective and reliable measurement method has not yet been established.

To establish a diagnostic method of confined α-particles in burning plasmas, a high-repetition and high-energy Transversely Excited Atmospheric (TEA) carbon dioxide (CO_2) laser (Fig. I.2.6-1) for a collective Thomson scattering (CTS) diagnostic has been developed. To excite a single-transverse and

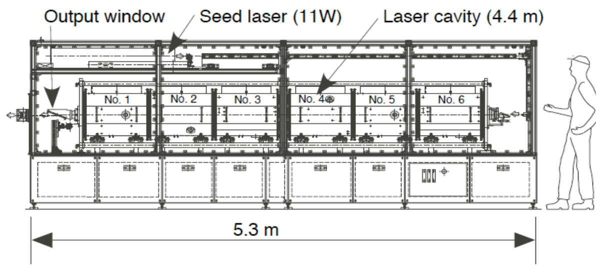

Fig. I.2.6-1 Schematic view of newly developed TEA CO_2 laser. The dimensions of the laser casing are 5.3m long, 1.9m high, 1.1m wide.

single longitudinal mode, the laser has an unstable resonator with a cavity length of ~4.4m and continuous wave seed laser is injected. Pulse energy of 10J with a repetition rate of 10Hz has been achieved in the single-mode operation. The beam size is 40mm in diameter. Pulse energy of 18J with a repetition rate of 10 Hz and 36J with single shot operation has also been achieved in the multimode operation. These results give an outlook for the CTS diagnostic on ITER, which requires single-mode energy of 20J with a repetition rate of 40Hz. A proof-of-principle test will be performed with the improved laser system on JT-60U.

2.6.2 Density Fluctuation Measurement Using Motional Stark Effect Optics [2.6-2]

The motional Stark effect (MSE) diagnostic system has been modified to work as a beam emission spectroscopic (BES) diagnostic. By fast sampling (0.5-1MHz) of the photo-multiplier signals, the system can simultaneously measure density fluctuation in addition to the pitch angle of the magnetic field. In the core plasmas, density fluctuation induced by rotating tearing mode islands has been observed. In the scrape-off layer of an ELMy H-mode plasma, outward propagation of strong intermittent emission coinciding with ELM crashes has been observed.

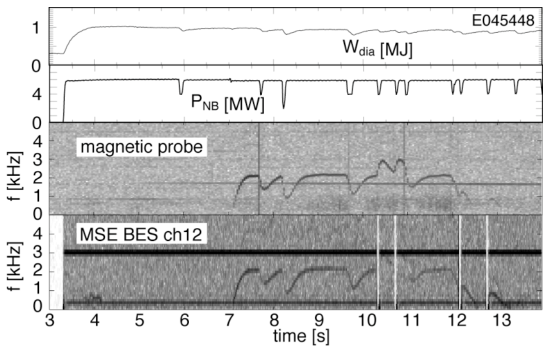

Fig. I.2.6-2 Time evolution of a discharge in which density fluctuation induced by rotating tearing mode islands was observed. Diamagnetic stored energy (W_{dia}), NB heating power (P_{NB}), spectrogram of magnetic fluctuation measured with a magnetic probe, and spectrogram of fluctuation in a photo-multiplier signal of the MSE diagnostic system.

Figure I.2.6-2 shows time evolution of a discharge in which density fluctuation induced by rotating tearing mode islands was observed. An MHD fluctuation is observed from t=7s at a frequency of ~2.2kHz, using magnetic probes. The poloidal and toroidal mode numbers are 2 and 1, respectively. Several channels of the MSE BES diagnostic near q=2 surface detected the MHD fluctuation having the same temporal evolution of frequency. The phase of the fluctuations measured by the MSE BES diagnostic is inverted at the q=2 surface measured by the MSE diagnostic, where the phase of the electron temperature fluctuations measured by an electron cyclotron emission diagnostic is also inverted. The phase inversion of the temperature and density fluctuations indicates a rotating island structure of the magnetic field.

2.6.3 Neutron Detector with Fast Digital Signal Processor [2.6-3]

Neutron emission profiles are routinely measured and used for transport studies of energetic ions. In order to measure neutrons effectively in the mixed neutron and gamma-ray filed, Stilbene neutron detectors (SNDs) have been used. The SND combines a Stilbene crystal scintillation detector (SD) with an analog neutron-gamma pulse shape discrimination (PSD) circuit to select only neutron events. Although the SND has many advantages as a neutron detector, the maximum count rate is limited up to ~ 1×10^5counts/s due to pile up effect in the analog PSD circuit. Under this situation, it is difficult to investigate transport of energetic ions due to MHD instabilities such as Alfvén Eigenmodes with frequency of ~ MHz range.

To overcome this issue, a digital signal processing system (DSPS) using a Flash ADC (Acqiris DC252, 8 GHz, 10bit) has been developed at Cyclotron and Radioisotope Center in Tohoku University. In this system anode signals from the photomultiplier of the SD are directory stored and digitized sequentially. Then, neutron-gamma PSD is performed using software. This system allows neutron measurements with a high counting rate of > 1×10^6counts/s. Good neutron-gamma

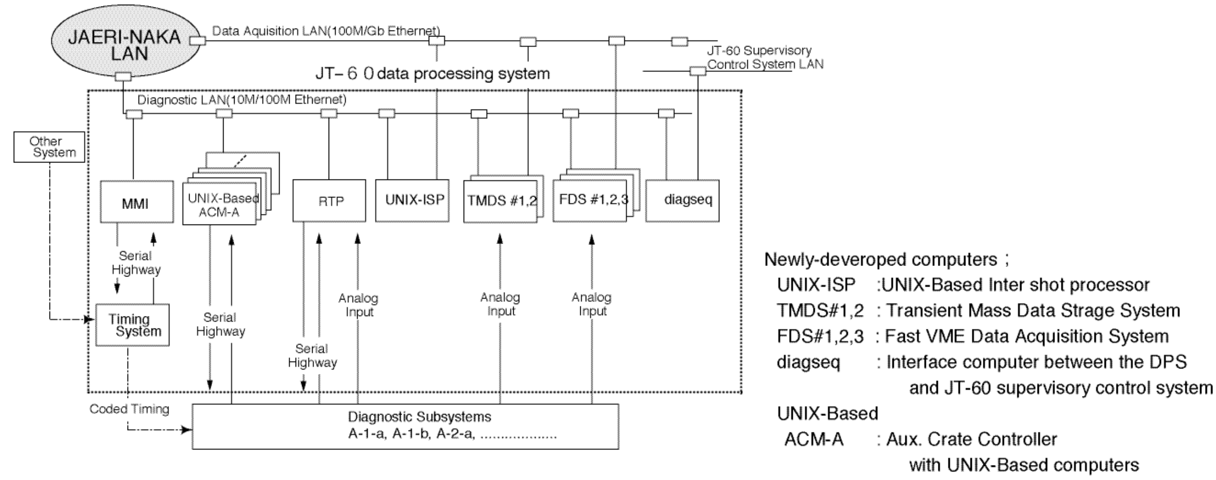

Fig.I. 2.6-3 The configuration of the new data processing system.

discrimination of this system was verified by performance tests using neutron-gamma sources. Then, it has been installed in the center channel of the vertical neutron collimator system in JT-60U and applied to deuterium experiments. As a result, it is confirmed that the PSD is sufficiently performed and collimated neutron flux are successfully measured with a count rate up to ~ 5×10^{5}counts/s without pile up of detected pulses. Thus, the performance of the DSPS as a neutron detector, which supersedes the SND, is demonstrated.

2.6.4 Data Processing System [2.6-4]

In order to meet demands for the advanced diagnostics, the JT-60 data processing system (DPS) has been modified from a three-level hierarchy system to a two-level hierarchy system. The old DPS had a mainframe computer at the top level of the hierarchy. The mainframe computer communicated with the JT-60 supervisory control system and supervised internal communication inside the DPS. The middle level of the hierarchy had minicomputers, and the bottom level had individual diagnostic subsystems. The mainframe computer at the top level limited the total performance of the DPS. The new DPS is a decentralized data processing system using UNIX-based workstations and network technology. The configuration of the new DPS is shown in Fig. I.2.6-3. The mainframe computer was replaced with a UNIX-based workstation. All the computers in the middle level of the hierarchy are now UNIX-based workstations. The new DPS started operation in October 2005.

References

2.6-1 Kondoh, T., *et al.*, “High-Repetition CO2 Laser for Collective Thomson Scattering Diagnostic of α-Particles in Burning Plasmas,” submitted to *Rev. Sci. Instrum.*.

2.6-2 Suzuki, T., *et al.*, “Density Fluctuation Measurement Using Motional Stark Effect Optics in JT-60U,” to be published in *Rev. Sci. Instrum.*.

2.6-3 Ishikawa, M., *et al.*, “Fast Collimated Neutron Flux Measurement using Stilbene Scintillator and Flash-ADC in JT-60U,” submitted to *Rev. Sci. Instrum.*.

2.6-4 Sakata, S., *et al.*, “Progress of Data Processing System in JT-60 -Development of Remote Experiment System-,” to be published in *Fusion Eng. Des.*.

II. THEORY AND ANALYSIS

Much progress was made in confinement, transport and MHD researches, such as beta dependence of ELMy H-mode confinement, ITB in reversed shear plasma, aspect ratio effect on external MHD modes and magnetic island evolution in rotating plasma. Integrated simulation code for burning plasma analysis is being developed and validated by fundamental researches of JT-60U experiments. Progress has been made in the NEXT project to investigate complex physical processes in MHD and transport phenomena. The behaviors of the collisionless MHD modes in high temperature plasmas, and the effect of MHD modes on current hole formation were shown. The dynamics of the zonal flows and geodesic acoustic modes (GAMs) were understood in reversed shear configuration and a new gyrokinetic Vlasov code was developed. Cross section data for atomic and molecular collisions and spectral data relevant to fusion research have been compiled and produced.

1. Confinement and Transport

1.1 Origin of the Various Beta Dependence of ELMy H-mode Confinement

Dependence of the energy confinement in ELMy H-mode tokamak on the beta has been investigated for a long time, but a common conclusion has not been obtained so far. Recent non-dimensional transport experiments in JT-60U demonstrated clearly the beta degradation. A database for JT-60U ELMy H-mode confinement was assembled. Analysis of this database is carried out, and the strong beta degradation consistent with above experiments is confirmed. Two subsets of ASDEX Upgrade and JET data in the ITPA H-mode confinement database are analyzed to find the origin of the various beta dependences. The shaping of the plasma cross section, as well as the fuelling condition, affects the confinement performance. The beta dependence is not identical for different devices and conditions. The shaping effect, as well as the fuelling effect, is a possible candidate to cause the variation of beta dependence. [1.1-1]

Reference

1.1-1 Takizuka, T., *et al*., *Plasma Phys. Control. Fusion*, **48**, 799 (2006).

1.2 Internal Transport Barriers in JT-60U Reversed-Shear Plasmas

Physics of strong internal transport barriers (ITBs) in JT-60U reversed-shear (RS) plasmas has been studied through the modeling on the 1.5 dimensional transport simulation. Key physics to produce two scalings on the basis of the JT-60U box-type ITB database are identified. Figure II.1.2-1 shows the ITB width, Δ_{ITB}, as a function of the ion poloidal gyroradius at the ITB centre, $\rho_{pi,ITB}$. The standard model reproduces the JT-60U scaling (Δ_{ITB}~$1.5\rho_{pi,ITB}$), while other models does not. As a result, as for the scaling for the narrow ITB width proportional to the ion poloidal gyroradius, the following three physics are important: (1) the sharp reduction of the anomalous transport below the neoclassical level in the RS region, (2) the autonomous formation of pressure and current profiles through the neoclassical transport and the bootstrap current, and (3) the large difference between the neoclassical transport and the anomalous transport in the normal-shear region. As for the scaling for the energy confinement inside ITB ($\varepsilon_f\beta_{p,core}$~0.25 where ε_f is the inverse aspect ratio at the ITB foot and $\beta_{p,core}$ is the core poloidal beta value), the value of 0.25 is found to be a saturation value due to the MHD equilibrium. The value of $\varepsilon_f\beta_{p,core}$ reaches the saturation value, when the box-type ITB is formed in the strong RS plasma with the large asymmetry of the poloidal magnetic field, regardless of details of the transport and the non-inductively driven current [1.2-1].

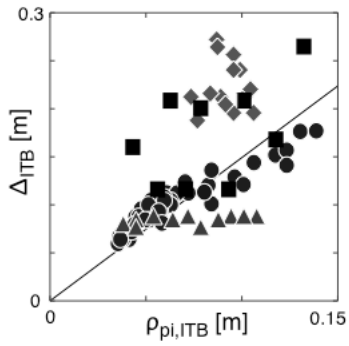

Fig. II.1.2-1 shows Δ_{ITB} versus $\rho_{pi,ITB}$ for several types of models. Standard model (●) is modified so that neoclassical transport is replaced by gyro-Bohm type (▲), anomalous transport is reduced even in normal-shear region (■), and current profile with weakly-reversed-shear is fixed (◆). Solid line denotes JT-60 scaling.

Reference

1.2-1 Hayashi, H., *et al*., *Plasma Phys. Control. Fusion,* **48**, A55 (2006).

2. MHD Stability

2.1 Aspect Ratio Effect on the Stability of the External MHD Mode in Tokamaks

The formulation for solving numerically the two-dimensional Newcomb equation is extended to calculate the vacuum energy integral. This extension realizes the stability analysis of ideal external MHD modes from low to high toroidal mode numbers. According to this extension, an effect of the aspect ratio on the achievable normalized plasma pressure (β_N), restricted by ideal external MHD modes whose toroidal mode number is from 1 to 10, is studied. Figure II.2.1-1 shows the decrease of the aspect ratio improves the achievable β_N value, and increases the toroidal mode number of the external mode restricting the achievable β_N when the conducting wall is placed close to the plasma surface. This aspect ratio effect is confirmed when the safety factor at the plasma surface is between 4 and 5. These represent the importance of the stability of external MHD modes whose toroidal mode number is larger than 3 to determine the achievable β_N.

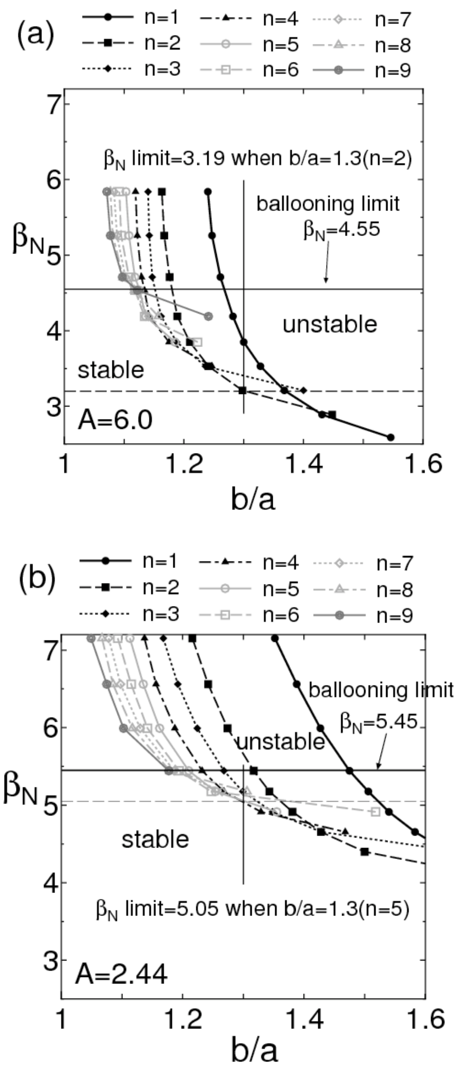

Fig. II.2.1-1 Dependence of the normalized pressure (β_N) limit on the wall position b/a when (a) A=6.00 and (b) A=2.44, where A is the aspect ratio. The edge safety factor is fixed as 4.44. The β_N limit improves and the toroidal mode number of the mode restricting the β_N limit increases as A decreases when the conducting wall is close to the plasma surface.

Reference

2.1-1 Aiba, N., *et al.*, "Analysis of an Aspect Ratio Effect on the Stability of External MHD Modes in Tokamaks with Newcomb Equation," to be published in *J.Plasma Phys.*.

2.2 Role of Anomalous Transport in Neoclassical Tearing Modes

Role of anomalous transport in onset and evolution of neoclassical tearing modes (NTMs) is investigated. A key role in the evolution NTMs belongs to the radial profiles of the perturbed plasma flow, temperature and density which are determined by the conjunction of the longitudinal and cross-field transport. The influence of anomalous perpendicular heat transport and anomalous ion perpendicular viscosity on early stages of NTM evolution are studied.

Several parallel transport mechanisms competitive with anomalous cross-island heat transport in the formation of the perturbed electron and ion temperature profiles within the island are considered. The partial contributions from the plasma electron and ion temperature perturbations in the bootstrap drive of the mode and magnetic curvature effect were taken into account in construction of a generalized transport threshold model of NTMs. This model gives more favourable predictions for NTM stability and qualitatively modifies the scaling law for β_{onset}. The anomalous perpendicular ion viscosity is shown to modify the collisionality dependence of the polarization current effect, reducing it to the low collisionality limit. In its turn a viscous contribution to the bootstrap drive of NTMs is found to be of the same order as a conventional bootstrap drive for the islands of width close to the characteristic one of the transport threshold model. A viscous contribution to the perturbed bootstrap current is destabilizing for the island rotating in the ion diamagnetic drift direction [2.2-1].

Reference

2.2-1 Konovalov, S.V., *et al.*, *Plasma Phys. Control. Fusion*, **47**, B223 (2005).

2.3 Magnetic Island Evolution in Rotating Plasma

It has been well understood that, in tokamak plasmas, magnetic islands resonant with the low q rational surface deteriorate the plasma confinement. Hence, the suppression and control of the magnetic islands is an urgent subject in a tokamak fusion research. Thus, the time evolution of the magnetic island formed at the tearing stable rational surface by the external magnetic flux perturbation in the plasma with poloidal flow is investigated numerically by using the resistive MHD model. It was found that the magnetic island growth phase is divided into four phases, 1) flow-suppressed phase, 2) rapid growth phase, 3) transient phase, and 4) Rutherford type phase. It was also found that the onset condition of this rapid growth depends on the resistivity, but does not much depend on the viscosity. On the other hand, the time constant of the rapid growth phase is almost independent on both the plasma resistivity and the viscosity. After the rapid growth phase, the island enters a transient phase, which becomes clear in the low resistivity regime. Then, the magnetic island grows slowly. This phase seems to be the Rutherford type phase [2.3-1].

Reference

2.3-1 Ishii, Y., *et al.*, "Magnetic Island Evolution in Rotating Plasmas," to be published in *J. Plasma Phys.*.

2.4 Mechanism of Rotational Stabilization of High-n Ballooning Modes

It has been clarified that ballooning modes in a shear toroidal rotating tokamak are stabilized by a countably infinite number of crossings among eigenvalues associated with ballooning modes in a static plasma. It was also found that the crossings cause energy transfer from an unstable mode to the infinite number of stable modes; such transfer works as the stabilization mechanism of the ballooning mode [2.4-1]. The method used in this research has been further explored from the view point of regularization of singular eigenfunctions of operators encountered often in plasma physics [2.4-2]. It has been confirmed that the set of regularized eigenfunctions does capture the transient behavior of the original equations of motion with singular operator for a finite time. Thus, this method will resolves the practical difficulties in analyzing various MHD phenomena with continuous spectra in tokamak plasmas.

References

2.4-1 Furukawa, M., *et al.*, *Phys. Rev. Lett.*, **94**, 175001 (2005).

2.4-2 Furukawa, M., *et al.*, *Phys. Plasmas,* **12**, 072517 (2005).

3. Integrated Simulation

3.1 Integrated Simulation Code for Burning Plasma Analysis

Strategy of integrated modeling for burning plasmas in Japan Atomic Energy Agency is as follows: In order to simulate the burning plasma which has a complex feature with wide time and spatial scales, a simulation code cluster based on the transport code TOPICS is being developed by the integration with heating and current drive, the impurity transport, edge pedestal model, divertor model, MHD and high energy behavior model. Developed integration models are validated by fundamental researches of JT-60U experiments and the simulation based on the first principle in our strategy.

The integration of MHD stability and the transport is progressed for three phenomena with different time scale of NTMs ($\sim\tau_{NTM}\sim10^{-2}\tau_R$), beta limits ($\sim\tau_{Alfven}$) and ELMs (intermittent of τ_E and τ_{Alfven}). Here, τ_R ,τ_{Alfven} and τ_E are the resistive skin time, the Alfven transit time and the energy confinement time, respectively. Integrated model of the NTM is produced by coupling the modified Rutherford equation with the transport equation. Integrated model of beta limits is developed by the low-n stability analysis of down streaming data from the TOPICS code. Integrated model of ELM is developed by the iterative calculation of the ideal MHD stability code MARG2D and the TOPICS code. These models are being validated by the data of JT-60 experiments and estimate the plasma performance for burning plasmas.

3.2 Development of Integrated SOL/Divertor code and Simulation Study

An integrated SOL/divertor code is being developed by the JAEA for interpretation and prediction studies of the behavior of plasmas, neutrals, and impurities in the SOL/divertor region [3.2-1]. A code system consists of the 2D fluid code for plasma (SOLDOR), the neutral Monte-Carlo code (NEUT2D), the impurity Monte-Carlo code (IMPMC), and the particle simulation code (PARASOL) as shown in Fig. II.3.2-1. The physical processes of neutrals and impurities are studied using the Monte Carlo (MC) code to accomplish highly accurate simulations. The so-called divertor code, SOLDOR/NEUT2D, has the following features: 1) a high-resolution oscillation-free scheme for solving fluid equations, 2) neutral transport calculation under the condition of fine meshes, 3) successful reduction of MC noise, and 4) optimization of the massive parallel computer. As a result, our code can obtain a steady state solution within 3 ~ 4 hours even in the first run of a series of simulations, allowing the performance of an effective parameter survey. The simulation reproduces the X-point MARFE in the JT-60U. It is found that the chemically sputtered carbon at the dome causes radiation peaking near the X-point. The performance of divertor pumping in the JT-60U is evaluated based on particle balances. In regard to the design of NCT (National Centralized Tokamak, renaming to the JT-60SA Satellite Tokamak at present) divertor [3.2-1, 3.2-2], the simulation indicates that pumping efficiency is determined by the balance between the incident and back-flow fluxes into and from the exhaust chamber, which depends on the divertor geometry and operational conditions.

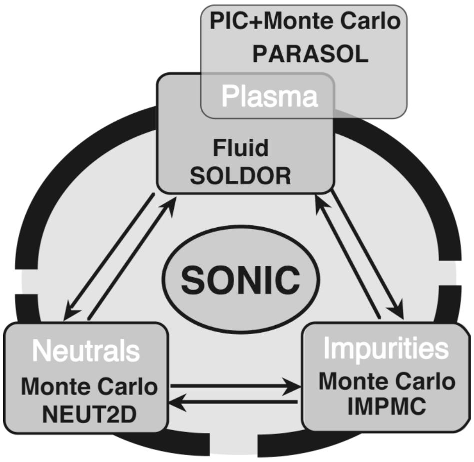

Fig. II.3.2-1 Development of SOL/divertor codes and integration in the JAEA [3.2-1].

References

3.2-1 Kawashima, H., *et al.*, *Plasma and Fusion Res.,* **1**, 031 (2006).

3.2-2 Kawashima, H., *et al.*, *Fusion Eng. Des.*, **81,** 1613 (2006).

3.3 Transient Behaviour of SOL-Divertor Plasmas after an ELM Crash

Enhanced heat flux to the divertor plates after an ELM crash in H-mode plasmas is a crucial issue for the tokamak reactor. Characteristic time of this heat flux is one of key factors of the influence on the plate. We investigate the transient behavior of SOL-divertor plasmas after an ELM crash with the use of a one-dimensional particle simulation code, PARASOL.

Influence of the collisionality and the recycling rate on characteristic times of the fast-time-scale response and of the slow-time-scale response are examined. The fast time scale is further classified into the supra-thermal-electron transit time scale and the thermal-electron-transit time scale. Supra-thermal electrons supplied by an ELM crash induce the large electron heat flux Q_e and the high sheath potential ϕ at the plate soon after the crash, while the time scale of electron temperature T_e is governed by the thermal electrons. Extremely large heat transmission factor and higher ϕ are observed in the low collisionality regime. In the higher collisionality regime, supra-thermal electrons are thermalized and the value of ϕ becomes proportional to T_e as usual. On the other hand, the slow-time-scale characteristic time is governed by the sound speed in the central SOL region, and is insensitive to the collisionality compared with the fast-time-scale one. The slow-time-scale phenomena are affected by the recycling condition in contrast to fast-time-scale behaviors being independent of the recycling. Peaks of particle and heat fluxes, Γ and Q, are delayed by the increase of recycling rate, though the arrival times of Γ and Q are not changed. Large recycling after the arrival of the enhanced Γ makes the flow speed small in the central SOL region, and the peaks are forced to be delayed. [3.3-1]

Reference

3.3-1 Takizuka, T., *et al.*, "Origin of the Various Beta Dependence of ELMy H-mode Confinement Properties," to be published in *Contrib. Plasma Phys.*.

4. Numerical Experiment of Tokamak (NEXT)

4.1 Nonlinear Behaviors of Collisionless Double Tearing and Kink Modes

In high temperature plasmas, the collisionless effects such as the electron inertia and the electron parallel compressibility become important for the magnetic reconnection in MHD modes. Thus, the behaviors of collisionless MHD modes were investigated by gyrokinetic particle simulations. The collisionless double tearing mode (DTM) grows at the Alfven time scale due to the electron inertia, and nonlinearly induces the internal collapse when the helical flux at the magnetic axis is less than that at the outer resonant surface. It was found that, after the internal collapse, the secondary reconnection is induced by the current concentration due to the convective flow, and a new reversed shear configuration with resonant surfaces can be generated [4.1-1]. The collisionless internal kink mode was also studied in the parameter region where the effects of electron inertia and electron parallel compressibility are competitive for magnetic reconnection. Although the linear growth of the mode is dominated by the electron inertia, it was found that the growth rate can be nonlinearly accelerated due to the electron parallel compressibility proportional to the ion sound Larmor radius. The acceleration of growth is also observed in the nonlinear phase of the DTM [4.1-2].

References

4.1-1 Matsumoto, T., *et al.*, *Nucl. Fusion*, **45**, 1264 (2005).
4.1-2 Matsumoto, T., *et al.*, *Phys. Plasmas*, **12**, 092505-1-7 (2005).

4.2 Stability of Double Tearing Mode and its Effects on Current Hole Formation

In tokamak plasmas with negative central current density, so called the current hole formation can be explained by the destabilization of m=1/n=0 resistive kink MHD mode. Here, a strong reversed magnetic shear configuration has two resonant surfaces for low mode numbers, thus DTM could become unstable before the hole formation. However, it was found that the stability of the resistive kink mode, so that the current density gradient to drive the mode, does not change much after a crash by DTM, although the current profile is flatten near the minimum safety factor region [4.2-1].

After a formation of the hole, no MHD activity identified to DTM was observed in experiments, and a resultant profile with two resonant surfaces could have a good stability for DTM. It was also found that the current profile with a strong peak around an inner resonant surface, as shown in Fig.II.4.2-1, is stable for DTM [4.2-2].

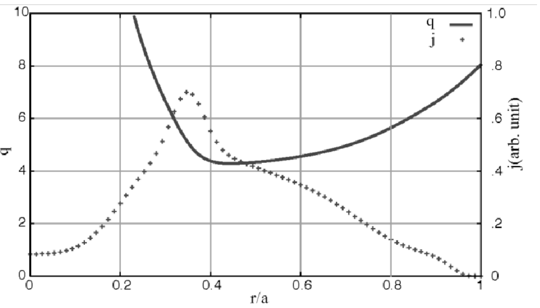

Fig. II.4.2-1 An example of stabilized current density ***j*** and safety factor ***q*** profiles. When a position of a current peak is shifted to an inner resonant surface for *m*/*n*=5/1 DTM, DTM becomes to be stable, where *m* and *n* are a poloidal and toroidal mode number, respectively.

References

4.2-1 Tuda, T., *et al*., "Roles of Double Tearing Mode on the Formation of Current Hole," to be published in *J. Plasma Phys.*.

4.2-2 Tuda, T., *et al*., "Stability of Double Tearing Mode in Current Hole Configuration," to be published in *J. Korean Phys. Soc.*.

4.3 ZF/GAM Dynamics and Ion Turbulent Transport in Reversed Shear Tokamaks

Zonal flow behavior and its effect on turbulent transport in reversed magnetic shear tokamaks were investigated by global simulations of electrostatic ion temperature gradient driven turbulence. In a high safety factor case (q_0=2.2), Fig.II.4.3-1 shows that turbulent heat transport is high in a broad radial region because oscillatory zonal flows or GAMs are dominant. When q_0 is reduced from 2.2 to 1.8 with keeping the other parameters unchanged, zonal flows change from the GAMs to stationary flows in the region around the minimum q surface. As a result of the change in zonal flow behavior, the ion thermal diffusivity is reduced, as shown in Fig.II.4.3-1. This result indicates that the change of zonal flow behavior may trigger the formation of ion transport barriers in the minimum q region.

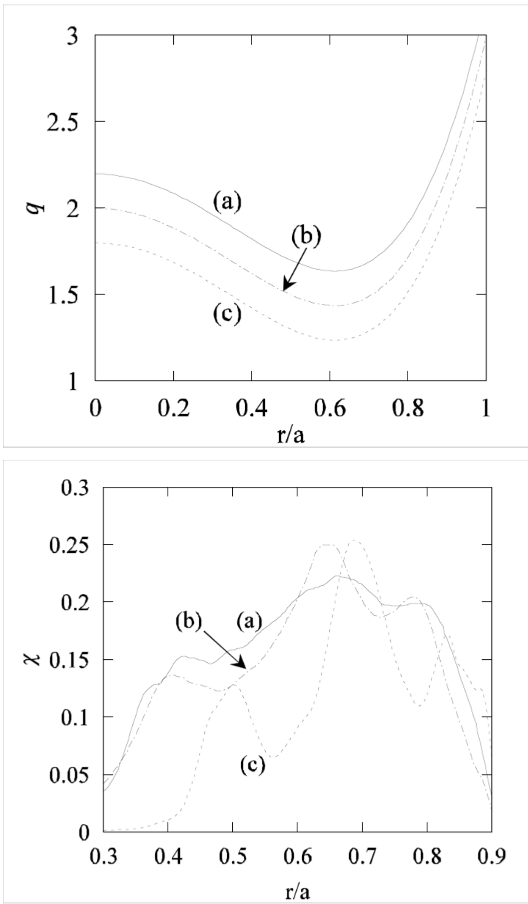

Fig. II.4.3-1 Radial profiles of the safety factor $q=q_0-3(r/a)^2+4(r/a)^4$ for (a) q_0=2.2, (b) q_0=2.0, and (c) q_0=1.8 (top), and the normalized ion thermal diffusivity χ (bottom).

Reference

4.3-1 Miyato, N., *et al*., "Zonal Flow and GAM Dynamics and Associated Transport Characteristics in Reversed Shear Tokamaks," to be published in *J. Plasma Phys.*.

4.4 Development of Gyrokinetic Vlasov CIP Code

A gyrokinetic simulation is an essential tool to study anomalous turbulent transport in tokamak plasmas. Although the δf Particle-In-Cell (PIC) method enabled an accurate gyrokinetic simulation of small amplitude turbulent fluctuations with ~1%, the method has a difficulty in implementing non-conservative effects such as heat and particle sources and collisions are important, which are essential in realistic long time turbulence simulations. To overcome the difficulty, a new gyrokinetic Vlasov code has been developed using the Constrained-Interpolation-Profile (CIP) method. The code is numerically stable and numerical oscillations, which have been a critical issue in the previous Vlasov simulations, are quite small. In the benchmark tests of ion temperature gradient driven

(ITG) turbulence simulations, the linear growth rates, the nonlinear saturation levels, the zonal flow structures, and the conservation properties are almost the same between the PIC and CIP codes. In addition, computational costs are almost comparable between two codes. A possibility of a long time turbulence simulation was demonstrated from the viewpoints of numerical properties and a computational cost.

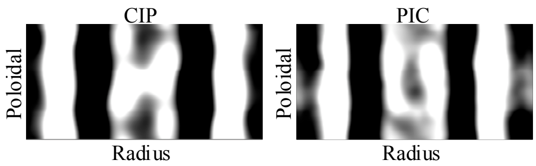

Fig. II.4.4-1 The radial-poloidal contour plots of f observed in the nonlinear quasi-steady phase of the ITG turbulence simulations with CIP (left) and PIC (right) codes. Both results show similar zonal flow patterns.

Reference

4.4-1 Idomura, Y., *et al*., "Comparisons of Gyrokinetic PIC and CIP Codes," *Proc. 32nd EPS Plasma Physics Conf.*, p1.044 (2005), to be published in *J. Plasma Phys.*.

5. Atomic and Molecular Data

We have been compiling and producing cross section data for atomic and molecular collisions and spectral data relevant to fusion research [5-1].

Cross sections for 74 processes in collisions of electrons with N_2 and N_2^+ have been compiled [5-2]. In tokamak fusion research, N_2 gas has been injected for heat control. The cross sections are plotted as a function of the electron collision energy, and recommended cross sections are expressed by analytic expressions to facilitate practical use of the data. Figure II.5-1 shows an example of the complied cross section data. The data have been included in Japanese Evaluated Atomic and Molecular Data Library (JEAMDL), which is available through the Web at the URL http://www-jt60.naka.jaea.go.jp/english/JEAMDL/index.html. As to the data production, cross sections for various carbon containing molecules, which are produced from carbon-based plasma-facing materials, have been measured [5-3,4]. Charge transfer cross sections of impurity ions produced from the plasma-facing materials: Be, B, C, Cr, Fe and Ni ions, with gaseous atoms and molecules have also been measured [5-5]. Cross sections of state-selective electron capture in collisions of C^{+4} ions with H* (n=2) atoms have been calculated using a molecular-bases close-coupling method [5-6].

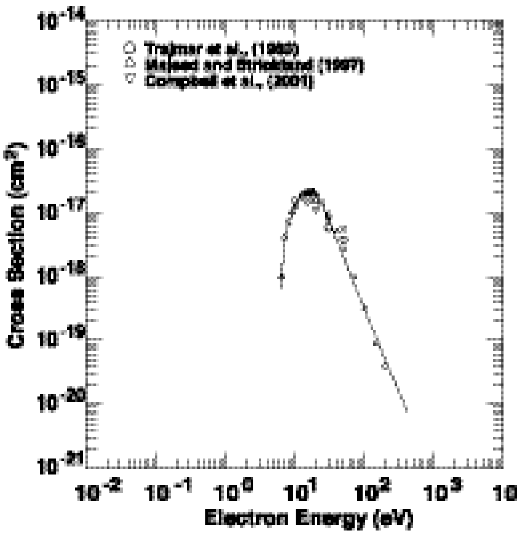

Fig. II.5-1 Cross sections of excitation to A $^3\Sigma_u^+$ for N_2 molecule. The data points indicate the measured cross sections, and the curve indicates an analytical fitting.

Regarding spectral data, wavelengths, energy levels, oscillator strengths, transition probabilities and ionization energies have been critically compiled for tungsten [5-7, 5-8] and gallium [5-9]. Tungsten is one of the candidate plasma-facing materials for future fusion devises, and gallium is a candidate material for liquid divertors.

References

5-1 Kubo, H., *et al.*, "Atomic and Molecular Data Activities for Fusion Research at JAERI," to be published in *J. Plasma Fusion Res.*.

5-2 Tabata, T., *et al.*, *Atomic Data and Nuclear Data Tables,* **92**, 375 (2006).

5-3 Makochekanwa, C., *et al.*, *J. Phys. Chem.,* **124**, 024323 (2006).

5-4 Kusakabe, T., *et al.*, "Cross Sections of Charge Transfer by Slow Doubly-Charged Carbon Ions from Various Carbon Containing Molecules," to be published in *J. Plasma Fusion Res.*.

5-5 Imai, M., *et al.*, "Production and Compilation of Charge Changing Cross Sections of Ion-Atom and Ion-Molecule Collisions," to be published in *J. Plasma Fusion Res.*.

5-6 Shimakura, N., *et al.*, "Electron Capture Processes in Low-Energy Collisions of C^{4+} Ions with Excited H Atoms Using Molecular-Bases Close-Coupling Method," to be published in *J. Plasma Fusion Res.*.

5-7 Kramida, A.E., *et al.*, "Compilation of Wavelengths, Energy Levels, and Transition Probabilities for W I and W II," to be published in *J. Phys. Chem. Ref. Data*.

5-8 Kramida, A.E., *et al.*, "Compilation of Wavelengths and Energy Levels of Tungsten, W III through W LXXIV," to be published in *J. Plasma Fusion Res.*.

5-9 Shirai, T., *et al.,* "Spectral Data for Gallium: Ga I through Ga XXXI," to be published in *J. Phys. Chem. Ref. Data.*

III.FUSION REACTOR DESIGN STUDY

1. Conceptual Design of DEMO Reactor

Fusion DEMO plant is requested to demonstrate 1) an electric power generation of 1GW level, 2) self-sufficiency of T fuel, 3) year-long continuous operation. From the economical aspect, the reactor size should be as compact as ITER. To meet these requirements, a DEMO reactor concept named SlimCS was proposed in 2005 [1-1].

SlimCS produces a fusion output of 2.95GW with a major radius of 5.5m, aspect ratio (A) of 2.6, normalized beta (β_N) of 4.3 and maximum field of 16.4T. The conceptual view is depicted in Fig.III.1-1. It is expected that the zero output at the sending end is obtained at $\beta_N = 2$, $n/n_{GW} = 0.4$ and $f_{BS} = 0.35$ and that a step-by-step power-up eventually attains 1GWe output at $\beta_N = 4.3$, $n/n_{GW} = 1.1$ and $f_{BS} = 0.77$, where n/n_{GW} and f_{BS} are the line-averaged electron density against the Greenwald density and the bootstrap fraction, respectively. SlimCS uses technologies foreseeable in 2020's such as Nb_3Al superconductor, water-cooled solid breeder blanket, low activation ferritic steel F82H as the blanket structural material, and tungsten monoblock divertor plate. Neutron wall load is designed at $3MW/m^2$. Divertor heat flux, which can be a critical issue for such a compact reactor, is mitigated to $10MW/m^2$ at the peak by small inclination (15º) of divertor plates and flux expansion in the divertor region.

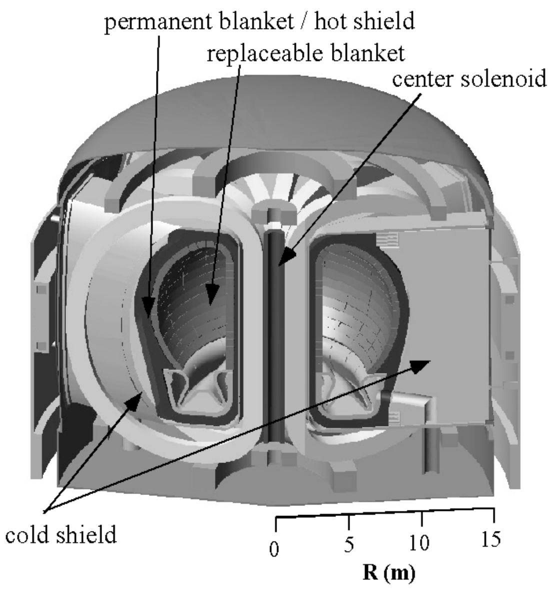

Fig. III.1-1 Conceptual view of SlimCS.

SlimCS can be as compact as advanced commercial reactor designs such as ARIES-RS and CREST (Fig.III.1-2), eIIIen with the assumption of relatively conservative plasma parameters. This is because such a low-A plasma, being stable for higher elongation (κ), can have higher n_{GW} and β_N limits. Another merit of low-A is that the first wall area on the low field side, where smaller electromagnetic (EM) force acts on disruptions, is wide compared with that of conventional-A. This means that tritium can be efficiently breeded with large blanket modules on the low field side. As a result, the demand for tritium breeding on the high field side is comparatively reduced so that small blanket modules, being robust to stronger EM force but less efficient for tritium breeding, can be arranged on the side.

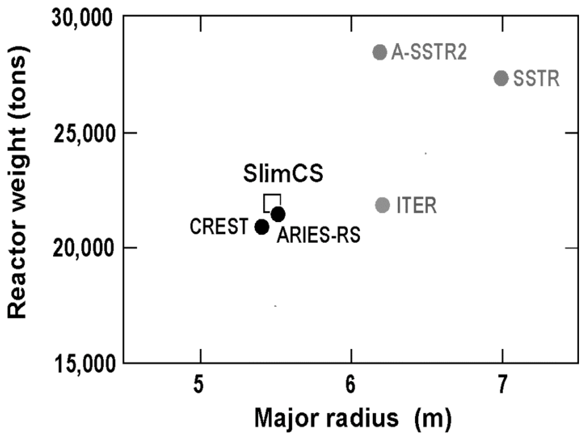

Fig. III.1-2 Comparison of major radius and reactor weight for various fusion reactors.

Reference

1-1 Tobita, K., *et al.*, *Fusion Eng. Des.*, **81**, 1151 (2006).

2. Non-Inductive Current Ramp Simulation

From the practical control aspect of a compact, CS-free tokamak reactor concept "VECTOR", a fully non-inductive, very slow current buildup scenario were investigated via a consistent simulation using Tokamak Simulation Code [2-1, 2-2, 2-3]. The L-mode based, improved core confinement transport model, *e.g.* current diffusive ballooning mode (CDBM), has clarified detailed dynamics of the stable formation of the internal transport barrier (ITB) by non-inductive means of off-axis current sources. First, in accordance with the strong ITB formation, the bootstrap (BS) current was confirmed to substantially increase by more than $f_{bs} > 50\%$ and to enhance the current buildup efficiency, saving a great deal of the driving power of the non-inductive current sources. Second, the integrated, non-inductive scenario was shown to meet the following control and physics requirements set by (a) plasma shaping compatible with recharging of the coil currents, (b) available NB-heating power, (c) avoidance of Current Hole formation under over driving, non-inductive current sources, (d) reasonable HH factor = $t_E/t_{E,y2} < 1.3$ and (e) allowable Greenwald density limit of $n < n_{GW}$. Third, a safe plasma takeoff from limiter to diverter configuration, as well as a safe landing to limiter structures at discharge termination, was also demonstrated. Furthermore, a new operation scenario was computationally examined to control the ITB structure by means of small, but long-duration perturbation (~ 80sec in reactor plasmas) of negative or positive inductive current sources. Thus, the q-profile was first shown to undergo a drastic change over a wide range from positive to negative magnetic shear configuration, and vice versa.

References

2-1 Nakamura, Y., *et al.*, "Simulation Modeling of Fully Non-Inductive Buildup Scenario in High Bootstrap Current Tokamaks without Center Solenoids," *Proc. 32nd EPS Conf. on Plasma Phys.*, P2-051 (2005).

2-2 Nakamura, Y., *et al.,* "Non-Inductive Operation Scenario of Plasma Current Ramp-Down in CS-Less, Advanced Tokamak Reactor," *Proc. 15th International Toki Conf. on "Fusion & Adv. Technol.,"* PS2-22 (2005).

2-3 Nakamura, Y., *et al.,* "Computational Study of Non-Inductive Current Buildup in Compact DEMO Plant with Slim Center Solenoid," *1st IAEA TM on First Generation of Fusion Power Plants -Design and Technology-,* PPCA1-V (2005).

3. Study of Advanced Shield Materials

In general, a hydrogen-rich material has the potential to be an effective neutron shield because the contained hydrogen nuclei work as a moderator of fast neutrons, reducing the fast neutron flux. It is notable that some hydrides have a considerably higher hydrogen content than polyethylene, water and solid hydrogen. The material that we have focused attention on is borohydrides which has been developed for a fuel cell [3-1]. The anticipated hydrogen concentration of $Mg(BH_4)_2$, which will probably be a new candidate shielding material, is as high as 1.32×10^{23} H-atoms/cm^3, surpassing those of already known VH_2 (1.05×10^{23} H-atoms/cm^3) and TiH_2 (9.1×10^{22} H-atoms/cm^3).

In order to assess capability of such hydrides as a advanced shield material, neutronics calculation was carried out for the SlimCS design [3-2]. In the design, the shields are located on the inboard and outboard sides, and originally they were designed to be 30 and 70cm in thickness, respectively, using steel-and-water. When the steel-andwater is replaced with steel-and-hydride, it was found that $Mg(BH_4)_2$, TiH_2 and ZrH_2 could reduce the thickness of the outboard shield by 23, 20 and 19%, respectively. When $Mg(BH_4)_2$ is mixed with ferritc steel (F82H) at the ratio of 1:1, the gamma-ray flux is reduced to 1/300 compared with that for pure $Mg(BH_4)_2$. These results indicates that borohydrides in conbination with steel can work as an attractive shield material for fusion.

References

3-1 Orimo, S., *et al*., *Mater. Sci. Eng.,* B **108**, 51 (2006).

3-2 Hayashi, T., *et al*., *Fusion Eng. Des.,* **81**, 1285 (2006).

Appendix

A.1 Publication List (April 2005 – March 2006)

A.1.1 List of JAERI/JAEA Report

1) Alvani, C., Casadio, S., (Tsuchiya, K.), et al., "Li Depletion Effects on Li_2TiO_3 Reaction with H_2 in Thermo-mechanical Environment Relevant to Breeding Blanket for Fusion Power Plant," JAERI-Review 2005-024 (2005).

2) Department of Fusion Engineering Research and Department of Materials Science, "Achievement of Element Technology Development for Breeding Blanket," JAERI-Review 2005-012 (in Japanese).

3) Department of Fusion Facilities and Department of Fusion Plasma Research, "Progress in JT-60 Innovative Technologies," JAERI-Review 2005-037 (2005) (in Japanese).

4) Honda, A., Okano, F., Ohshima, K., et al., "PLC Control of NBI Cryogenic Facility for JT-60U" JAEA-Technology 2006-020 (2006) (in Japanese).

5) Ida, M., Nakamura, H., Yamamura, T. et al., "Thermal Analysis of IFMIF Target Assembly," JAEA-Technology 2006-003 (2006) (in Japanese).

6) Ida, M., Nakamura, H., Chida, T., et al., "Review of JAEA Activities on the IFMIF Liquid Lithium Target in FY2005," JAEA-Review 2006-009 (2006).

7) IFMIF International Team, "Minutes of the IFMIF Technical Meetings May 17-20, 2005 Tokyo, Japan," JAERI-Review 2005-027 (2005).

8) JT-60 Team., "Review of JT-60U Experimental Results in 2003 and 2004," JAEA-Review 2005-005 (2005).

9) Kikuchi, K., Akino, N., Ikeda, Y., et al., "Characteristics of Voltage Holding and Outgassing on the Accelerator of JT-60 N-NBI Ion Source," JAEA-Technology 2006-016 (2006) (in Japanese).

10) Kondo, K., Ochiai, K., Kubota, N., et al., "Development of Measurement Technique for Charged-particle Emission Double-differential Cross section using Pencil-beam Neutron Source," JAEA-Research 2006-016 (2006).

11) Nakamichi, M., Kawamura, H., "An Irradiation Experiment for Qualification of Insulating Coating," JAERI-Research 2005-015 (2005).

12) Nishitani, T., Yamauchi, M., Izumi, M., et al., "Design of Micro Fission Chambers for ITER Low Power Operations," JAERI-Tech 2005-047 (2005).

13) Obara, K., Kakudate, S., Yagi, T., et al., "Continuous Running Test of Radiation Residence Motor Driving Equipment under High Gamma Irradiation," JAEA-Technology 2006-023 (2006) (in Japanese).

14) Ogawa, H., Sugie, T., Katsunuma, A., et al., "Design of Impurity Influx Monitor (Divertor) for ITER," JAEA-Technology 2006-015 (2006).

15) Ohmori, J., Nakahira, M., Takeda, N., et al., "Applicability Assessment of Plug Weld to ITER Vacuum Vessel by Crack Propagation Analysis," JAEA-Technology 2006-017 (2006).

16) Sato, K., Hashimoto, M., Nagamatsu, N., et al., "Study of the Layout Plan in the Tokamak Complex Building for ITER," JAEA-Technology (2006) (in Japanese).

17) Sato, K., Uehara, M., Tamura, K., et al., "Study of Site Layout in the Rokkasho Site," JAEA-Technology 2006-024 (2006) (in Japanese).

18) Sato, S., Yamauchi, M, Nishitani, T., et al., "Analysis of Heat Load in ITER NBI Duct and Neutron Streaming through Pressure Relief Line," JAEA-Technology 2006-032 (2006).

19) Sueoka, M., Suzuki, T., Hosoyama, H., "Development of a Profile Control System for the JT-60 Plasma Equilibrium Control," JAEA-Technology 2006-022 (2006) (in Japanese).

20) Takeda, N., Kakudate, S., Nakahira, M., et al., "Study on Compact Design of Remote Handling Equipment for ITER Blanket Maintenance," JAEA-Technology 2006-025 (2006).

21) Tsuchiya, K., Kawamura, H., Nagao, Y., “Breeding Blanket Development -Tritium Release from Breeder-,” JAEA-Technology 2005-003 (2005).

22) Tsuchiya, K., Kawamura, H., Nakamichi, M., “Fabrication Test and Characterization of Lithium Zirconate Pebbles Fabricated by a Rotating Granulation Method,” JAEA-Technology 2006-002 (2006)(in Japanese).

23) Uehara, K., and Nagashima, T., “Current Profiles and Major Disruptions in a Lower-Hybrid Current Drive Tokamak,” JAEA-Research 2006-002 (2006).

24) Watanabe, K., Takayanagi, T., Okumura, Y., et al., “H^- Ion Beam Acceleration in a Single Gap Multi-Aperture Accelerator,” JAEA-Technology 2005-002 (2006).

25) Yamada, H., Kawamura, H., “Neutron Irradiation Test of Copper Alloy/Stainless Steel Joint Materials,” JAEA-Technology 2005-001 (2005).

26) Yamaki, D., Nakazawa, T., Tanifuji, T., et al., “Observation of Microstructural Changes in Li_2TiO_3 Caused by Multi-ion Beam Irradiation,” JAEA-Review 2005-001, 212 (2006).

27) Yamamoto, M., Okano., F., Tsuzuki, K., et al., “The development of the boron coating device for the JFT-2M,” JAERI-Tech 2005-061(2005).

28) Yamamoto, M., Tsuzuki, K., Kimura, H., et al., “The development of the device for 3D-Measurement of the Magnetic Field Profile in the Toroidal Direction,” JAERI-Tech 2005-060(2005).

29) Yutani, T., Nakamura, H., Sugimoto, M., “Compatibility of Reduced Activation Ferritic/ Martensitic Steel Specimens with Liquid Na and NaK in Irradiation Rig of IFMIF,” JAERI-Tech 2005-036 (2005).

A.1.2 List of papers published in journals

1) Akino, N., Ebisawa, N., Honda, A., et al., “Long Pulse Operation of NBI Systems for JT-60U,” Fusion Sci. Technol., **47** 758 (2005).

2) Amemiya, H., and Uehara, K., “Method for Detection of Separatrix Surface Using Differential Double Probe,” Jpn. J. Appl. Phys., **45**, 247 (2006).

3) Angelone, M., Pillon, M., (Ochiai, K.), et al., “Radiation Hardness of a Polycrystalline Chemical-Vapor-Deposited Diamond Detector Irradiated with 14 MeV Neutrons,” Rev. Sci. Instrum. **77**, 23505 (2006).

4) Asai, K., Iguchi, T., (Nishitani, T.), et al., “Improved In-situ Calibration Technique for ITER Ex-Vessel Neutron Yield Monitor,” Fusion Eng. Des., **81**, 1497 (2006).

5) Bakhtiari, M., Kramer, G. J., (Kusama, Y.), et al., “Role of Bremsstrahlung Radiation in Limiting the Energy of Runaway Electrons in Tokamaks,” Phys. Rev. Lett., **94**, 215003 (2005).

6) Bakhtiari, M., Tamai, H., (Kawano, Y.), et al., “Study of Plasma Termination using High-Z Noble Gas Puffing in the JT-60U Tokamak,” Nucl. Fusion, **45**, 318 (2005).

7) Batistoni, P., Angelone, M., (Ochiai, K.), et al., “International Comparison of Measuring Techniques of Tritium Production for Fusion Neutronics Experiments Status and Preliminary Results,” Fusion Eng. Des., **75-79**, 911 (2005).

8) Baylor, L.R., Combs, S.K., (Maruyama, S.), et al., “Pellet Fueling Technology Development Leading to Efficient Fueling of ITER Burning Plasmas,” Physics of Plasmas, **12**, 056103 (2005).

9) Combs, S. K., Baylor, L. R., (Maruyama, S.), et al., “Pellet Delivery and Survivability through Curved Guide Tubes for Fusion Fueling and its Implication for ITER,” Fusion Eng. Des., **75-79**, 691 (2005).

10) Cordey, J.G. , Thomsen, K. , (Takizuka, T.), et al. , “Scaling of the Energy Confinement Time with β and Collisionality Approaching ITER Conditions,” Nucl. Fusion, **45**, 1078 (2005).

11) Costley,A.E., Sugie,T., Vayakis,G., et al., “Technological Challenges of ITER Diagnostics,” Fusion Eng. Des., **74**, 109 (2005).

12) Donne, A.J.H, Fasoli, J., (Ozeki, T.), et. al., “Summary of the International Energy Agency Workshop on Burning Plasma Physics and Simulation”, Fusion Sc. Technol., **49**, 79 (2006).

13) Elio, F., Ioki, K., Utin, Y., et al., “Special Blanket Design in the NB Region of ITER,” Fusion Eng. Des., **75-79**, 601 (2005).

14) Enoeda, M., Akiba, M., Tanaka, S., et al., “Overview of Design and R&D of Test Blankets in Japan,” Fusion Eng. Des., **81**, 415 (2006).

15) Enoeda, M., Akiba, M., Tanaka, S., et al., “Plan and Strategy for ITER Blanket Testing in Japan,” Fusion Sci. Technol., **47**, 1023 (2005).

16) Enoeda, M., Hatano, T., Tsuchiya, K., et al., “Development of Solid Breeder Blanket at JAERI,” Fusion Sci. Technol., **47**, 1060 (2005).

17) Ezato, K., Suzuki, S., Dairaku, M., et al., “Critical Heat Flux Testing on Screw Cooling Tube made of RAFM-Steel F82H for Divertor Application,” Fusion Eng. Des., **75-79**, 313 (2005).

18) Ezato, K., Suzuki, S., Dairaku, M., et al., “Experimental Examination of Heat Removal Limitation of Screw Cooling Tube at High Pressure and Temperature Conditions,” Fusion Eng. Des., **81**, 347 (2006).

19) Fujii, T. and JT-60 Team, “Operational Progress of the 110GHz-4MW ECRF Heating System in JT-60U,” J. Physics, **25**, 45 (2005).

20) Fujita, T., Suzuki, T., Oikawa, T., et al., “Current Clamp at Zero Level in JT-60U Current Hole Plasmas,” Phys. Rev. Lett., **95**, 075001 (2005).

21) Fujita, T. and the JT-60 team, “Steady State Operation Research in JT-60U with Extended Pulse Length,” Nucl. Fusion, **46**, S3 (2006).

22) Furukawa, M. and Tokuda, S., “Mechanism of Stabilization of Ballooning Modes by Toroidal Rotation Shear in Tokamaks,” Phys. Rev. Lett., **94**, 175001 (2005).

23) Furukawa, M., Yoshida, Z. and Tokuda, S., “Regularization of Singular Eigenfunctions of an Operator with Continuous Spectra: with Applications for Ballooning Modes in Toroidally Rotating Tokamaks,” Phys. Plasmas, **12**, 072517 (2005).

24) Giancarli, L., Chuyanov, V., (Akiba, M.), et al.,” Breeding Blanket Modules Testing in ITER: An International Program on the Way to DEMO,” Fusion Eng. Des., **81**, 393 (2006).

25) Hagiwara, M., Itoga, T., (Sugimoto, M.), et al., “Measurement of Neutron Emission in Li(d,xn) Reaction with Thick and Thin Targets for 40-MeV Deuterons,” Fusion Sci. Eng., **48**, 1320 (2005).

26) Hamada, K., Nakajima, H., Takano, K., et al., “Fatigue Assessments of the ITER TF Coil Case based on; JJ1 Fatigue Tests,” Fusion Eng. Des., **75**, 87(2005)

27) Hanada, M., Seki, T., Takado, N., et al, “Experimental Study on Spatial Uuniformity of H- Ion Beam in a Large Negative Ion Source,” Fusion Eng. Des., **74**, 311 (2005).

28) Hayashi, N., Takizuka, T., Ozeki, T., “Profile Formation and Sustainment of Autonomous Tokamak Plasma with Current Hole Configuration,” Nucl. Fusion, **45**, 933 (2005).

29) Hayashi, T., Ochiai, K., Masaki, K., et al., “Deuterium depth profiling in JT-60U W-shaped divertor tiles by nuclear reaction analysis,” J. Nucl. Mater., **349**, 6 (2006).

30) Hayashi, T., Tobita, K., Nishio, S., et al., “Neutronics Assessment of Advanced Shield Materials Using Metal Hydride and Boron hydride for Fusion Reactors,” Fusion Eng. Des., **81**, 1285 (2006).

31) Hayashi, T., Itoh, T., Kobayashi, K., et al., “Safety Handling Characteristics of High-Level Tritiated Water,” Fusion Eng. Des., **81**, 1365 (2006).

32) Hayashi, T., Suzuki, T., Yamada, M., et al., “Tritium Accounting Stability of a ZrCo Bed with “in-bed” Gas Flowing Calorimetry,” Fusion Sci. Technol., **48**, 317 (2005).

33) Hegeman, J. B. J., van der Laan, J. G., Kawamura, H., et al., “The HFR Petten High Dose Irradiation Programme of Beryllium for Blanket Application,” Fusion Eng. Des., **75-79,** 769 (2005).

34) Hino, T., Yoshida, H., Akiba, M., et al., “Deutrium Retention in Carbon flakes and Tungsten-Carbon mixed flakes produced by Deuterium Arc Discharge,” Nucl. Fusion, **45**, 893 (2005).

35) Hirai, T., Ezato, K., Majerus, P., “ITER Relevant High Heat Flux Testing on Plasma Facing Surfaces,” Mater. Trans., **46-3**, 412 (2005).

36) Hirohata, Y., Shibahara T., (Arai, T.), et al., “Retention of hydrogen isotopes in divertor tiles used in JT-60U,” Fusion Sci. Technol.,**48**, , 557(2005).

37) Hirohata, Y., Shibahara, T., (Arai, T.), et al., “Hydrogen Retention in Divertor Tiles in JT-60 for Hydrogen Discharge Period,” J. Nucl. Mater., **337-339**, 609 (2005).

38) Hirose, T., Shiba, K., Ando, M., et al., “Joining Technologies of Reduced Activation Ferritic/Martensitic Steel for Blanket Fabrication,” Fusion Eng. Des., **81**, 645 (2006).

39) Hoshino, K., Yamamoto, T., Tamai, H., et al., “Heating, Current Drive, and Advanced Plasma Control in JFT-2M,” Fusion Sci. Technol., **49**, 139 (2006).

40) Hoshino, T., Tsuchiya, K., Hayashi, K., et al, “Non-stoichiometry of Li_2TiO_3 under Hydrogen Atmosphere Condition,” Fusion Eng. Des., **75-79**, 939 (2005).

41) Hoshino, T., Yasumoto, M., Tsuchiya, K., et al., “Vapor Species Evolved from Li_2TiO_3 Heated at High Temperature under Various Conditions,” Fusion Eng. Des., **81**, 555 (2005).

42) Ichimasa, M., Awagakubo, S., Takahashi, M., et al., “Tritium Elimination Syatem Using Tritium Gas Oxidizing Bacteria,” Fusion Sci. Technol., **48**, 759 (2005).

43) Ida, M., Nakamura, H., Shimizu, K., et al., “Thermal and Thermal-Stress Analyses of IFMIF Liquid Lithium Target Assembly,” Fusion Eng. Des., **75-79**, 847 (2005).

44) Ide, S., and the JT-60 team, “Long Pulse Operation of High Performance Plasmas in JT-60U,” Plasma Sci. Technol., **8**, 1 (2006).

45) Ide, S., and the JT-60 team, “Overview of JT-60U Progress towards Steady-State Advanced Tokamak,” Nucl. Fusion, **45**, S48 (2005).

46) Ido, T., Miura, Y., Hoshino, K., et al., “Observation of the Interaction between the Geodesic Acoustic Mode and Ambient Fluctuation in the JFT-2M Tokamak,” Nucl. Fusion, **46**, 512 (2006).

47) Ido, T., Miura, Y., Kamiya, K., et al., “Geodesic-Acoustic-Mode in JFT-2M Tokamak Plasmas,” Plasma Phys. Control. Fusion, **48**, S41 (2006).

48) Idomura, Y., Tokuda, S. and Kishimoto, Y., “Global Profile Effects and Structure Formations in Toroidal Electron Temperature Gradient Driven Turbulence,” Nucl. Fusion, **45**, 1571 (2005).

49) Iida, H., Petrizzi, L., Khripunov, V., et al., “Nuclear Analyses of Some Key Aspects of the ITER Design with Monte Carlo Codes,” Fusion Eng. Des., **74**, 133 (2005).

50) Imbeaux, F., Artaud, J. F., (Fujita, T.), et al., “Multi-machine transport analysis of hybrid discharges from the ITPA profile database,” Plasma Phys. Control. Fusion, **47**, B179 (2005).

51) Inagaki, S., Takenaga, H., Ida, K., et al., “Comparison of Transient Electron Heat Transport in LHD Helical and JT-60U Tokamak Plasmas,” Nucl. Fusion, **46**, 133 (2006).

52) Inoue, T., Hanada, M., Kashiwagi, M., “Design Study of a Neutral Beam Injector for Fusion DEMO Plant at JAERI,” Fusion Eng. Des., **81**, 1291 (2006).

53) Inoue, T., Taniguchi, M., Morishita, T., et al., “R&D on a Hhigh Energy Accelerator and a Large Negative Ion Source for ITER,” Nucl. Fusion **45**, 790 (2005).

54) Ioki, K., Elio, F., Maruyama, S., et al., “Selection of Design Solutions and Fabrication Methods and Supporting R&D for Procurement of ITER Vessel and FW/Blanket,” Fusion Eng. Des., **74**, 185 (2005).

55) Ioki, K., Elio, F., Nakahira, M., et al., “Recent Progress of ITER FW/Blanket Design and Preparations for Fabrication,” Fusion Eng. Des., **81**, 443 (2006).

56) Isayama, A. and the JT-60 Team, “Steady-State Sustainment of High-β Plasmas through Stability Control in Japan Atomic Energy Research Institute Tokamak-60 Upgrade,” Phys. Plasmas, **12**, 056117 (2005).

57) Isayama, A. and the JT-60 Team, “Suppression of Neoclassical Tearing Modes towards Stationary High-Beta Plasmas in JT-60U,” Plasma Sci. Technol., **8**, 36 (2006).

58) Isayama, A., Inagaki, S., Watanabe, K.Y., “Observation of Localized Oscillations at m/n=2/1 Rational Surface during Counter Neutral Beam Injection in the Large Helical Device,” Plasma Phys. Control. Fusion, **48**, L45 (2006).

59) Ishikawa, M., Takechi, M., Shinohara, K., et al., “Energetic Ion Transport by Abrupt Large-Amplitude Event Induced by Negative-Ion-Based Neutral Beam Injection in the JT-60U,” Nucl. Fusion, **45**, 1474 (2005).

60) Ishikawa. M., Takechi, M., (Nishitani, T.), et al., “Energetic Ion Transport by Abrupt Large-Amplitude Event Induced by Negative-Ion-Based Neutral Beam Injection in the JT-60U,” Nucl. Fusion, **45**, 1474 (2005).

61) Isobe, K., Nakamura, H., Kaminaga, A., et al., “Characterization of JT-60U Exhaust Gas during Experimental Operation,” Fusion Eng. Des., **81**, 827 (2006).

62) Isono, T., Koizumi, N., Okuno, K., et al., “Design Study of Superconducting coils for the Fusion DEMO Plant at JAERI,” Fusion Eng. Des., **81**, 1257 (2006)

63) Iwai, Y., Hayashi, T., Kobayashi, K., et al., “Case Study on Unexpected Tritium Release Happened in a Ventilated Room of Fusion Reactor,” Fusion Sci. Technol., **48**, 460 (2005).

64) Iwai, Y., Yamanishi, T., Hayashi, T., et al., “Study on Tritium Removal Performance by Gas Separation Membrane with Reflux Flow for Tritium Removal System of Fusion Reactor,” Fusion Sci. Technol., **48**, 456 (2005).

65) Iwai, Y., Yamanishi, T., Isobe, K., et al., “Distinctive radiation durability of ion exchange membrane in SPE water electrolyzer for ITER water detritiation system,” Fusion Eng. Des., **81**, 815 (2006).

66) Iwai, Y., Yamanishi, T., Nishi, M., et al., “Application of Pressure Swing Adsorption to Water Detritiation Process,” J. Nucl. Sci. Technol., **42**, 566 (2005).

67) Iwai, Y., Yamanishi, T., Nishi, M., et al., “Durability of Irradiated Polymers in Solid-Polymer-Electrolyte Water Electrolyzer,” J. Nucl. Sci. Technol., **42**, 636 (2005).

68) Joffrin, E., Sips, A.C.C, (Isayama, A.), et al., "The 'Hybrid' Scenario in JET: towards Its Validation for ITER," Nucl. Fusion, **45**, 626 (2005).

69) Jones, L., Bianchi, A., (Ioki, K.), et al., "ITER Vacuum Vessel Sector Manufacturing Development in Europe," Fusion Eng. Des., **75-79**, 607 (2005).

70) Kajijta, S., Ohno, N., Takamura, S., et al., "Comparison of He I Line Intensity Ratio Method and Electrostatic Probe for Electron Density and Temperature Measurements in NAGDIS-II," Phys. Plasmas, **13**, 013301 (2006).

71) Kajiwara, K. and JT-60 Team, "Electron Cyclotron Heating Assisted Startup in JT-60U," Nucl. Fusion, **45**, 694 (2005).

72) Kamada, Y., Oyama, N., Ide, S., et al., "Impact of the Edge Pedestal Characteristics on the Integrated Performance in Advanced Tokamak Operation Modes on JT-60U," Plasma Phys. Control. Fusion, **48**, A419 (2006).

73) Kamiya, K., Kawashima, H., Ido, T., et al., "Reduced Divertor Heat Loads, Plasma Shape Effects, and Radial Electric Field Structures in JFT-2M HRS H-mode Plasmas," Nucl. Fusion, **46**, 272 (2006).

74) Kamiya, K., Oyama, N., Ido, T., et al., "Characterization of Coherent Magnetic Fluctuations in JFT-2M High Recycling Steady High-Confinement Mode Plasmas," Phys. Plasmas, **13**, 032507 (2006).

75) Kaneko, J., Tanaka, T., (Ochiai, K.), et al., "Radiation Detector Made of a High-Quality Polycrystalline Diamond," Diamond & Related Materials, **14**, 2027 (2005).

76) Kasai, S., Kamiya, K., Shinohara, K., et al., "Plasma Diagnostics in JFT-2M," Fusion Sci. Technol., **49**, 225 (2006).

77) Kawamura, Y., Enoeda, M., Yamanishi, T., et al., "Feasibility Study on The Blanket Tritium Recovery System Using The Palladium Membrane Diffuser," Fusion Eng. Des., **81**, 809 (2006).

78) Kawamura, Y., Iwai, Y., Nakamura, H., et al., "Tritium Recovery from Solid Breeder Blanket by Water Vapor Addition to Helium Sweep Gas," Fusion Sci. Technol., **48**, 654 (2005).

79) Kawano, Y., Nakano, T., Asakura, N., et al., "Electron Density Behavior during Fast Termination Phase of Post-Disruption Runaway Plasma," J. Plasma Fusion Res., **81**, 743 (2005).

80) Kawano, Y., Nakano, T., Isayama, A., et al., "Characteristics of Post-disruption Runaway Electrons with Impurity Pellet Injection," J. Plasma Fusion Res., **81**, 593 (2005).

81) Kawashima, H., Sakurai, S., Shimizu, K., et al., "Divertor Modeling for the Design of the National Centralized Tokamak with High Beta Steady-State Plasmas," Fusion Eng. Des., **81**, 1613 (2006).

82) Kawashima, H., Shimizu, K., Takizuka, T., et al., "Development of Integrated SOL/Divertor code and Simulation Study in JAEA," Plasma and Fusion Res., **1**, 031 (2006).

83) Kawashima, H., Sengoku, S., Uehara, K., et al., "Study of SOL/Divertor Plasmas in JFT-2M," Fusion Sci. Technol., **49**, 168 (2006).

84) Khomyakov, S., Elio, F., Ioki, K., et al., "Dynamic Amplification of Reaction Forces in the Blanket Module Attachment during Plasma Disruption of ITER," Fusion Eng. Des., **81**, 485 (2006).

85) Kikuchi, M., Nishio, S., Kurita, G., et al., "Blanket–Plasma Interaction in Tokamaks: Implication from JT-60U, JFT-2M and Reactor Studies," Fusion Eng. Des., **81**, 1589 (2006).

86) Kimura, A., Kasada, R., (Jitsukawa, S.), et al., "Ferritic steel-blanket systems integration R&D - Compatibility Assessment," Fusion Eng. and Des., **81**, 909 (2006)

87) Kinjyo, T., Nishikawa, M., (Enoeda, M.), et al., "Introduction of Tritium Transfer Step at Surface Layer of Breeder Grain for Modeling of Tritium Release Behavior from Solid Breeder Materials," Fusion Eng. Des., **81**, 573 (2006).

88) Kishimoto, H., Ishida, S., Kikuchi, M., et al., "Special Topic: Advanced Tokamak Reseach on JT-60," Nucl. Fusion, **45**, 986 (2005).

89) Klix, A., Verzilov, Y., Nishitani, T., et al., "Tritium Breeding Experiments with Blanket Mock-ups Containing ^{6}Li-Enriched Lithium Titanate and Beryllium Irradiated with DT Neutrons," Fusion Eng. Des., **75-79**, 881 (2005).

90) Kobayashi, K., Hayashi, T., Nishi, M., et al., “Sorption and Desorption of Tritiated Water on Four Kind of Materials for ITER,” Fusion Eng. Des., **81**, 1379 (2006).

91) Kobayashi, K., Terada, O., Miura, H., et al., “The Oxidation Performance Test of Detritiation System under Existence of CO and CO_2,” Fusion Sci. Technol., **48**, 476 (2005).

92) Kohyama, A., Abe, K., (Jitsukawa, S.), et al., “Recent Accomplishments and Future Prospects of Materials R & D in Japan,” Fusion Sci. and Technol., **47**, 836 (2005).

93) Koizumi, N., Matsui, K., Kume, K., et al., “Rapid Normal Zone Propagation Observed in a 13T-46kA Nb_3Al Cable-in-Conduit Conductor,” IEEE Trans. ASC, **15**, 1363 (2005).

94) Koizumi, N., Takeuchi, T., Okuno, K., “Development of Advanced Nb_3Al Superconductors for a Fusion DEMO Plant,” Nucl. Fusion, **45**, 431 (2005).

95) Kondo, H., Fujisato, A. (Nakamura, H.), et al., “Surface Wave on High Speed Liquid Lithium Flow for IFMIF,” Fusion Eng. Des., **75-79**, 865 (2005).

96) Kondo, H., Fujisato, A., (Nakamura, H.), et al., “Experimental Study of Lithium Free-Surface Flow for IFMIF Target Design,” Fusion Eng. Des., **81**, 687 (2006).

97) Kondo, K., Takagi, S., Murata, I., et al., “New Approach to Measure Double-Differential Charged-Particle Emission Cross Sections of Several Materials for A Fusion Reactor,” Fusion Eng. Des., **81**, 1527 (2006).

98) Konovalov1, S.V., Mikhailovskii1, A.B., Ozeki, T., et al., “Role of Anomalous Transport in Onset and Evolution of Neoclassical Tearing Modes,” Plasma Phys. Control. Fusion, **47**, B223 (2005).

99) Krasilnikov, A., Sasao, M., (Nishitani, T.), et al., “Status of ITER Neutron Diagnostic Development,” Nucl. Fusion, **45**, 1503 (2005).

100) Kubo, H. and the JT-60 Team, “Study of Particle Behavior for Steady-State Operation in JT-60U,” Plasma Sci. Technol., **8**, 50 (2005).

101) Kubota, N., Ochiai, K., Kutsukake, C., et al., “Beam Analyses of Hydrogen Isotopes for the TFTR Tiles used in the D-T Experiment,” Fusion Eng. Des., **81**, 227 (2006).

102) Kulsartov, T. V., Hayashi, K., Nakamichi, M., et al., “Investigation of Hydrogen Isotope Permeation through F82H Steel with and without a Ceramic Coating of Cr_2O_3-SiO_2 Including $CrPO_4$ (Out-of-Pile Tests),” Fusion Eng. Des., **81**, 701 (2005).

103) Kurihara, K., Kawamata, Y., Sueoka, M., et al., “The Basic Methods for Understanding of Plasma Equilibrium toward Advanced Control,” Fusion Eng. Des., **74**, 527 (2005).

104) Kurita, G., Bialek, J., Tuda, T., et al., “Critical β Analyses with Ferromagnetic and Plasma Rotation Effects and Wall Geometry for a High β Steady State Tokamak,” Nucl. Fusion, **46**, 383 (2006).

105) Kusama, Y. and JFT-2M group, “JFT-2M Program,” Fusion Sci. Technol., **49**, 89 (2006).

106) La Haye, R.J., Prater, R., (Isayama, A.), et al., “Cross-Machine Benchmarking for ITER of Neoclassical Tearing Mode Stabilization by Electron Cyclotron Current Drive,” Nucl. Fusion, **46**, 451 (2006).

107) Li, J. Q., Kishimoto, Y., Dong, J. Q., et al., “Dynamics of Secondary Large-scale Structure in ETG Turbulence Simulations,” Plasma Sci. and Technol., **8**, 1 (2006).

108) Lorenzetto, P., Boireau, B., (Ioki, K.), et al., “Manufacture of Blanket Shield Modules for ITER,” Fusion Eng. Des., **75-79**, 291 (2005).

109) Lorenzetto, P., Peacock, A., (Ioki, K.), et al., “EU R&D on the ITER First Wall,” Fusion Eng. Des., **81**, 355 (2006).

110) Lukash, V., Sugihara, M., Gribov, Y., et al., “Analysis of the Direction of Plasma Vertical Movement during Major Disruptions in ITER,” Plasma Phys. Control. Fusion, **47**, 2077 (2005).

111) Luo, G.–N., Shu, W.M. and Nishi, M.F., “Incident Energy Dependence of Blistering at Tungsten Irradiated by Low Energy High Flux Deuterium Plasma Beams,” J. Nucl. Mater., **347**, 111 (2005).

112) Luo, G.–N., Shu, W.M. and Nishi, M.F., “Influence of Blistering on Retention in W Irradiated by High Flux Deuterium Plasmas of Tens of eV,” Fusion Eng. Des., **81**, 957 (2006).

113) Maebara, S., Moriyama, S., Saigusa, M., et al., “Power-Balance Control by Slug Tuner for the 175MHz Radio-Frequency Quadrupole (RFQ) Linac in IFMIF Project,” Fusion Sci. Technol., **47**, 941 (2005).

114) Maebara, S., Moriyama, S., Saigusa, M., et al., “Development of an RF-Input Coupler with a Multi-Loop Antenna for the RFQ Linac in IFMIF Project,” Fusion Eng. Des., **75-79**, 823 (2005).

115) Makochekanwa, C., Kato, H., Hoshino, M., et al., “Experimental and Theoretical Clastic Cross Sections for Electron Collisions with the C_3H_6 Isomers,” J. Phys. Chem., **124**, 024323 (2006).

116) Masaki, K., Sugiyama, K., Hayashi, T., et al., “Retention Characteristics of Hydrogen Isotopes in JT-60U,” J. Nucl. Mater., **337-339**, 553 (2005).

117) Matsuhiro, K., Nakamura, H., Hayashi, T., et al., “Evaluation of Tritium Permeation from Lithium Loop of IFMIF Target System,” Fusion Sci. Technol., **48**, 625 (2005).

118) Matsumoto, T., Naitou, H., Tokuda, S., et al., “Nonlinear Acceleration of the Electron Inertia-Dominated MHD Modes due to Electron Parallel Compressibility,” Phys. Plasmas, **12**, 092505-1-7(2005).

119) Matsumoto, T., Naitou, H., Tokuda, S., et al., “Nonlinear Behaviors of Collisionless Double Tearing Mode induced by Electron Inertia,” Nucl. Fusion, **45**, 1264 (2005).

120) Miyato, N., Li, J. Q. and Kishimoto, Y., “Study of a Drift Wave-Zonal Mode System Based on Global Electromagnetic Landau-fluid ITG Simulation in Toroidal Plasmas,” Nucl. Fusion, **45**, 425 (2005).

121) Moeslang, A., Heinzel, V., (Sugimoto, M.), et al., “The IFMIF Test Facilities Design,” Fusion Eng. Des., **81**, 863 (2006).

122) Mori, M., “Japanese activities in ITER Transitional Arrangements,” Fusion Eng. Des., **81**, 69 (2006).

123) Morioka, A., Nishimura, S., Muroga, T., et al., “Nuclear Technology and Potential Ripple Effect of Superconducting Magnets for Fusion Power Plant,” Fusion Eng. Des., **81**, 1675 (2006).

124) Morioka, A., Sakurai, S., Okuno, K., et al., “Development of a Heat-Resistant Neutron Shielding Resin for the National Centralized Tokamak,” J. Plasma Fusion Res., **81**, 645 (2005).

125) Moriyama, S. and JT-60 Team, “Conpact Antenna for Tow-Dimensional Beam Scan in the JT-60U Electron Cyclotron Heating /Current Drive System,” Rev. Sci. Instrum., **76**, 113504-1 (2005).

126) Moriyama, S. and JT-60 Team, “Development and Contribution of RF Heating and Current Drive System to Long Pulse, High Performance Experiments in JT-60U,” Fusion Eng. Des., **74**, 343 (2005).

127) Moriyama, S. and Shinozaki, S., “Concept and Results of New Operation Scheme with Improved Control System for Radio Frequency Heating in JT-60U,” Jpn. J. Appl. Phys., **44**, 6224 (2005).

128) Munakata, K., Kawamura, H., Uchida, M., “Reaction of Titanium Beryllide with Water Vapor,” Fusion Eng. Des., **75-79,** 997 (2005).

129) Murata, I., Yamamoto, Y., (Kondo, K.), et al., “Fusion-Driven Hybrid System with ITER Model,” Fusion Eng. Des., **75-79**, 871 (2005).

130) Nagao, Y., Tsuchiya, K., Ishida, T., et al., “Development of Tritium Production M for In-Pile Tests of Fusion Blanket in the JMTR,” Fusion Eng. Des., **81**, 619 (2006).

131) Nagasaki, K., Isayama, A., Hayashi, N., et al., “Stabilization of Neoclassical Tearing Mode by ECCD and Its Evolution Simulation on JT-60U Tokamak,” Nucl. Fusion, **45**, 1608 (2005).

132) Nagashima, Y., Hoshino, K., Ejiri, A., et al., “Observation of Nonlinear Coupling between Small-Poloidal Wave-Number Potential Fluctuations and Turbulent Potential Fluctuations in Ohmically Heated Plasmas in the JFT-2M Tokamak,” Phys. Rev. Lett., **95**, 095002-1(2005).

133) Nagashima, Y., Itoh, K., Itoh, S-I., et al., “Bispectral Analysis Applied to Coherent Floating Potential Fluctuations Obtained in the Edge Plasmas on JFT-2M,” Plasma Phys. Control. Fusion, **48**, S1 (2006).

134) Nagata, M., Ogawa, H., Yatsu, S., et al., “Experimental Studies of the Dynamics of Compact Toroid Injected into the JFT-2M Tokamak,” Nucl. Fusion, **45**, 1056 (2005).

135) Nakamura, H., Hayashi, T., Kobayashi K., et al., “Evaluation of Tritium Behavior in the Epoxy Painted Concrete wall of ITER Hot Cell,” Fusion Sci. Technol., **48**, 452 (2005).

136) Nakamura, H., Sakurai, S., Suzuki, S., et al., “Case Study on Tritium Inventory in the Fusion DEMO Plant at JAERI,” Fusion Eng. Des., **81**, 1339 (2006).

137) Nakamura, H., Takemura, M., Yamauchi, M., et al., “Accessibility Evaluation of the IFMIF Liquid Lithium Loop Considering Activated Erosion/Corrosion Materials Deposition,” Fusion Eng. Des., **75-79**, 1169 (2005).

138) Nakano, T., Koide, Y., Honda, A., et al., “Relation Between the Oxygen Contents in the Neutral Beam and in the Core Plasma in JT-60U,” J. Plasma Fusion Res., **81**, 708 (2005).

139) Nishi, H., “Notch Toughness Evaluation of Diffusion-Bonded Joint of Alumina Dispersion- strengthened Copper to Stainless Steel,” Fusion Eng. Des., **81**, 269 (2006).

140) Ninomiya, H., “Conference Summary: Progress in Experiments on Confinement, Plasma-Material Interactions and Innovative Confinement Concepts,” Nucl. Fusion, **45**, 513 (2005).

141) Nishi, M., Yamanishi, T., Hayashi, T., et al., “Study on Tritium Accountanct in Fusion DEMO Plant at JAERI,” Fusion Eng. Des., **81**, 745 (2006).

142) Nishimura, A., Hishinuma, Y., (Okuno, K.), et al., “14 MeV Neutron Irradiation Effect on Superconducting Magnet Materials for Fusion Device,” Adv. Cryog. Eng. (Material), **52**, 208 (2006).

143) Nishimura, A., Hishinuma, Y., Tanaka, T., et al., “Design, Fabrication and Installation of Cryogenic Target System for 14 MeV Neutron Irradiation on Superconducting Magnet Materials,” Fusion Eng. Des., **75-79**, 173 (2005).

144) Nishimura, A., Muroga, T., (Nishitani, T.), et al., “Nuclear Technology of Superconducting Magnet for Fusion Power Plant and Potential Ripple Effect,” Fusion Eng. Des., **81**, 1675 (2006).

145) Nishio, S., Enoeda, M., Tobita, K., et al, “Consideration on Blanket Structure for Fusion DEMO Plant at JAERI,” Fusion Eng. Des., **81**, 1271 (2006).

146) Nishio, S., Ohmori, J., Kuroda, T., et al, “Consideration on Blanket Structure for Fusion DEMO Plant at JAERI,” Fusion Eng. Des., **81**, 1271 (2006).

147) Nishitani, T., Sugie, T., Morishita, N., et al., “Temperature Dependence of the Transmission Loss in KU-1 and KS-4V Quartz Glasses for the ITER Diagnostic Window,” Fusion Eng. Des., **74**, 871 (2005).

148) Nishitani, T., Yamauchi, M., Nishio, S., et al., “Neutronics Design of the Low Aspect Ratio Tokamak Reactor, VECTOR,” Fusion Eng. Des., **81**, 1245 (2006).

149) Nomoto, Y., Suzuki, S., Ezato, K., et al., “Structural Design of Japanese Solid Breeder Test Blanket Modules for ITER,” Fusion Eng. Des., **81**, 719 (2006).

150) O’hira, S., Luo, G. -N., Nakamura, H., et al., “New Conceptual Design of a Test Module Assembly for Tritium Permeation Experiment,” Fusion Sci. Technol., **48**, 621 (2005).

151) O’hira, S., Yamanishi, S., Hayashi, T., “Operation Scenarios and Design Requirements for Fuel Processing in Future Fusion Reactor Facilities,” J. Nucl. Sci. Technol., **43**, 354 (2005).

152) Ochiai, K., Nakao, M., Hori, J., et al., “Measurements of Deuteron-Induced Activation Cross Sections for IFMIF Accelerator Structural Materials in the Energy Range of 22-40 MeV,” Fusion Eng. Des., **81**, 1459 (2006).

153) Ochiai, K., Velzilov, Y., Nishitani, T., et al., “International Benchmark Activity of Tritium Production Measurement for Blanket Neutronics,” Fusion Sci. Technol., **48**, 378 (2005).

154) Ochiai, K., Kondo, K., Murata, I., et al., “Measurement of Energetic Charged Particles Produced in Fusion Materials with 14 MeV Neutron Irradiation,” Fusion Eng. Des., **75-79**, 859 (2005).

155) Ogawa, H., Ogawa, T., Tsuzuki, K., “CT Injection Experiments in JFT-2M,” Fusion Sci. Technol., **49**, 209 (2006).

156) Ogiwara, H., Kohyama, A., Tanigawa, H., et al., “Irradiation-induced hardening mechanism of ion irradiated JLF-1 to High Fluences”, Fusion Eng. and Des., **81**, 1091(2006)

157) Ohwaki, H., Sugihara, M., Hatayama, A., “Modeling of Plasma Current Decay during Disruptions Caused by Massive Impurity Injection,” Plasma Fusion Res., **1**, 16 (2006).

158) Oikawa, T., Isayama, A., Fujita, T., et al., “Evolution of the Current-density Profile Associated with Magnetic-Island Formation in JT-60U,” Phys. Rev. Lett., **94**, 125003-1 (2005).

159) Oikawa, T., Suzuki, T., Isayama, A., et al., “Observation of the Bootstrap Current Reduction at Magnetic Island in a Neoclassical Tearing Mode Plasma,” Nucl. Fusion, **45**, 1101 (2005).

160) Okano, K., Suzuki, T., Umeda, N., et al., “Experimental Validation of Beam Particle Self Interaction in JT-60U by Use of N-NB,” J. Plasma Fusion Res., **81**, 579 (2005).

161) Okubo, N., Wakai, E., Matsukawa, S., et al., “Heat Treatment effects on microstructures and DBTT of F82H steel doped with boron and nitrogen,” Mater. Trans., **46**, 193(2005)

162) Okubo, N., Wakai, E., Matsukawa, S., et al., “Tempering treatment effect on mechanical properties of F82H steel doped with boron and nitrogen,” Mater. Trans., **46**,1779 (2005)

163) Olivares, R. U., Oda, T., (Tsuchiya, K.), et al., “Behavior of Li_2TiO_3 under Varied Surface Condition,” Fusion Eng. Des., **75-79**, 765 (2005).

164) Onozuka, M., Shimizu, K., (Shibanuma, K.), et al., “Investigation of the Dynamic Behavior of the ITER Tokamak Assembly using a 1/5.8-scale Model,” Fusion Eng. and Des., 81, 155(2006).

165) Oyama, N., Sakamoto, Y., Isayama A., et al., “Energy Loss for Grassy ELMs and Effects of Plasma Rotation on the ELM Characteristics in JT-60U,” Nucl. Fusion, **45**, 871 (2005).

166) Polevoi, A. R., Shimada, M., Sugihara, M., et al., “Requirements for Pellet Injection in ITER Scenarios with Enhanced Particle Confinement,” Nucl. Fusion, **45**, 1451 (2005).

167) Sakamoto, K., Kasugai, A., Minami, R., et al., “Development of Long Pulse and High Power 170GHz Gyrotron,” J. Phys. Conf. Series. **25**, 8 (2005).

168) Sakamoto, K., Takahashi, K., Kasugai, A., et al., “Conceptual Study of ECH/ECCD System for Fusion DEMO Plant,” Fusion Eng. and Des., **81**, 1263(2006).

169) Sakamoto,Y., and the JT-60 Team, “Enhanced performance and control issues in JT-60U long pulse discharges,” Plasma Phys. Control. Fusion, **47**, B337 (2005).

170) Sakamoto, Y., Fujita, T., Ide, S., et al., “Stationary High Confinement Plasmas with Large Bootstrap Current Fraction in JT-60U,” Nucl. Fusion, **45**, 574 (2005).

171) Sakasegawa, H., Ohtsuka, (Tanigawa, H.), et al., “Microstructural evolution during creep of 9Cr-ODS steels,” Fusion Eng. and Des., **81**, 1013(2006).

172) Sato, K., Ezato, K., Taniguchi, M., et al., “Proposal of Hot-pressed, Rod-shaped Tungsten Armor Concept for ITER Divertor and its High-Heat-flux Performance,” J. Nucl. Sci. Technol., **42-7**, 643 (2005).

173) Sato, K., Yoshiie, T., (Kutsukake, C.), et al., “Point Defect Formation in V-4Cr-4Ti and F82H Irradiated with Fission and Fusion Neutrons,” Mater. Trans., **46**, 445 (2005).

174) Sato, M., Sakurai, S., Nishio, S., et al., “Concept of Core and Divertor Plasma for Fusion DEMO Plant at JAERI,” Fusion Eng. Des., **81**, 1277 (2006).

175) Sato, S., Iida, H., Yamauchi, M., et al., “Shielding Design of the ITER NBI Duct for Nuclear and Bremsstrahlung Radiation,” Radiat. Prot. Dosimetry, **116**, 28 (2005).

176) Sato, S., Nakao, M., Verzilov, Y., et al., “Experimental Studies on Tungsten-Armor Impact on Nuclear Responses of Solid Breeding Blanket,” Nucl. Fusion, **45**, 656 (2005).

177) Sato, S., Verzilov, Y., Nakao, M., et al., “Neutronics Experiments using Small Partial Mockup of the ITER Test Blanket Module with Solid Breeder,” Fusion Sci. Technol., **47**, 1046 (2005).

178) Sato, S., Verzilov, Y., Ochiai, K., et al., “Progress in the Blanket Neutronics Experiments at JAERI/FNS,” Fusion Eng. Des., **81**, 1183 (2006).

179) Seki, M., Moriyama, S., Shinozaki, S., et al., “Performance of the LH Antenna with Carbon Grill in JT-60U,” Fusion Eng. Des., **74**, 273 (2005).

180) Shiba, K., Hirose, T., “Deformation Behavior of Reduced Activation Martensitic Steel during Tensile Test,” Fusion Eng. Des., **81**, 1051 (2006).

181) Shikama, T., Toh, K., (Yamauchi, M.), et al., “Radiation Sensitive Scintillator/Optical Fibre System for Radiation Dosimetry in Burning Plasma Machine,” Nucl. Fusion, **46**, 46 (2006).

182) Shimizu, T., Miyazaki, I., (Nishitani, T.), et al., “Measurements of (n,n’) Reaction Cross-Sections of ^{79}Br, ^{90}Zr, ^{197}Au and ^{207}Pb with Pulsed d-D Neutrons,” Annals of Nucl. Energy, **32**, 949 (2005).

183) Shimomura, Y., et al., “Preparation of ITER Construction and Operation,” Fusion Eng. Des., **81**, 3 (2006).

184) Shinohara, K., Sato, M., Kawashima, H., et al., “Ripple Reduction with Ferritic Insert in JFT-2M,” Fusion Sci. Technol., **49**, 187 (2006).

185) Shinohara, K., Suzuki, Y., Sakurai, S., et al., “Orbit Following Calculation of Energetic Ions in the Design of Ferritic Insertion in the JT-60U,” Plasma Fusion Res., **1**, 007 (2006).

186) Shinohara, K., Takechi, M., Ishikawa, M., et al., “Instability in the Frequency Range of Alfvén Eignemode Induced by Negative-Ion-Based Neutral Beam in JT-60U,” J. Plasma Fusion Res., **81**, 547 (2005).

187) Shu, W.M., Matsuyama, M., Suzuki T., et al., “Monitoring of Tritium in Diluted Gases by Detecting Bremsstrahlung X-rays,” Fusion Eng. Des. **81**, 803 (2006).

188) Shu, W.M., Ohira, S., Suzuki, T., et al., “Radiochemical Reactions between Tritium Molecule and Carbon Dioxide,” Fusion Sci. Technol., **48**, 684 (2005).

189) Stober, J., Lomas, P. J.,Saibene, G., et al., “Small ELM Regimes with Good Confinement on JET and Comparison to Those on ASDEX Upgrade, Alcator C-mod and JT-60U,” Nucl. Fusion, **45**, 1213 (2005).

190) Suzuki, S., Enoeda, M., Hatano, T., et al., “Key Achievements in Elementary R&D on Water-Cooled Solid Breeder Blanket for ITER Test Blanket Module in JAERI,” Nucl. Fusion, **46**, 285 (2005).

191) Suzuki, S., Ezato, K., Hirose, T., et al., “First Wall and Divertor Engineering Research for Power Plant in JAERI,” Fusion Eng. Des., **81**, 93 (2006).

192) Takahashi, K., Illy, S., Heidinger, R., et al., “Development of Reliable Diamond Window for EC Launcher on Fusion Reactors,” Fusion Eng. Des. **74** , 305 (2005).

193) Takahashi, K., Kobayashi, N., Kasugai, A., et al., “Design and Development of EC H&CD Antenna Mirrors for ITER,” Fusion Eng. Des. **81**, 281 (2006).

194) Takahashi, K., Kobayashi, N., Kasugai, A., et al., “Development of EC Launcher Components for ITER,” J. Phys. Conf. Series. **25**, 75 (2005).

195) Takahashi, H., Kudo, Y., Tsuchiya, K., et al., “Fracture Mechanics Analysis Including the Butt Joint Geometry for the Superconducting Conductor Conduit of the National Centralized Tokamak,” Fusion Eng. Des., **81**, 1005 (2006).

196) Takahashi, Y., Yoshida, K., Mitchell, N., “Quench Detection Using Pick-up Coils for the ITER Central Solenoid,” IEEE Trans. Appl. Supercond., **15**, 1395 (2005).

197) Takechi, M., Fujita, T., Ishii, Y., et al., “MHD Instabilities Leading to Disruptions in Low Beta JT-60U Reversed Shear Plasmas,” Nucl. Fusion, **45**, 1694 (2005).

198) Takechi, M., Fukuyama, A., Ishikawa, M., “Alfvén Eigenmodes in Reversed Shear Plasmas in JT-60U Negative-Ion-Based Neutral Beam Injection Discharges,” Phy. Plasmas, **12**, 082509 (2005).

199) Takenaga, H., Asakura, N., Higashijima, S., et al., “Study of Plasma Wall Interactions in the Long-Pulse NB-Heated Discharges of JT-60U towards Steady-State Operation,” J. Nucl. Mater., **337**, 802 (2005).

200) Takenaga, H., Asakura, N., Kubo, H., et al., “Compatibility of Advanced Tokamak Plasma with High Density and High Radiation Loss Operation in JT-60U,” Nucl. Fusion, **45**, 1618 (2005).

201) Takenaga, H., Nakano, T., Asakura, N., et al., “Study of Global Wall Saturation Mechanisms in Long-Pulse ELMy H-Mode Discharges on JT-60U,” Nucl. Fusion, **46**, S39 (2006).

202) Tamai, H., Akiba, M., Azechi, H., et al., “Design Study of National Centralized Tokamak Facility for the Demonstration of Steady State High-β Plasma Operation,” Nucl. Fusion, **45**, 1676 (2005).

203) Tani, K., Tobita, K., Tsuji-Iio, S., et al., “Confinement of Alpha Particles in a Low Aspect Ratio Tokamak Reactor,” IEEJ Trans., FM **125**, 938 (2005).

204) Tanifuji, T., Yamaki, D., Jitsukawa, S., “Tritium Release from Neutron-irradiated Li_2O: Transport in Porous Sintered Pellets,” Fusion Eng. Des., **81**, 595 (2005).

205) Tanigawa, H., Sakasegawa, H., Klueh, R.L., “Irradiation Effects on Precipitation in Reduced-Activation Ferritic/Martensitic Steels,” Materials Transactions, **46,** 469 (2005)

206) Tobita, K., Nishio, S., Enoeda, M., et al., “Design Study of Fusion DEMO Plant at JAERI,” Fusion Eng. Des., **81**, 1151 (2006).

207) Tsuchiya, B., Nagata, S., (Yamauchi, M.), et al., “Radiation Damage of Proton Conductive Ceramics under 14 MeV Fast Neutron Irradiation,” Fusion Sci. Technol., **47**, 891 (2005).

208) Tsuchiya, K., Akiba, M., Azechi, H., et al., “Engineering Design and Control Scenario for Steady-State High-Beta Operation in National Centralized Tokamak,” Fusion Eng. Des., **81**, 1599 (2006).

209) Tsuchiya, K., Kawamura, H., Casadio, S., et al., “Effect of Gelation and Sintering Conditions on Granulation of Li_2TiO_3 Pebbles from Li-Ti Complex Solution,” Fusion Eng. Des., **75-79**, 877 (2005).

210) Tsuchiya, K., Kawamura, H., Tanaka, S., “Evaluation of Contact Strength of Li_2TiO_3 Pebbles with Different Diameters,” Fusion Eng. Des., **81**, 1065 (2005).

211) Tsuchiya, K., Uchida, M., Kawamura, H., “General Properties on Compatibility between Be-Ti Alloy and SS 316LN,” Fusion Eng. Des., **81**, 1057 (2005).

212) Tsuzuki, K., Hirai, T., Kusama, Y., et al., “Exposure of Reduced Activation Ferritic Steel F82H to TEXTOR Plasma,” Fusion Eng. Des., **81**, 925 (2005).

213) Umeda, N., Yamamoto, T., Hanada, M., “Recent Progress of Negative Ion Based Neutral Beam Injector for JT-60U,” Fusion Eng. Des., **74**, 385(2005).

214) Umeda, N., Ikeda, Y., Hanada, M., “Beam Deflection by PG Filter in the Negative Ion Source for JT-60U NBI System,” Rev. Sci. Instrum. **77**, 03A529 (2006).

215) Urano, H., Kamada, Y., Takizuka, T., et al., “Pedestal Characteristics of H-Mode Plasmas in JT-60U and ASDEX Upgrade,” J. Plasma Fusion Res., **81**, 280 (2005).

216) Urano, H., Kamiya, K., Koide, Y., et al., “Roles of Plasma Rotation and Toroidal Field Ripple on H-mode Pedestal Structure in JT-60U,” Plasma Phys. Control. Fusion, **48**, A193 (2006).

217) Urano, H., Takizuka, T., Kamada, Y., et al., “Reduced Heat Transport between Edge-Localized-Mode Bursts at Low Collisionality and Small Poloidal Larmor Radius,” Phys. Rev. Lett., **95**, 035003-1 (2005).

218) Usigome, M., Ide, S., Itoh, S., et al., “Development of Completely Solenoidless Tokamak Operation in JT-60U,” Nucl. Fusion, **46**, 207 (2006).

219) Utin, Y., Chuyanov, V., (Ioki, K.), et al., “Design Progress of the ITER Vacuum Vessel and Ports,” Fusion Eng. Des., **75-79**, 571 (2005).

220) Verzilov, Y., Nishitani, T., Ochiai, K., et al., “Development of a New Fusion Power Monitor based on Activation of Flowing Water,” Fusion Eng. Des., **81**, 1477 (2006).

221) Verzilov, Y., Ochiai, K., Nishitani, T., “Methods for the Tritium Production Rate Measurement in Design-Oriented Blanket Experiments,” Fusion Sci. Technol., **48**, 650 (2005).

222) Wakai, E., Ando, M., Matsukawa, S., et al., “Effect of Initial Heat Treatment on DBTT of F82H Steel Irradiated by Neutrons,” Fusion Sci. and Technol., **47,** 856 (2005).

223) Wakai, E., Jitsukawa, S., Tomita, et al., “Radiation Hardening and -Embrittlement due to He Production in F82H Steel Irradiated at 250 °C in JMTR,” J. Nucl. Mater., **343,** 285 (2005).

224) Wakai, E., Ohtsuka, H., Matsukawa, et al., “Mechanical Properties of Small Size Specimens of F82H Steel,” Fusion Eng. and Des., **81**, 1077 (2006).

225) Wakai, E., Sato, M., Okubo, N., et al., “Effect of Heat Treatments on Mechanical Properties and Microstructures of ^{8}Cr-^{2}W(F82H) Steel Doped with Boron or Boron and Nitrogen,” J. Jpn. Inst. of Met., **69**, 460 (2005).

226) Wakai, E., Taguchi, T., Yamamoto, S., et al., “Effects of Helium Production and Heat Treatment on Neutron Irradiation Hardening of F82H Steels Irradiated with Neutrons,” Mater. Trans., **46**, 481 (2005).

227) Wakisaka, M., Kaneko, J., (Ochiai, K.), et al., "Analysis of Neutron Propagation from the Skyshine Port of a Fusion Neutron Source Facility," Nucl. Instrum. Methods, **A 554**, 347 (2005).

228) Walker, C.I, Barnsley, R., (Itami, K.), et al., "ITER Diagnostics: Maintenance and Commissioning in the Hot Cell Test Bed," Fusion Eng. Des., **74**, 685 (2005).

229) Yamada, H., Kawamura, H., Tsuchiya, K., et al., "The Effect of Neutron Irradiation on Mechanical Properties of YAG Laser Weldaments Using Previously Irradiated Material," J. Nucl. Mater., **340**, 57 (2005).

230) Yamada, H., Sato, S., Mohri, K., et al., "Neutron Irradiation Effect on Mechanical Properties of SS/SS Hip Joint Materials for ITER Shielding Blankets," Fusion Eng. Des., **81**, 631 (2005).

231) Yamaki, D., Jitsukawa, S., "Model Calculation of Tritium Release Behavior from Lithium Titanate," Fusion Eng. Des., **81**, 589 (2005).

232) Yamanishi, T., Hayashi, T., Kawamura, Y., et al., "Interlinked Test Results for Fusion Fuel Processing and Blanket Tritium Recovery Systems Using Cryogenic Molecular Sieve Bed," Fusion Sci. Technol., **48**, 63 (2005).

233) Yamanishi, T., Iwai, Y., Kawamura, Y., et al., "A Design Study for Tritium Recovery System from Cooling Water of a Fusion Power Plant," Fusion Eng. Des., **81**, 797 (2006).

234) Yamauchi, M., Hori, J., Ochiai, K., et al., "Analysis of Sequential Charged Particle Reaction Experiments for Fusion Reactors," Fusion Eng. Des., **81**, 1577 (2006).

235) Yamauchi, M., Nishitani, T., Nishio, S., "Neutron Shielding and Blanket Neutronics Study on Low Aspect Ratio Tokamak Reactor," IEEJ Trans. FM., **125**, 943 (2005).

236) Yamauchi, M., Ochiai, K., Morimoto, Y., et al., "Experiment and Analyses for 14 MeV Neutron Streaming through Dogleg Duct," Radiat. Prot. Dosimetry, **116**, 542 (2005).

237) Yamauchi, M., Takemura, M., Nakamura, H., et al., "Activity Estimation for the IFMIF Liquid Lithium Loop due to the Erosion and Corrosion of Target Back-wall," Fusion Sci. Technol., **47**, 1008 (2005).

238) Yoshida, H., Yokoyama, K., Taniguchi, M., et al., "High Flux Ion Beam Acceleration at the 100-eV Level for Fusion Plasma Facing Material Studies," Fusion Eng. Des., **81**, 361 (2006).

239) Yoshida, K., Takahashi, Y., Isono, T., et al., "Updating the Design of the Feeder Components for the ITER Magnet System," Fusion Eng. Des., **75-79**, 241 (2005).

240) Yoshida, H., Yamauchi, Y., (Arai, T.), et al., "Hydrogen Retention in Divertor Tiles in JT-60 for Hydrogen Discharge Period," J. Nucl. Mater., **337-339**,604 (2005).

241) Yoshikawa, A., Shibahara T., (Arai, T.), et al., "Depth Profile Of Hydrogen And Its Retention In Divertor Target Tile of JT-60 Exposed to Hydrogen Discharges," Fusion Eng. Des., **81**, 289 (2006).

242) Yoshino, R., "Neural-Net Predictor for Beta Limit Disruption in JT-60U," Nucl. Fusion, **45**, 1232 (2005).

243) Zanino, R., Egorov, S., (Takahashi, Y.), et al., "Preparation of the ITER Poloidal Field Conductor Insert (PFCI) Test," IEEE Trans. Appl. Supercond., **15**, 1346 (2005).

A.1.3 List of papers published in conference proceedings

1) Abe, K., Nakajima, H., Hamada, K., et al., “Manufacturing Study and Trial Fabrication of Radial Plate for ITER Toroidal Field Coil,” Proc. 19th Inter. Conf. on Magnet Technology (2005), to be published in IEEE Trans. ASC..

2) Aiba, N., Tokuda, S., Ishizawa, T., “Analysis of an Aspect Ratio Effect on the Stability of External MHD Modes in Tokamaks with Newcomb Equation,” 19th Inter. Conf. on Numerical Simulation of Plasmas and 7th Asia Pacific Plasma Theory Conf. (2005).

3) Aiba, N., Tokuda, S., Ishizawa, T., et. al., “Ideal MHD Stability Code MARG2D for the Analysis of External MHD Modes in JT-60U Plasma," Proc. 47th Annual Meeting of DPP-APS (2005).

4) Asakura, N., Takechi, M., Matshunaga, G., et al.,“ELM Propagation and Fluctuations in SOL and Divertor on JT-60U Tokamak,” Proc. 32nd EPS Conf. on Plasma Phys., P5-006(CD-ROM) (2005).

5) Barabash,V., the ITER International Team, (Akiba, M.), et al., “Materials Challenges for ITER -Current Status and Future Activities,” 12th Int. Conf. on Fusion Reactor Materials (2005), to be published in J. Nucl. Mater..

6) Baylor, L.R., Combs, S.K., Maruyama, S., et al., “Pellet Fueling of ITER Burning Plasmas,” Proc. 21st Symp. on Fusion Eng. (2005) (CD-ROM).

7) Combs, S. K., Baylor, L. R., Maruyama, S., et al., “Experimental Study of Pellet Delivery to the ITER Inner Wall through a Curved Guide Tube at Steady-State Pressure,” Proc. 21st Symp. on Fusion Eng. (2005) (CD-ROM).

8) Ebisawa, N., Akino, N., Grisham, L., et al “Recent Activities of Negative Ion Based NBI System on JT-60U,” Proc. 21st Symp. on Fusion Eng. (2005) (CD-ROM).

9) Fukumoto, N. and JFT-2M group, “Compact Toroid Injection System for JFT-2M,” Proc. 15th Int. Toki Conf., PS2-15 (2005).

10) Giancarli, L.,Chuyanov, V., (Akiba, M.), et al., “Test Blanket Modules in ITER; An Overview on Proposed Designs and Required DEMO-Relevant Materilas,” 12th Int. Conf. on Fusion Reactor Materials (2005), to be published in J. Nucl. Mater..

11) Hamada, K., Nakajima, H., Takano, K., et al., “Demonstration of JK2LB Jacket Fabrication for ITER Central Solenoid,” Proc. 19th Inter. Conf. on Magnet Technology (2005), to be published in IEEE Trans. ASC..

12) Hamamatsu, K., Takizuka, T., Hayashi, N., et. al., “Monte-Carlo Simulation of Electron Cyclotron Current Drive in NTM Magnetic Islands,” Proc. 32nd EPS Conf. on Plasma Phys., P5-098(CD-ROM) (2005).

13) Hatae, T., Kondoh, T., Naito, O., et al., “Recent R&D of Thomson Scattering Diagnostics for JT-60U and ITER,” Proc. 12th Int. Symp. on Laser-Aided Plasma Diagnostics (CD-ROM), 309 (2006).

14) Hatae, T., Nakatsuka, M., Yoshida, H., et al., “Application of Phase Conjugate Mirrors to Thomson Scattering Diagnosticsin JT-60U and ITER,” Proc. 5th Conf. of Asia Plasma & Fusion Association (2005), to be published in J. Korean Phys. Soc..

15) Hayashi, N., Takizuka, T., Sakamoto, Y., et. al., “Structural Mechanism of Strong Internal Transport Barrier in JT-60U Reversed-Shear Plasma,” 10th IAEA Technical Meeting on H-mode Physics and Transport Barriers (2005).

16) Hayashi, T., Tobita, K., Nishio, S., et al., “Possibility of Tritium Self-Sufficiency in Low Aspect Ratio Tokamak Reactor with the Outboard Blanket Only,” 15th Int. Toki Conf., (2005), to be published in Fusion Eng. Des..

17) Hirohashi, M., Ishiyama, A., (Koizumi, N.), et al., “Numerical Simulation of the Critical Current and n-Value in Nb_3Sn Strand Subjected to Bending Strain,” Proc. 19th Inter. Conf. on Magnet Technology (2005), to be published in IEEE Trans. ASC..

18) Hirohata, Y., Oya, Y., Yoshida. H., et al., “Depth Profile and Retention of Hydrogen Isotopes in Graphite Tiles Used in the W-Shaped Divertor of JT-60U,” Proc. 12th Int. Conf. on Fusion Reactor Materials (2005), to be published in J. Nucl. Mater..

19) Hirohata, Y., Tanabe, T., (Arai, T.), et al., “Deuterium and Hydrogen Retention Properties of the JT-60 and JT-60U Divertor Tiles,” Satellite meeting of the 7th Int. Symp. of Fusion Nuclear Technology (2005), to be published in Fusion Eng. Des..

20) Hirose, T., Shiba, K., Enoeda, M., et al., “Stress Corrosion Cracking Susceptibility of Ferritic/Martensitic Steel in Super Critical Pressurized Water,” 12th Int. Conf. on Fusion Reactor Materials (2005), to be published in J. Nucl. Mater..

21) Ida, M., Nakamura, H. and Sugimoto, M., “Analytical Estimation of Accessibility to Activated Lithium Loop in IFMIF,” 12th Int. Conf. on Fusion Reactor Materials (2005), to be published in J. Nucl. Mater..

22) Idomura, Y., “Gyrokinetic Simulations of ETG Turbulence and Zonal Flows in Positive/Reversed Shear Tokamaks," Proc. Festival de Theorie 2005 (2005).

23) Ikeda Y., the NBI group, the NCT Design Team, “Progress of Neutral Beam Injection System on JT-60U for Long Pulse Operation,” Proc. 5th General Scientific Assembly of Asia Plasma and Fusion Association (2005), to be published in J. Korea Phy. Soc..

24) Ikeda, Y., Umeda, N., Akino, N., et al., “Present Status of Negative Ion Based NBI System for Long Pulse Operation on JT-60U,” Proc. 4th IAEA Technical meeting on Negative Ion Based Neutral Beam Injectors (2005), to be published in Nucl. Fusion.

25) Isayama, A., Oyama, N., Urano, H., et al., “Measurement of Toroidal Structure of Electron Temperature with Electron Cyclotron Emission Diagnostic in JT-60U,” Proc. 21st Symp. on Fusion Eng. (2005) (CD-ROM).

26) Ishii. Y., Azumi, M. and Smolyakov, A., “Magnetic Island Evolution in Rotating Plasmas,” Proc. Joint Conf. of 19th Inter. Conf. on Numerical Simulation of Plasma and 7th Asia Pacific Plasma Theory Conf., 300 (2005).

27) Ishii. Y., Azumi, M., Smolyakov, A., “Rapid Evolution of the Magnetic Island in the Rotating Plasma,” Proc. 47th Annual Meeting of DPP-APS, 237 (2005).

28) Ishimoto, Y., Gotoh, Y., Arai, T., et al., “Transport of Carbon Impurity Using $^{13}CH_4$ Gas Puffing in JT-60U,” Proc. 12th Int. Conf. on Fusion Reactor Materials (2005), to be published in J. Nucl. Mater..

29) Isobe, K., Nakamura, H., Kaminaga, A., et al., “Characterization of JT-60U Exhaust Gas during Experimental Operatin,” Proc. 7th Int. Symp. on Fusion Nuclear Technology (2005), to be published in Fusion Eng. Des..

30) Itami, K., Sugie, T., Vayakis, G., et al., “Study of an Erosion Monitor for the ITER Diverter Target Plates,” Proc. 32nd EPS Conf. on Plasma Phys., P4-091(CD-ROM) (2005).

31) Kagei, Y., Kishimoto, Y., Miyoshi, T., “A Finite Volume Approach to the Fully Compressible MHD Simulation of High Beta Tokamak Plasmas,” Proc. 47th Annual Meeting of DPP-APS, 240 (2005).

32) Kasugai, A., Minami R., Takahashi K., et al., “Development of a 170GHz High-Power and CW Gyrotron for Fusion Application,” Digest of Int. Conf. of Infrared and Millimeter Waves, TB4-1 (2005).

33) Kawamura, H., Mishima, Y., Yoshida, N., et al., “Status of Beryllium R&D in Japan,” Proc. 7th Int. Workshop on Beryllium Technology (2005), to be published in Nucl. Technol..

34) Kawano, Y., Nakano, T., Isayama, A., et al., “Characteristics of Runaway Plasmas in JT-60U,” Proc. 32nd EPS Conf. on Plasma Phys., P2-068(CD-ROM) (2005).

35) Kikuchi, M., Suzuki, T., Sakamoto, Y., et al., “Measurement of Local Electrical Conductivity and Thermodynamical Coefficients in JT-60U,” Proc. 32nd EPS Conf. on Plasma Phys., P1-043(CD-ROM) (2005).

36) Kimura, A., Kasada, R., (Tanigawa, H.), et al., “Recent Progress in US-Japan Collaborative Research on Ferritic Steels R&D,” 12th Int. Conf. on Fusion Reactor Materials (2005), to be published in J. Nucl. Mater..

37) Kinjyo, T., Nihikawa, M., Enoeda, M., “Estimation of Tritium Release Behavior from Solid Breeder Materials under the Condition of ITER Test Blanket Module,” 12th Int. Conf. on Fusion Reactor Materials (2005), to be published in J. Nucl. Mater..

38) Kobayashi, Y., Isobe, K., Kaminaga, A., et al., “Analysis of Exhaust Gas In JT-60U Tokamak Operation,” Proc. 21th Symp. on Fusion Eng. (2005) (CD-ROM).

39) Koizumi, N., Nunoya, Y., Okuno, K., “A New Model to Simulate Critical Current Degradation of a Large CICC by Taking into Account Strand Bending,” Proc. 19th Inter. Conf. on Magnet Technology (2005), to be published in IEEE Trans. ASC..

40) Kondoh, T., Hayashi, T., Kawano, Y., et al., “CO2 laser Collective Thomson Scattering for Alpha-Particle Diagnostics,” Proc. 9th IAEA Technical Meeting on Energetic Particles in Magnetic Confinement Systems, NIFS-PROC-63, 189 (2006).

41) Konoshima, S. and the JT-60 team, “Radiated Power Profile Observed by a Tangentially Viewing IR Imaging Bolometer in JT-60U Tokamak,” Proc. 32nd EPS Conf. on Plasma Phys. P4-092(CD-ROM) (2005).

42) Konovalov, S.V., Mikhailovskii, A.B., Ozeki, T., et al., “Role of Anomalous Transport in Onset and Evolution of Neoclassical Tearing Modes,” Proc. 32nd EPS Conf. on Plasma Phys. I4-004(CD-ROM)(2005).

43) Kudo, Y., Sawai, T., Sakurai, S., et al., “Fabrication of ^{8}Cr-^{2}W Ferritic Steel Tile for Reduction in Toroidal Magnetic Field Ripple on JT-60U,” Proc. 5th Asia Plasma & Fusion Association (2005), to be published in Supplementary Issue of J. of Korean Physical Society.

44) Kurihara, K. and the JT-60 team, “Current Status of Experimental Study and Device Modifications in JT-60U,” Proc. of the 21st Symp. on Fusion Eng. (2005) (CD-ROM)

45) Maebara, S., Moriyama, S., Sugimoto, M., et al., “A 175MHz RFQ design for IFMIF project,” Proc. the 2005 Particle Accelerator Conference (2005), TPPT004 (CD-ROM).

46) Matsumoto, T., Kishimoto, Y., Li, J. Q., “Statistical Characteristics of Turbulent Plasmas Dominated by Zonal Flows,” Proc. Joint Conf. of 19th Inter. Conf. on Numerical Simulation of Plasma and 7th Asia Pacific Plasma Theory Conf., 258 (2005).

47) McDonald, D.C., ITPA H-mode Threshold Database WG, (Takizuka, T.), et al., “The Impact of Statistical Models on Scalings Derived from Multi-Machine H-mode Threshold Experiments,” 10th IAEA Technical Meeting on H-mode Physics and Transport Barriers (2005).

48) Mishima, Y., Yoshida, N., Kawamura, H., et al., “Recent Results on Beryllium and Beryllides in Japan,” 12th Int. Conf. on Fusion Reactor Materials (2005), to be published in J. Nucl. Mater..

49) Miura, Y., Takenaga, H., Kubo, H., et al., “Burn Control Study Using Burning Plasma Simulation Experiments in JT-60U,” Proc. 32nd EPS Conf. on Plasma Phys., P2-069 (CD-ROM) (2005).

50) Miyato, N., Kishimoto, Y. and Li, J. Q., “Zonal Flow and GAM Dynamics and Associated Transport Characteristics in Reversed Shear Tokamaks,” Proc. Joint Conf. of 19th Inter. Conf. on Numerical Simulation of Plasma and 7th Asia Pacific Plasma Theory Conf., 32 (2005).

51) Miyoshi, H., Ohno, N., (Asakura, N.), et al., “Intermittent Fluctuation Property of JT-60U Edge Plasmas,” Proc. 32nd EPS Conf. on Plasma Phys., P1-045(CD-ROM) (2005).

52) Nagashima, Y., Itoh, K., Itoh, S-I., et al., “Observation of Coherent Bicoherence and Biphase in Potential Fluctuations around Geodesic Acoustic Mode Frequency on JFT-2M,” 10th IAEA Technical Meeting on H-mode Physics and Transport Barriers (2005).

53) Nakahata, T., Yoshikawa A., (Ishimoto, Y.), et al., “Dynamics of Deuterium Implanted in Boron Coating Film for Wall Conditioning,” Proc. 12th Int. Conf. on Fusion Reactor Materials (2005), to be published in J. Nucl. Mater..

54) Nakamura, H., Ida, M., Chida., T., et al., “Thermo-Structural Design of the Replaceable Backwall in IFMIF Liquid Lithium Target,” 12th Int. Conf. on Fusion Reactor Materials (2005), to be published in J. Nucl. Mater..

55) Nakamura, H., Kobayashi, K., Yokoyama S., et al., “Measurement of Tritium Trapped in the Irradiation Defects Produced by High Energy Proton and Spallation Neutron in SS316,” 12th Int. Conf. on Fusion Reactor Materials (2005), to be published in J. Nucl. Mater..

56) Nakamura, Y., Tobita, K., Tsutsui, H., et al., “Computational Study of Non-Inductive Current Buildup in Compact DEMO Plant with Slim Center Solenoid,” PPCA1-V, 1st IAEA Technical Meeting on First Generation of Fusion Power Plants -Design and Technology (2005)

57) Nakamura, Y., Tsutsui, H., Tobita, K., et al., “Simulation Modeling of Fully Non-Inductive Buildup Scenario in High Bootstrap Current Tokamaks without Center Solenoids,” Proc. 32nd EPS Conf. on Plasma Phys., P2-051(CD-ROM) (2005).

58) Nakamura, Y., Tobita, K., Takei, N., et al., “Non-inductive Operation Scenario of Plasma Current Ramp-down in CS-less, Advanced Tokamak Reactor,” 15th International Toki Conference, "Fusion & Advanced Technology", PS2-22, (2005).

59) Nakano, T., Tsuzuki, K., Higashijima, S., et al., "Emission Rates of CH/CD and C2 Spectral Bands for Hydrocarbon-Loss-Events Measured in JT-60U Divertor Plasmas," Proc. 32nd EPS Conf. on Plasma Phys., P5-007(CD-ROM) (2005).

60) Neudatchin, S.V., Inagaki, S., Takizuka, T., et al., "Common Features of Heat Pulse Propagation across Internal Transport Barriers in JT-60U, LHD and T-10," 10th IAEA Technical Meeting on H-mode Physics and Transport Barriers (2005).

61) Neudatchin, S.V., Inagaki, S. , Takizuka, T., et al., "Comparison of Heat Pulse Propagation across Internal Transport Barriers in JT-60U, LHD and T-10 Plasmas in a Presence of ECRH," 6th Int. Workshop on Strong Microwaves in Plasmas (2005).

62) O'hira, S., Shu, W., Hayashi, T., et al., "Radiochemical Characteristics of Tritium to be Considered in Fusion Reactor Facility Design," 5th Asia-Pacific Symp. on Radiochemistry (2005), to be published in J. Radioanal. & Nucl. Chem..

63) Oda,Y., Kawamura, K., (Takahashi, K.), et al., "An Experimental Study on a Thrust Generation Model for Microwave Beamed Energy Propulsion," Proc. 44th AIAA Aerospace Sciences Meeting and Exhibition, AIAA2006-0765 (2006).

64) Oda,Y., Komurasaki, K., Takahashi ,K., et al., "Application of High Power Millimeter-Wave to Space Propulsion," Digest of Int. Conf. of Infrared and Millimeter Waves, MA3-4 (2005).

65) Oda, Y., Komurasaki, K., Takahashi, K., et al., "Experimental Study on Microwave Beaming Propulsion Using a 1MW-Class Gyrotron," 56th Int. Astronautical Conf., IAC-05-C4.6.01 (2005).

66) Oda, Y., Ushio, M., (Takahashi, K.), et al., "Pressure History Measurement in a Microwave Beaming Thruster," Proc. of 4th Int. Symp. on Beaming Energy Propulsion, (2005).

67) Ogiwara, H., Kohyama, A.,Tanogawa, H. et al., " Helium effect of Microstructural Evolution in Ion-Irradiated Redeuced Activation Ferritic/Martensitic Steel to High Fluences," 12th Int. Conf. on Fusion Reactor Materials (2005), to be published in J. Nucl. Mater..

68) Ohwaki, H., Sugihara, M., Kawano, Y., et al., "Modeling of Plasma Current Decay during the Disruption," Proc. 32nd EPS Conf. on Plasma Phys., P5-099(CD-ROM) (2005).

69) Okuno, K., Nakajima, H., Koizumi, N., "From CS and TF Model Coil to ITER : Lessons Learnt and Further Progress," Proc. 19th Inter. Conf. on Magnet Technology (2005), to be published in IEEE Trans. ASC..

70) Okuno, K., Nakajima, H., Sugimoto, H., et al. "Japanese Contributions to the Procurement of the ITER Superconducting Magnet," 15th Int. Toki Conf., (2005), to be published in Fusion Eng. Des..

71) Oya, Y., T. Tanabe, M., (Ishimoto, Y.), et al, "Hydrogen Isotope Behavior in the First Wall of JT-60U after DD Discharge," Proc. 12th Int. Conf. on Fusion Reactor Materials (2005), to be published in J. Nucl. Mater..

72) Ozeki, T., Aiba, N., Hayashi, N., et al., "Modeling of MHD Stability Consistent to the Transport," Proc. 32nd EPS Conf. on Plasma Phys. (2005).

73) Ozeki, T., Aiba, N., Hayashi, N., et al., "Integrated Simulation Code for Burning Plasma Analysis," IEA Large Tokamak Workshop on Burning Plasma Physics and Simulation (2005).

74) Peterson, B. J., Alekseyev, A. G., Konoshima, S., et al., "Imaging Bolometer Development for Application to Fusion Reactor Diagnostics," Proc. 47th Annual Meeting of DPP-APS, QP1. 00055 (2005).

75) Sakata, S., Totsuka, T., Kiyono, K., et al., "Progress of Data Processing System in JT-60 – Development of Remote Experiment System," 5th IAEA Technical Meeting on Control, Data Acquisition, and Remote Participation for Fusion Research (2005).

76) Sato, M., Isayama, A., Inagaki, S., et al., "Relativistic Downshift Frequency on ECE Measurements of Electron Temperature and Density in Torus Plasma," Proc. 32nd EPS Conf. on Plasma Phys., P4-090(CD-ROM) (2005).

77) Seki, M., "The Role of ITER and Associated Facilities on the Pthway towards Fusion Energy" 12th Int. Conf. on Fusion Reactor Materials (2005), to be published in J. Nucl. Mater..

78) Shiba, K., Nakata, T., Ando, M., et al., "Thermal creep Behavior of Japanese Reduced Activation Martensitic Steels," 12th Int. Conf. on Fusion Reactor Materials (2005), to be published in J. Nucl. Mater..

79) Shu, W.M., "Blistering and Retention in the Near-Surface Region of Tungsten Exposed to High Flux Deuterium Plasmas of Tens of eV," Proc. 3rd Int. Workshop on Tritium-Material Interactions, 27 (2005).

80) Shu, W.M., Luo, G.-N. and Yamanishi, T., "Mechanisms of Retention and Blistering in Near-Surface Region of Tungsten Exposed to High Flux Deuterium Plasmas of Tens of eV," 12th Int. Conf. on Fusion Reactor Materials (2005), to be published in J. Nucl. Mater..

81) Sokolov, M.A., Tanigawa, H., Odette, G.R., et al., "Fracture Toughness and Charpy Impact Properties of Several RAFS Before and After Irradiation in HFIR," 12th Int. Conf. on Fusion Reactor Materials (2005), to be published in J. Nucl. Mater..

82) Sugihara, M., Ohwaki, H., Kawano, Y., et al., "Extrapolation of Plasma Current Quench Time during Disruptions from Existing Machines to ITER," Proc. 32nd EPS Conf. on Plasma Phys., P2-067(CD-ROM) (2005).

83) Sugiyama, K., Tanabe, T., Masaki, K., et al., "Tritium Distribution Measurement of the Tile Gap of JT-60U," Proc. 12th Int. Conf. on Fusion Reactor Materials (2005), to be published in J. Nucl. Mater..

84) Suzuki, S., Akiba, M.,"Materials and Design Interface of In-Vessel Components for Fusion Reactors," 12th Int. Conf. on Fusion Reactor Materials (2005), to be published in J. Nucl. Mater..

85) Suzuki, T., Isayama, A., Ide, S., et al., "Recent RF Experiments and Application of RF Waves to Real-Time Control of Safety Factor Profile in JT-60U," Radio Frequency Power in Plasmas (Proc. 16th Topical Conf. on Radio Frequency Power in Plasmas), 279 (2005).

86) Takatsu, H., Sugimoto, M., Jitsukawa, S., et al., "The Role of IFMIF in the Roadmap Toward Fusion Power Systems," 12th Int. Conf. on Fusion Reactor Materials (2005), to be published in J. Nucl. Mater..

87) Takechi, M., Fujita, T., Ishii, Y., et al., "MHD Instabilities Observed in Extremely Reversed Shear Discharges on JT-60U," Proc. 32nd EPS Conf. on Plasma Phys. P2-049(CD-ROM) (2005).

88) Takenaga, H., Oyama, N., Isayama, A., "Transient Electron Heat Transport and Reduced Density Fuctuation after Pellet Injection in JT-60U Reversed Shear Plasmas," Proc. 32nd EPS Conf. on Plasma Phys. P1-042(CD-ROM) (2005).

89) Takeuchi, T., Tagawa, K., (Koizumi, N.), et al., "Internally Cu-stabilized RHQT Nb3Al Superconductors with Ta Matrix," Proc. 19th Inter. Conf. on Magnet Technology (2005), to be published in IEEE Trans. ASC..

90) Takizuka, T., Urano, H., Takenaga, H., et al., "Origin of the Various Beta Dependence of ELMy H-Mode Confinement Properties," 10th IAEA Technical Meeting on H-mode Physics and Transport Barriers (2005).

91) Tani, K., Nishio, S., Tobita, K., et al., "Ripple Loss of Alpha Particles in a Low-Aspect -Ratio Tokamak Reactor," Proc. 19th IAEA Technical Meeting on Energetic Particles in Magnetic Confinement Systems (2005).

92) Tanigawa, H., Sokolov, M.A., Klueh, R.L., "Microstructural Inhomogeneity of Reduced-Activation Ferritic/Martensitic Steel," 12th Int. Conf. on Fusion Reactor Materials (2005), to be published in J. Nucl. Mater..

93) Tanigawa, H., Sakaseagawa, H., Hashimoto, N., et al., "Irradiation Effects on Precipitation and its Impact on the Mechanical Properties of Reduced-Activation Ferritic/Martensitic Steels," 12th Int. Conf. on Fusion Reactor Materials (2005), to be published in J. Nucl. Mater..

94) Taniguchi, M., Inoue, T., Kashiwagi, M., et al., "Acceleration of 100A/m2 Negative Hydrogen Ion Beams in a 1 MeV Vacuum Insulated Beam Source," Proc. 10th Int. Symp. on Production and Neutralization of Negative Ions and Beams, AIP Conf. Proc., 763, 168 (2005).

95) Tomita, Y., Smirnov, R., Takizuka, T., et al., "Charging of Spherical Dust Particle on Plasma-Facing Wall," 19th Int. Conf. on Numerical Simulation of Plasmas and 7th Asia Pacific Plasma Theory Conf. (2005).

96) Tsuchiya, K., Ishitsuka, E., Kawamura, H., et al., "Contact Strength of Irradiated Beryllium Pebbles," Proc. 7th Int. Workshop on Beryllium Technology (2005), to be published in Nucl. Technol..

97) Tsuchiya, K., Kawamura, H., Ishida, T., "Compatibility between Be-Ti Alloys and F82H Steel," 12th Int. Conf. on Fusion Reactor Materials (2005), to be published in J. Nucl. Mater..

98) Tsuchiya, K., Kawamura, H., Ishida, T., "Effect of α Be on Compatibility between Be-Ti and SS316LN," Proc. 7th Int. Workshop on Beryllium Technology (2005), to be published in Nucl. Technol..

99) Tuda, T., Kurita G. and Fujita T., "Roles of Double Tearing Mode on the Formation of Current Hole," Proc. 19th Int. Conf. on Numerical Simulation of Plasmas and 7th Asia Pacific Plasma Theory Conf., 236 (2005).

100) Tuda, T., Kurita, G. and Fujita, T., "Stability of Double Tearing Mode in Current Hole Configuration," Proc. 5th Asia Plasma Fusion Association, 88 (2005).

101) Urano, H., Kamiya, K., Koide, Y., et al., "Roles of Plasma Rotation and Toroidal Field Ripple on H-Mode Pedestal Structure in JT-60U," 10th IAEA Technical Meeting on H-mode Physics and Transport Barriers (2005).

102) Wakai, E., Ando, M., Sawai, T., et al., "Effect of Heat Treatments on Tensile Properties and Microstructures of F82H Steel Ittadiated by Neutrons," 12th Int. Conf. on Fusion Reactor Materials (2005), to be published in J. Nucl. Mater..

103) Yamauchi. M., Sato, S., Nishitani, T., et al., "Shielding Design of ITER Pressure Suppression System," Proc. 21st Symp. on Fusion Eng. (2005), (CD-ROM).

104) Ying, A., Akiba, M., Boccaccini, L.V., et al., "Staus and Perspectives of the R&D on Solid Breeder Materials fro testing in ITER TBMs," 12th Int. Conf. on Fusion Reactor Materials (2005), to be published in J. Nucl. Mater..

105) Yoshida, M., Kobayashi, S., Urano, et al, "Observations of the Collapse and Recovery of the Temperature Pedestal by Using Diagnostics with the Fast Temporal Resolution in JT-60U," 10th IAEA Technical Meeting on H-mode Physics and Transport Barriers (2005).

106) Yoshikawa, A., Shibahara, T., (Arai, T.), et al., "Depth Profile Of Hydrogen And Its Retention In Divertor Target Tile Of Jt-60 Exposed To Hydrogen Discharges," Proc. 7th Int. Symp. on Fusion Nuclear Technology (2005), to be published in Fusion Eng. Des..

A.1.4 List of other papers

1) Akasaka, H., Takano, S., Kawamata, Y., "Reconfiguration Study of the JT-60 Timing System Using FPGA," Proc. 17th Topical Meeting on Eng. and Technol. (CD-ROM), (2006) (in Japanese).

2) Akiba, M., Matsui, H., Takatsu, H., et al., "Technology and Material Research in Fusion Power Plant Development," J. Plasma Fusion Res., **81**, 863 (2005) (in Japanese).

3) El-Guebaly, L.A., Forrest, R.A., (Tobita, K.), et al., "Current Challenges Facing Recycling and Clearance of Fuision Radioactive Materials," Fusion Technology Institute Report at University of Wisconsin, UWFDM-1285 (2005).

4) Hamada, K., Nakajima, H, Kawano, K., et al., "Optimization of JK2LB Chemical Component for ITER Central Solenoid Jacket Material," J. Cryog. Eng. Soc. Japan, **41**, 131 (2006) (in Japanese).

5) Ido, T., Hamada, Y., Miura, Y., et al., "Zonal Flow Study with Heavy Ion Beam Probes II," J. Plasma Fusion Res., **81**, 987 (2005) (in Japanese).

6) Idomura, Y., "df Simulations of Microturbulence," J. Plasma Fusion Res. **81**, 581 (2005) (in Japanese).

7) Ikeda, Y., Kubo, S., "Plasma Profile Control by Using Local Heating and Current Drive with EC Waves," J. Plasma Fusion Res. **81**, 160 (2006) (in Japanese).

8) Ikeda, Y., Oikawa, T., Ide, S., "N-NBI Heating and Current Drive in JT-60U towards Steady-State Tokamak," J. Plasma Fusion Res., **81**, 773 (2005) (in Japanese).

9) Inoue, N., Yoshino, R., "Tokoton Yasashii Kakuyugou Enerugii no Hon (Book of Fusion Energy Thoroughly Understandable)," Nikkan Kogyou Shimbun, Ltd., Tokyo (2005) (in Japanese).

10) Inoue, T., "Background and Latest R&D Achievements," J. Plasma Fusion Res., **81**, 764 (2005) (in Japanese).

11) Inoue, T., Hanada, M., "R&D Progress of a Negative Ion Source and an Accelerator for Fusion Reactors," J. Plasma Fusion Res., **81**,785 (2005) (in Japanese).

12) Ishimoto, Y., Gotoh, Y., Arai, T., et al., "Thermal Properties and Structure of Redeposition Layers in JT-60U," 2005 Japan-US Workshop on Heat Removal and Plasma Materials Interactions for Fusion, Fusion High Power Density Components and System, and IEA workshop on Solid Surface Plasma Facing Components (2005).

13) Ishio, K., Hamada, K., Nakajima, H., "Effects of Nitrogen, Niobium, Phosphorous and Carbon on the Mechanical Properties of Aged 316LN Stainless Steels at Cryogenic Temperature, 4 K," Tetsu-to-Hagane, **92**, 30 (2006) (in Japanese).

14) Ishio, K., Nakajima, H., "Effects of Nitrogen on the Material Properties of 316LN Stainless Steels," Tetsu-to-Hagane, **92**, 38 (2006) (in Japanese).

15) Kamada, Y., "Plasama Properties for the Design of the Thermonuclear Reactor," J. Atomic Energy Soc. Jpn., **47**, 45 (2005) (in Japanese).

16) Kamada, Y., Shimada, M., Ogawa, Y., et al., "Fusion Plasma Research toward Fusion Power Plants," J. Plasma Fusion Res., **81**, 849 (2005) (in Japanese).

17) Kawamata, Y., Kurihara, K., "Development of an Innovative Integrator Being Resistant to an Excessive High Voltage Input at Plasma Instabilities toward ITER," Proc. 22nd Annual Meeting on Plasma Fusion Research, 173 (2005) (in Japanese).

18) Koizumi, N., Nishimura, A., "Intelligible Seminar on Fusion Reactors – (9) Superconducting Coil to Generate Magnetic Field for Plasma Confinement," J. Energy Soc. Jpn., 47, 703 (2005) (in Japanese).

19) Konishi, S., Enoeda, M., "Intelligible Seminor on Fusion Reactors – (6) Blanket that converts Energy, and Produces Fuels," J. At. Energy Soc. Jpn., **47**, 488 (2005) (in Japanese).

20) Krylov, A., Inoue, T., "ITER NB System: Compact Beamline and Design Against Radiation," J. Plasma Fusion Res., 81, No.10, 779 (2005).

21) Kubota, N., Ochiai, K., Kutsukake, C., et al., "Measurement of Light Element Distribution near the Surface of TFTR Plasma Facing Component using Nuclear Reaction Analysis," J. Plasma and Fusion Res., **81**, 296 (2005) (in Japanese).

22) Kurihara, K., “Conference Report on the 21st IEEE/NPSS Symp. on Fusion Eng. (21st SOFE, Sept. 26-29, 2005, Knoxville, Tennessee),” J. Plasma Fusion Res., **82**, 111 (2006) (in Japanese).

23) Kurihara, K., Kawamata, Y., Sueoka, M., et al., “A New Method of Current Profile Reconstruction based on the Exact Solution of Fredholm Integral Equation of the First Kind,” Proc. 22nd Annual Meeting on Plasma Fusion Research, 109 (2005) (in Japanese).

24) Kusama, Y., Ishikawa, M., “Application of Diamond to Plasma Diagnostic,” New Diamond, **21**, 24 (2005) (in Japanese).

25) Maebara, S. and Watanabe, K., “Development of Accelerator for IFMIF,” J. Plasma Fusion Res, **82**, 21 (2005) (in Japanese).

26) Masaki, K., “Analyses of Dust in JT-60U,” 2005 Japan-US Workshop on Heat Removal and Plasma Materials Interactions for Fusion, Fusion High Power Density Components and System, and IEA workshop on Solid Surface Plasma Facing Components (2005).

27) Minami, R., Kasugai, A., Takahashi, K., et al., “Development of High Power Gyrotron for CW Operation,” Inst. Elec. Info. Comm. Engineers Technical Report, **105**, 498, 39 (2005).

28) Miura, Y., “Measurement and Control of Tokamak Plasma by Light,” Hikarikagaku-no-Saizensen (in Japanese).

29) Morioka, A., Okuno, K., “Development of High Heat-Resistance Resin for Neutron Shielding,” Plastics, **57**, 148 (2006) (in Japanese).

30) Nakahira, M., Takeda, N., “An Approach for Development of Technical Structural Standard in ITER,” Maintenology **4**, 47 (2006) (in Japanese).

31) Nakamura, H., and Higashijima, S., “Hydrogen Isotopes Removal from the Vacuum Vessel Using Discharges,” J. Vacuum Soc. Japan. **49**, 62 (2006) (in Japanese).

32) Nakamura, H., Horiike, H., Kondo, H., et al., “Development of Liquid Lithium Target System in the IFMIF,” J. Plasma and Fusion Res., **82**, 16 (2005) (in Japanese).

33) Nishitani, T., “Burning Plasma Diagnostics by Radiation Measurement,” Housyasen, **31**, 97 (2005) (in Japanese).

34) O’hira, S., “Intelligible Seminar on Fusion Reactors- (11) Safety of Fusion Reactor - Safety Characteristics and Requirements -,” J. At. Energy Soc. Japan, **47**, 839 (2005) (in Japanese).

35) Ohmori, Y., Kurihara, K., Matsukawa, M., et al., “Trouble of a Transformer with the No-Voltage Tap Changer,” Proc. 17th Topical Meeting on Eng. and Technol. (CD-ROM), (2006) (in Japanese).

36) Okano, F., Honda, A., Ohshima, K., et al., “Application of PLC to Dynamic Feedback Control of a Large Liquid-He Refrigerator System on Nuclear Fusion Facility,” Keiso **49**, 22 (2006) (in Japanese).

37) Okano, K., Kikuchi, M., Tobita, K., et al., “Path toward Commercial Fusion Power Plants,” J. Plasma Fusion Res. **81**, 839 (2005) (in Japanese).

38) Okano, K., Kurihara, K., Tobita, K., “Intelligible Seminar on Fusion Reactors, 12; Next Step toward the Realization of Fusion Reactors -Future Vision of Fusion Energy Research and Development-,” J. Nucl. Sci. Technol., **48**, 48 (2006) (in Japanese).

39) Oya, Y., Hirohata, Y., (Masaki, K.,) et al., “Hydrogen and Deuterium Distributions and Erosion/Deposition Profile in JT-60U,” 2005 Japan-US Workshop on Heat Removal and Plasma Materials Interactions for Fusion, Fusion High Power Density Components and System, and IEA Workshop on Solid Surface Plasma Facing Components (2005).

40) Shibanuma, K., “Intelligible Seminar on Fusion Reactors – (10) Remote Maintenance Robot for In-Vessel Components – Advanced Robot Technology for Handling of Large-Heavy Components with High Positioning Accuracy,” J. At. Energy Soc. Japan **47**, 761 (2005) (in Japanese).

41) Sueoka, M., Kawamata, Y., Kurihara, K., “Web-Based Information Distribution Plan in JT-60 (Plasma Shape Real-Time Display and Broadcasting by Using Web Service),” Proc. 22nd Annual Meeting on Plasma Fusion Research, 116 (2005) (in Japanese).

42) Sugie, T., “Radiation from High Temperature Plasmas and Spectroscopy,” in Basis and Application of Plasma Diagnostic, Corona Publishing Co. Ltd. (in Japanese).

43) Sugimoto, M., "Status of Design and Development of International Fusion Materials Irradiation Facility (IFMIF) – Central Control/Common Instrumentation and Conventional Facilities," J. Plasma and Fusion Res., **82**, 26 (2005) (in Japanese).

44) Sugimoto, M., "Status of Design and Development of International Fusion Materials Irradiation Facility (IFMIF) – Summary," J. Plasma and Fusion Res., **82**, 28 (2005) (in Japanese).

45) Tanaka, S., Akiba, M, Enoeda, M., et al., "Present Status of ITER Test Blanket Development," J. Plasma Fusion Res., **81**, 434 (2005) (in Japanese).

46) Tobita, K., Konishi, S., Tokimatsu, K., et al., "Challenge to Innovative Technologies and the Expected Market Appeal," J. Plasma Fusion Res., **81**, 875 (2005) (in Japanese).

47) Totsuka, T., Sakata, S., Iba, K., "Status and Development of JT-60 Remote Experiment (Discharge Parameter Set-Up and Pulse Scheduling from Remote-Site)," Proc. 22nd Annual Meeting on Plasma Fusion Research, 116 (2005) (in Japanese).

48) Wang, F., Nakamura, (Kurihara, K.), et al., "Magnetic Sensor Dependence of CCS Method to Reproduce ST Plasma Shape," Proc. Kyushu-Okinawa-Yamaguchi Local Meeting on Plasma Fusion Res., (2005).

49) Watanabe, K., Andoh, Y., "Application of NBI Technologies," J. Plasma Fusion Res., **81**,792 (2005) (in Japanese).

50) Watanabe, T., Sugama, H., Idomura, Y., "Prospects of Microturbulence Simulation," J. Plasma Fusion Res., **81**, 698 (2005) (in Japanese).

A.2 Organization

A.2.1 Organization of Naka Fusion Research Establishment

(As of September 30, 2005)

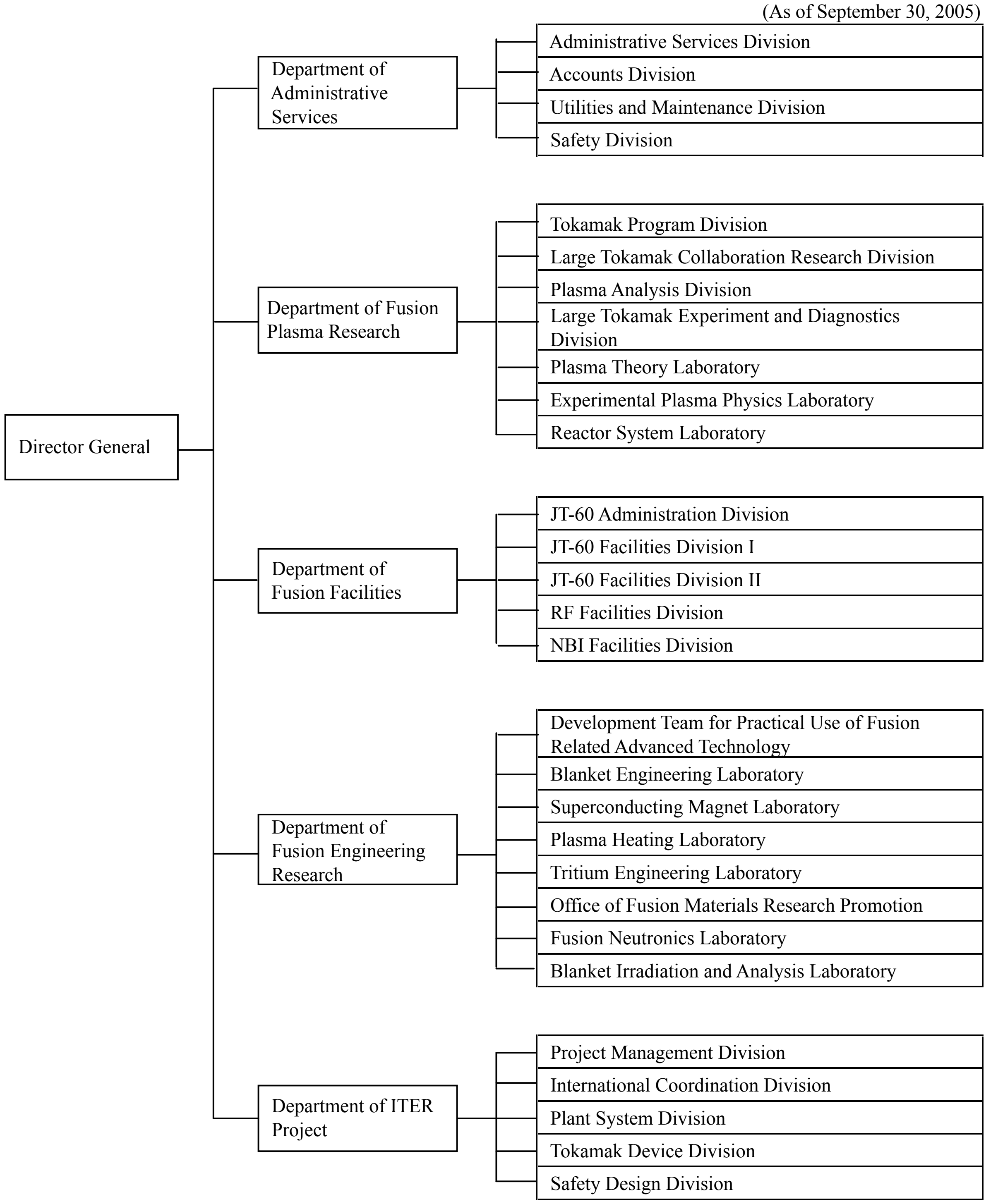

A.2.2 Organization of Fusion Research and Development Directorate

(As of March 31, 2006)

- Director General
  - Research and Development Co-ordination and Promotion Office
  - ITER Project Promotion Group
  - Broader Approach Promotion Group
  - Research Coordination Group
  - Division of Advanced Plasma Research
    - JT-60 Advanced Program Group
    - Collaborative Research Group
    - Tokamak Analysis Group
    - Tokamak Experimental Group
    - Plasma Theory & Simulation Group
    - Tokamak Diagnostics Grooup
    - Fusion Reactor Design Group
  - Division of Tokamak System Technology
    - Tokamak Control Group
    - Tokamak Device Group
    - RF Heating Group
    - NBI Heating Group
  - Division of Fusion Energy Technology
    - Group of Fusion Advanced Technology for Practical Use
    - Blanket Technology Group
    - Superconducting Magnet Technology Group
    - Plasma Heating Technology Group
    - Tritium Technology Group
    - Fusion Materials Development Group
    - Fusion Neutronics Group
    - Blanket Irradiation and Analysis Group
  - Division of ITER Project
    - ITER Project Management Group
    - ITER International Coordination Group
    - ITER Plant System Group
    - ITER Tokamak Device Group
    - ITER Safety Design Group

For more information on JAEA organization, please see the following URL:
http://www.jaea.go.jp/english/01/1_5.shtml

A.3 Personnel Data

A.3.1 Scientific Staff in the Naka Fusion Research Establishment of JAERI (April 2005 - September 2005)

Naka Fusion Research Establishment

SEKI Masahiro	(Director General)
SHIMOMURA Yasuo	(Scientific Consultant)
MATSUI Hideki	(Invited Researcher)
KOHYAMA Akira	(Invited Researcher)
IDA Katsumi	(Invited Researcher)
KISHIMOTO Yasuaki	(Invited Researcher)
USHIGUSA Kenkichi	(Staff for Director General)
ISEI Nobuaki	(Staff for Director General)
OOHARA Hiroshi	(Staff for Director General)

Department of Fusion Plasma Research

NINOMIYA Hiromasa	(Director)
KIKUCHI Mitsuru	(Deputy Director)
NAGAMI Masayuki	(Prime Scientist)
TANI Keiji	
TERAKADO Yuichi	(Administrative Manager)

Tokamak Program Division

MIURA Yukitoshi (General Manager)

ANDO Toshinari (*18)	FUJITA Takaaki	HATAE Takaki
KURIHARA Ryoichi	KURITA Gen-ichi	MATSUMURA Hiroshi (*2)
MORI Katsuharu (*7)	MORIOKA Atsuhiko	OGURI Shigeru (*7)
OIKAWA Akira	SAKURAI Shinji	SATO Fujio (*7)
SHIINA Tomio	TAMAI Hiroshi	TSUCHIYA Katsuhiko
YAMAZAKI Takeshi (*7)		

Large Tokamak Collaboration Research Division

MIURA Yukitoshi (General Manager)

KONOSHIMA Shigeru	SHINOHARA Kouji

Plasma Analysis Division

OZEKI Takahisa (General Maneger)

AIBA Nobuyuki (*21)	HAMAMATSU Kiyotaka	HAYASHI Nobuhiko
KIYONO Kimihiro	KOBAYASHI Masayuki (*23)	KONOVALOV Sergei (*6)
NAITO Osamu	OHASA Kazumi	OHSHIMA Takayuki
SAKATA Shinya	SATO Minoru	SUZUKI Mitsuhiro (*30)
TAKIZUKA Tomonori		

Large Tokamak Experiment and Diagnostics Division

KAMADA Yutaka (General Manager)

ASAKURA Nobuyuki	CHIBA Shinichi	FUJIMOTO Kayoko (*21)
HAMANO Takashi (*19)	HAYASHI Toshimitsu (*17)	HOSHINO Katsumichi
IDE Shunsuke	INOUE Akira (*19)	ISAYAMA Akihiko
ISHIKAWA Masao (*21)	KAMIYA Kensaku	KASHIWA Yoshitoshi
KAWASHIMA Hisato	KITAMURA Shigeru	KOIDE Yoshihiko
KOKUSEN Shigeharu (*18)	KUBO Hirotaka	MATSUNAGA Go (*21)
MIYAMOTO Atsushi (*18)	NAGAYA Susumu	NAKANO Tomohide
OYAMA Naoyuki	SAKAMOTO Yoshiteru	SAKUMA Takeshi (*19)
SUNAOSHI Hidenori	SUZUKI Takahiro	TAKECHI Manabu
TAKENAGA Hidenobu	TSUBOTA Naoaki (*18)	TSUKAHARA Yoshimitsu
TSUZUKI Kazuhiro	UEHARA Kazuya	URANO Hajime
YOSHIDA Maiko (*21)		

Plasma Theory Laboratory

KISHIMOTO Yasuaki (Head)

IDOMURA Yasuhiro	ISHII Yasutomo	KAGEI Yasuhiro (*21)
MATSUMOTO Taro	MIYATO Naoaki	SUGAHARA Akihiro (*23)
TOKUDA Shinji	TUDA Takashi	

Experimental Plasma Physics Laboratory

KUSAMA Yoshinori (Head)

KASAI Satoshi	KAWANO Yasunori	KONDOH Takashi
OGAWA Hiroaki		

Reactor System Laboratory

TOBITA Kenji (Head)

NAKAMURA Yukiharu	NISHIO Satoshi	SATO Masayasu
SONG Yuntao (*4)		

Department of Fusion Facilities

KURIYAMA Masaaki	(Director)
HOSOGANE Nobuyuki	(Deputy Director)
YAMAMOTO Takumi	

JT-60 Administration Division

TERAKADO Yuichi (General Manager)

JT-60 Facilities Division I

KURIHARA Kenichi (Head)

AKASAKA Hiromi	FURUKAWA Hiroshi (*19)	HOSOYAMA Hiromi (*8)
KAWAMATA Youichi	MATSUKAWA Makoto	OHMORI Shunzo
OHMORI Yoshikazu	OKANO Jun	SEIMIYA Munetaka
SHIBATA Kazuyuki (*19)	SHIBATA Takatoshi	SHIMADA Katsuhiro
SUEOKA Michiharu	TAKANO Shoji (*30)	TERAKADO Hiroyuki (*7)
TERAKADO Tsunehisa	TOTSUKA Toshiyuki	YAMASHITA Yoshiki (*7)
YONEKAWA Izuru		

JT-60 Facilities Division II

MIYA Naoyuki (Head)

ARAI Takashi	HAGA Saburo (*18)	HAYASHI Takao
HIRATSUKA Hajime	HONDA Masao	ICHIGE Hisashi
ISAKA Masayoshi	ISHIMOTO Yuki (*21)	KAMINAGA Atsushi
KIZU Kaname	MASAKI Kei	MATSUZAWA Yukihiro (*18)
MIYO Yasuhiko	NISHIYAMA Tomokazu	SASAJIMA Tadayuki
SHIBAMA Yusuke	SUZUKI Yutaka (*16)	TAKAHASHI Ryukichi (*2)
UEHARA Toshiaki (*19)	YAGISAWA Hiroshi (*2)	
YAGYU Jun-ichi	YAMAMOTO Masahiro	

RF Facilities Division

FUJII Tsuneyuki (Head)

ANNO Katsuto	HIRANAI Shinichi	HASEGAWA Koichi
IGARASHI Koichi (*18)	ISHII Kazuhiro (*19)	KIKUCHI Kazuo
MORIYAMA Shinichi	SATO Fumiaki (*18)	SAWAHATA Masayuki
SEKI Masami	SHIMONO Mitsugu	SHINOZAKI Shin-ichi
SUZUKI Sadaaki	TAKAHASHI Masami (*25)	TANI Takashi
TERAKADO Masayuki	YOKOKURA Kenji	

NBI Facilities Division

IKEDA Yoshitaka (Head)

AKINO Noboru	EBISAWA Noboru	GRISHAM Larry (*22)
HONDA Atsushi	KAWAI Mikito	KAZAWA Minoru
KIKUCHI Katsumi (*19)	KOMATA Masao	MOGAKI Kazuhiko
NOTO Katsuya (*18)	OHGA Tokumichi	OKANO Fuminori
OSHIMA Katsumi (*18)	TAKENOUCHI Tadashi (*28)	TANAI Yutaka (*19)
UMEDA Naotaka	USUI Katsutomi	YAMAZAKI Haruyuki (*2)

Department of Fusion Engineering Research

SEKI Shogo	(Director)
TAKATSU Hideyuki	(Prime Scientist and Deputy Director)
KATOGI Takeshi	(Administrative Manager)

SHIHO Makoto

Development Team for Practical Use of Fusion Related Advanced Technology

ABE Tetsuya (Team Leader)

Blanket Engineering Laboratory

AKIBA Masato (Head)

ENOEDA Mikio	EZATO Koichiro	HIROSE Takanori
HOMMA Takashi	NISHI Hiroshi	NOMOTO Yasunobu (*12)
SUZUKI Satoshi	TANIGAWA Hisashi	TANZAWA Sadamitsu
YOKOYAMA Kenji		

Superconducting Magnet Laboratory

OKUNO Kiyoshi (Head)

ABE Kanako (*5)	HAMADA Kazuya	ISONO Takaaki
KAWANO Katsumi	KOIZUMI Norikiyo	NABARA Yoshihiro
NAKAJIMA Hideo	NUNOYA Yoshihiko	OSHIKIRI Masayuki (*19)
SUGIMOTO Makoto	TAKANO Katsutoshi (*19)	TSUTSUMI Fumiaki (*30)

Plasma Heating Laboratory

SAKAMOTO Keishi (Head)

DAIRAKU Masayuki	HANADA Masaya	IKEDA Yukiharu
INOUE Takashi	KASHIWAGI Mieko	KASUGAI Atsushi
KOBAYASHI Noriyuki (*29)	KOMORI Shinji (*19)	MINAMI Ryutaroh (*21)
ODA Yasuhisa (*31)	SEKI Takayoshi (*2)	TAKAHASHI Koji
TANIGUCHI Masaki	TOBARI Naoyuki (*21)	WATANABE Kazuhiro

Tritium Engineering Laboratory

YAMANISHI Toshihiko (Head)

HAYASHI Takumi	ISOBE Kanetsugu	KAWAMURA Yoshinori
KOBAYASHI Kazuhiro	LUO Guang-Nan (*6)	MIURA Hidenori (*12)
NAKAMURA Hirofumi	SHU Wataru	SUZUKI Takumi
UZAWA Masayuki (*16)	YAMADA Masayuki	

Office of Fusion Materials Research Promotion

SUGIMOTO Masayoshi (Head)

ANDO Masami	CHIDA Teruo (*3)	IDA Mizuho (*5)
MATSUHIRO Kenjiro (*21)	NAKAMURA Hiroo	NAKAMURA Kazuyuki
TANIGAWA Hiroyasu	UMETSU Tomotake (*14)	YUTANI Toshiaki (*29)

Fusion Neutron Laboratory

NISHITANI Takeo (Head)

ABE Yuichi	KAWABE Masaru (*19)	KONDO Keitaro (*20)
KUBOTA Naoyoshi (*21)	KUTSUKAKE Chuzo	NAKAO Makoto (*12)

OCHIAI Kentaro
OKADA Kouichi (*27)
SATO Satoshi
SEKI Masakazu
TANAKA Shigeru
YAMAUCHI Michinori (*29)

Blanket Irradiation and Analysis Laboratory

HAYASHI Kimio (Head)
HOSHINO Tsuyoshi (*21)
ISHIDA Takuya (*19)
TSUCHIYA Kunihiko
YAMADA Hirokazu (*12)

Department of ITER Project

TSUNEMATSU Toshihide (Director)
YOSHINO Ryuji (Deputy Director)
TADA Eisuke
MATSUMOTO Hiroyuki (Administrative Manager)
KOIZUMI Koichi
ODAJIMA Kazuo
SHOJI Teruaki

Project Management Division

MORI Masahiro (General Manager)
ITAMI Kiyoshi
SENGOKU Seio
SHIMIZU Katsuhiro
SUGIE Tatsuo
YOSHIDA Hidetoshi

International Coordination Division

ANDO Toshiro (Head)
HONDA Tsutomu (*29)
IIDA Hiromasa
IOKI Kimihiro (*16)
KATAOKA Yoshiyuki (*2)
MARUYAMA So
MORIMOTO Masaaki (*16)
NAGAHAMA Tetsushi (*24)
OIKAWA Toshihiro
OKADA Hidetoshi (*2)
SAKASAI Akira
SATO Kouichi (*30)
SHIMADA Michiya
SUGIHARA Masayoshi
TAKAHASHI Yoshikazu
TERASAWA Atsumi (*15)
YOSHIDA Kiyoshi

Plant System Division

NEYATANI Yuzuru (Head)
KATAOKA Takahiro (*15)
NAGAMATSU Nobuhide (*9)
OHMORI Junji (*29)
OOHASHI Hironori (*10)
SATO Kazuyoshi
SEKIYA Shigeki (*14)
TAKAHASHI Hideo (*26)
TAMURA Kousaku (*13)
YAGENJI Akira (*1)
YAMAMOTO Shin

Tokamak Device Division

SHIBANUMA Kiyoshi (Head)
KAKUDATE Satoshi
KITAMURA Kazunori (*29)
MOHRI Kensuke (*11)
NAKAHIRA Masataka
OBARA Kenjiro
TAKEDA Nobukazu

Safety Design Division

O’HIRA Shigeru (Head)

HIGUCHI Masahisa,	MARUO Takeshi	TADO Shigeru (*15)
TAKEI Nahoko	TAKEMURA Morio (*11)	TSURU Daigo

Collaborating Laboratories

Tokai Research Establishment

Department of Material Science

Research Group for Radiation Effects and Analysis

JITSUKAWA Shiro (Leader)

FUJII Kimio	NAITO Akira	NAKAZAWA Tetsutya
OKUBO Nariaki	SAWAI Tomotsugu	SHIBA Kiyoyuki
TANIFUJI Takaaki	WAKAI Eiichi	YAMADA Reiji
YAMAKI Daiju		

Department of Nuclear Energy System

Research Group for Reactor Structural Materials

MIWA Yukio

Neutron Science Research Center

Research Group for Neutron Scattering from Functional Materials

IGAWA Naoki

Research Group for Nanostructure

TAGUCHI Tomitsugu

Center for Proton Accelerator Facilities

Accelerator Group

HIROKI Seiji

Office of Planning

Division of Collaborative Activities

NEMOTO Masahiro

*1 Hazama Corporation

*2 Hitachi, Ltd.

*3 Hitachi Engineering & Services Co., Ltd.

*4 Institute of Plasma Physics, Academia Science (China)
*5 Ishikawajima-Harima Heavy Industries Co., Ltd.

*6 JAERI Fellowship
*7 JP HYTEC Co., Ltd.
*8 Japan EXpert Clone Corp.
*9 Kajima Corporation
*10 Kandenko Co., Ltd.

*11 Kawasaki Heavy Industries, Ltd.
*12 Kawasaki Plant Systems, Ltd.
*13 Konoike Construction Co., Ltd.
*14 Kumagai Gumi Co., Ltd.
*15 Mitsubishi Electric Corporation

*16 Mitsubishi Heavy Industries, Ltd.
*17 NEC Corporation
*18 Nippon Advanced Technology Co., Ltd.
*19 Nuclear Engineering Co., Ltd.
*20 Osaka University

*21 Post-Doctoral Fellow
*22 Princeton Plasma Physics Laboratory (USA)
*23 Research Organization for Information Science & Technology
*24 Shimizu Corporation
*25 Sumitomo Heavy Industries, Ltd.

*26 Taisei Corporation
*27 Tohoku University
*28 Tomoe Shokai Co., Ltd.
*29 Toshiba Corporation
*30 Total Support Systems

*31 University of Tokyo

A.3.2 Scientific Staff in Fusion Research and Development Directorate of JAEA (October 2005 - March 2006)

Fusion Research and Development Directorate

SEKI Masahiro	(Director General)
SHIMOMURA Yasuo	(Scientific Consultant)
MATSUI Hideki	(Invited Researcher)
KOHYAMA Akira	(Invited Researcher)
IDA Katsumi	(Invited Researcher)
KISHIMOTO Yasuaki	(Invited Researcher)

Research and Development Co-ordination and Promotion Office

SEKI Shogo (General Manager)

GUNJI Masato	HAGA Junji	KATOGI Takeshi
KAWASAKI Minoru	KIZAKI Eiko	KUROSAWA Hiroshi
MATSUMOTO Hiroyuki	OHNAWA Tetsuya	SUGIKAWA Yukari
TERAKADO Yuichi	TSUDA Kazuko	YOSHINARI Shuji

ITER Project Promotion Group

OKUMURA Yoshikazu (Leader)

DOI Kenshin	EJIRI Shintaro	IWAI Yasunori
MATSUMOTO Hiroshi	OGAWA Toshihide	

Fusion Research Coordination Group

USHIGUSA Kenkichi (Leader)

ISEI Nobuaki	OOHARA Hirochi

Broader Approach Promotion Group

USHIGUSA Kenkichi (Acting Leader)

Division of Advanced Plasma Research

NINOMIYA Hiromasa	(Unit Manager)
KIKUCHI Mitsuru	(Senior Principal Researcher)
NAGAMI Masayuki	(Supreme Researcher)
TANI Keiji	(Senior Principal Researcher)

JT-60 Advanced Program Group

MIURA Yukitoshi (Leader)

ANDO Toshinari (*14)	FUJITA Takaaki	HATAE Takaki
KURIHARA Ryoichi	KURITA Gen-ichi	MATSUMURA Hiroshi (*2)
MORI Katsuharu (*5)	MORIOKA Atsuhiko	OGURI Shigeru (*5)

OIKAWA Akira	SAKURAI Shinji	SATO Fujio (*5)
SHIINA Tomio	TAMAI Hiroshi	TSUCHIYA Katsuhiko
YAMAZAKI Takeshi (*5)		

Collaborative Research Group

KIMURA Haruyuki (Leader)

KONOSHIMA Shigeru	SHINOHARA Kouji	

Tokamak Analysis Group

OZEKI Takahisa (Leader)

AIBA Nobuyuki (*17)	HAMAMATSU Kiyotaka	HAYASHI Nobuhiko
KIYONO Kimihiro	KOBAYASHI Masayuki (*19)	NAITO Osamu
OHASA Kazumi	OHSHIMA Takayuki	SAKATA Shinya
SATO Minoru	SUZUKI Mitsuhiro (*26)	TAKIZUKA Tomonori

Tokamak Experimental Group

KAMADA Yutaka (Leader)

ASAKURA Nobuyuki	CHIBA Shinichi	FUJIMOTO Kayoko (*17)
HAMANO Takashi (*15)	HAYASHI Toshimitsu (*13)	HOSHINO Katsumichi
IDE Shunsuke	INOUE Akira (*15)	ISAYAMA Akihiko
ISHIKAWA Masao (*17)	KAMIYA Kensaku	KASHIWA Yoshitoshi
KAWASHIMA Hisato	KITAMURA Shigeru	KOIDE Yoshihiko
KOKUSEN Shigeharu (*14)	KUBO Hirotaka	MATSUNAGA Go(*17)
MIYAMOTO Atsushi (*14)	NAKANO Tomohide	NAGAYA Susumu
OYAMA Naoyuki	SAKAMOTO Yoshiteru	SAKUMA Takeshi (*15)
SUNAOSHI Hidenori	SUZUKI Takahiro	TAKECHI Manabu
TAKENAGA Hidenobu	TSUBOTA Naoaki (*14)	TSUKAHARA Yoshimitsu
TSUTSUMI Kazuyoshi (*14)	TSUZUKI Kazuhiro	UEHARA Kazuya
URANO Hajime	YOSHIDA Maiko (*17)	

Plasma Theory & Simulation Group

KISHIMOTO Yasuaki (Leader)

IDOMURA Yasuhiro	ISHII Yasutomo	KAGEI Yasuhiro
MATSUMOTO Taro	MIYATO Naoaki	SUGAHARA Akihiro (*19)
TOKUDA Shinji	TUDA Takashi	

Tokamak Diagnostics Group

KUSAMA Yoshinori (Leader)

KASAI Satoshi	KAWANO Yasunori	KONDOH Takashi
OGAWA Hiroaki		

Fusion Reactor Design Group

TOBITA Kenji (Leader)

NAKAMURA Yukiharu	NISHIO Satoshi	SATO Masayasu

Division of Tokamak System Technology

KURIYAMA Masaaki	(Unit Manager)
HOSOGANE Nobuyuki	(Senior Principal Researcher)
YAMAMOTO Takumi	(Senior Principal Researcher)

Tokamak Control Group

KURIHARA Kenichi (Leader)

AKASAKA Hiromi	FURUKAWA Hiroshi (*15)	HOSOYAMA Hiromi (*6)
KAWAMATA Youichi	MATSUKAWA Makoto	OHMORI Yoshikazu
OKANO Jun	SEIMIYA Munetaka	SHIBATA Kazuyuki (*15)
SHIBATA Takatoshi	SHIMADA Katsuhiro	SUEOKA Michiharu
TAKANO Shoji (*26)	TERAKADO Hiroyuki (*5)	TERAKADO Tsunehisa
TOTSUKA Toshiyuki		

Tokamak Device Group

MIYA Naoyuki (Leader)

ARAI Takashi	HAGA Saburo (*14)	HAYASHI Takao
HIRATSUKA Hajime	HONDA Masao	ICHIGE Hisashi
ISAKA Masayoshi	KAMINAGA Atsushi	KIZU Kaname
MASAKI Kei	MATSUZAWA Yukihiro (*14)	MIYO Yasuhiko
NISHIYAMA Tomokazu	SASAJIMA Tadayuki	SHIBAMA Yusuke
SUZUKI Yutaka (*12)	TAKAHASHI Ryukichi (*2)	UEHARA Toshiaki (*15)
YAGISAWA Hiroshi (*2)	YAGYU Jun-ichi	YAMAMOTO Masahiro

RF Heating Group

FUJII Tsuneyuki (Leader)

HIRANAI Shinichi	HASEGAWA Koichi	IGARASHI Koichi (*14)
ISHII Kazuhiro (*15)	KIKUCHI Kazuo	MORIYAMA Shinichi
SATO Fumiaki (*14)	SAWAHATA Masayuki	SEKI Masami
SHIMONO Mitsugu	SHINOZAKI Shinichi	SUZUKI Sadaaki
TAKAHASHI Masami (*21)	TANI Takashi	TERAKADO Masayuki
YOKOKURA Kenji		

NBI Heating Group

IKEDA Yoshitaka (Leader)

AKINO Noboru	EBISAWA Noboru	GRISHAM Larry (*18)
HONDA Atsushi	KAWAI Mikito	KAZAWA Minoru
KIKUCHI Katsumi (*15)	KOMATA Masao	MOGAKI Kazuhiko
NOTO Katsuya (*14)	OHGA Tokumichi	OKANO Fuminori
OSHIMA Katsumi (*14)	TAKENOUCHI Tadashi (*24)	TANAI Yutaka (*15)
UMEDA Naotaka	USUI Katsutomi	YAMAZAKI Haruyuki (*2)

Division of Fusion Energy Technology

TAKATSU Hideyuki	(Unit Manager)
SHIHO Makoto	(Senior Principal Researcher)

Group of Fusion Advanced Technology for Practical Use

ABE Tetsuya (Leader)

Blanket Technology Group

AKIBA Masato (Leader)

ENOEDA Mikio	EZATO Koichiro	HIROSE Takanori
HOMMA Takashi	NISHI Hiroshi	NOMOTO Yasunobu (*8)
SUZUKI Satoshi	TANIGAWA Hisashi	TANZAWA Sadamitsu
YOKOYAMA Kenji		

Superconducting Magnet Technology Group

OKUNO Kiyoshi (Leader)

ABE Kanako (*4)	HAMADA Kazuya	ISONO Takaaki
KAWANO Katsumi	KOIZUMI Norikiyo	NABARA Yoshihiro
NAKAJIMA Hideo	NUNOYA Yoshihiko	OSHIKIRI Masayuki (*15)
SUGIMOTO Makoto	TAKANO Katsutoshi (*15)	TSUTSUMI Fumiaki (*26)

Plasma Heating Group

SAKAMOTO Keishi (Leader)

DAIRAKU Masayuki	HANADA Masaya	IKEDA Yukiharu
INOUE Takashi	KASHIWAGI Mieko	KASUGAI Atsushi
KOBAYASHI Noriyuki (*25)	KOMORI Shinji (*15)	MINAMI Ryutaroh (*17)
ODA Yasuhisa (*27)	SEKI Takayoshi (*2)	TAKAHASHI Koji
TANIGUCHI Masaki	TOBARI Naoyuki (*17)	WATANABE Kazuhiro

Tritium Technology Group

YAMANISHI Toshihiko (Leader)

HAYASHI Takumi	ISOBE Kanetsugu	KAWAMURA Yoshinori
KOBAYASHI Kazuhiro	MIURA Hidenori (*8)	NAKAMURA Hirofumi
SHU Wataru	SUZUKI Takumi	UZAWA Masayuki (*12)
YAMADA Masayuki		

Fusion Materials Development Group

SUGIMOTO Masayoshi (Leader)

ANDO Masami	CHIDA Teruo (*3)	IDA Mizuho (*4)
MATSUHIRO Kenjiro (*17)	NAKAMURA Hiroo	NAKAMURA Kazuyuki
TANIGAWA Hiroyasu	UMETSU Tomotake (*10)	YUTANI Toshiaki (*25)

Fusion Neutronics Group

NISHITANI Takeo (Leader)

ABE Yuichi	KAWABE Masaru (*15)	KONDO Keitaro (*16)
KUBOTA Naoyoshi (*17)	KUTSUKAKE Chuzo	NAKAO Makoto (*8)
OCHIAI Kentaro	OKADA Kouichi (*23)	SATO Satoshi
TANAKA Shigeru	YAMAUCHI Michinori (*25)	

Blanket Irradiation and Analysis Group

HAYASHI Kimio (Leader)

HOSHINO Tsuyoshi (*17)	ISHIDA Takuya (*15)	NAKAMICHI Masaru
TSUCHIYA Kunihiko	YAMADA Hirokazu (*8)	

Division of ITER Project

TSUNEMATSU Toshihide	(Unit Manager)
YOSHINO Ryuji	(Supreme Researcher)
TADA Eisuke	(Senior Principal Researcher)
SUGIHARA Masayoshi	(Senior Principal Researcher)
KOIZUMI Koichi	ODAJIMA Kazuo

ITER Project Management Group

MORI Masahiro (Leader)

ITAMI Kiyoshi	SENGOKU Seio	SHIMIZU Katsuhiro
SHOJI Teruaki	SUGIE Tatsuo	YOSHIDA Hidetoshi

ITER International Coordination Group

ANDO Toshiro (Leader)

HONDA Tsutomu (*25)	IIDA Hiromasa	IOKI Kimihiro (*12)
KATAOKA Yoshiyuki (*2)	MARUYAMA So	MORIMOTO Masaaki (*12)
NAGAHAMA Tetsushi (*20)	OIKAWA Toshihiro	OKADA Hidetoshi (*2)
SAKASAI Akira	SATO Kouichi (*26)	SHIMADA Michiya
TAKAHASHI Yoshikazu	TERASAWA Atsumi (*11)	YOSHIDA Kiyoshi

ITER Plant System Group

NEYATANI Yuzuru (Leader)

OHMORI Junji (*25)	SATO Kazuyoshi	SEKIYA Shigeki (*10)
TAKAHASHI Hideo (*22)	TAMURA Kousaku (*9)	YAGENJI Akira (*1)
YAMAMOTO Shin		

ITER Tokamak Device Group

SHIBANUMA Kiyoshi (Leader)

KAKUDATE Satoshi	KITAMURA Kazunori (*25)	MOHRI Kensuke (*7)
NAKAHIRA Masataka	OBARA Kenjiro	TAKEDA Nobukazu

ITER Safety Design Groupe

O'HIRA Shigeru (Leader)

HIGUCHI Masahisa TAKEI Nahoko TAKEMURA Morio (*7)

TSURU Daigo

Collaborating Laboratories

Tokai Research and Development Center

Nuclear Science and Engineering Directorate

Irradiation Field Materials Research Group

JITSUKAWA Shiro (Leader)

FUJII Kimio OKUBO Nariaki TANIFUJI Takaaki

WAKAI Eiichi YAMAKI Daiju

Research Group for Corrosion Damage Mechanism

MIWA Yukio

Quantum Beam Science Directorate

Nanomaterials Synthesis Group

TAGUCHI Tomitsugu

Accelerator Group

HIROKI Seiiji

Industrial Collaboration Promotion Department

Administration Section

NEMOTO Masahiro

Oarai Research and Development Center

Advanced Nuclear System Research and Development Directorate

Innovative Technology Group,

ARA Kuniaki

Technology Development Department

Advanced Liquid Metal Technology Experiment Section

YOSHIDA Eiichi

*1 Hazama Corporation
*2 Hitachi, Ltd.
*3 Hitachi Engineering & Services Co., Ltd.
*4 Ishikawajima-Harima Heavy Industries Co., Ltd.
*5 JP HYTEC Co., Ltd.

*6 Japan EXpert Clone Corp.
*7 Kawasaki Heavy Industries, Ltd.
*8 Kawasaki Plant Systems, Ltd.
*9 Konoike Construction Co., Ltd.
*10 Kumagai Gumi Co., Ltd.

*11 Mitsubishi Electric Corporation
*12 Mitsubishi Heavy Industries, Ltd.
*13 NEC Corporation
*14 Nippon Advanced Technology Co., Ltd.
*15 Nuclear Engineering Co., Ltd.

*16 Osaka University
*17 Post-Doctoral Fellow
*18 Princeton Plasma Physics Laboratory (USA)
*19 Research Organization for Information Science & Technology
*20 Shimizu Corporation

*21 Sumitomo Heavy Industries, Ltd.
*22 Taisei Corporation
*23 Tohoku University
*24 Tomoe Shokai Co., Ltd.
*25 Toshiba Corporation

*26 Total Support Systems
*27 University of Tokyo